# INFORMATION TO USERS

This manuscript has been reproduced from the microfilm master. UMI films the text directly from the original or copy submitted. Thus, some thesis and dissertation copies are in typewriter face, while others may be from any type of computer printer.

**The quality of this reproduction is dependent upon the quality of the copy submitted.** Broken or indistinct print, colored or poor quality illustrations and photographs, print bleedthrough, substandard margins, and improper alignment can adversely affect reproduction.

In the unlikely event that the author did not send UMI a complete manuscript and there are missing pages, these will be noted. Also, if unauthorized copyright material had to be removed, a note will indicate the deletion.

Oversize materials (e.g., maps, drawings, charts) are reproduced by sectioning the original, beginning at the upper left-hand corner and continuing from left to right in equal sections with small overlaps. Each original is also photographed in one exposure and is included in reduced form at the back of the book.

Photographs included in the original manuscript have been reproduced xerographically in this copy. Higher quality 6" x 9" black and white photographic prints are available for any photographs or illustrations appearing in this copy for an additional charge. Contact UMI directly to order.

UMI

University Microfilms International
A Bell & Howell Information Company
300 North Zeeb Road Ann Arbor MI 48106-1346 USA
313 761-4700 800 521-0600

Order Number 9510728

# Microcellular planning for a 2.0 GHz, direct sequence spread spectrum, code division multiple access personal communication network in a dense urban environment

Taylor, Maxwell M., Ph.D.

City University of New York, 1994

U·M·I
300 N. Zeeb Rd.
Ann Arbor, MI 48106

# MICROCELLULAR PLANNING FOR A 2.0 GHz, DIRECT SEQUENCE SPREAD SPECTRUM, CODE DIVISION MULTIPLE ACCESS PERSONAL COMMUNICATION NETWORK IN A DENSE URBAN ENVIRONMENT

by

Maxwell M. Taylor

A dissertation submitted to the Graduate Faculty in Engineering in partial fulfillment of the requirements for the degree of Doctor of Philosophy, The City University of New York

1994

This manuscript has been read and accepted for the Graduate Faculty in Engineering in satisfaction of the dissertation requirement for the degree of Doctor of Philosophy.

Sept. 1, 1994
Date

Professor Donald L. Schilling
Chairman, Examining Committee

Sept. 1, 1994
Date

Dean Gerard G. Lowen
Executive Officer

Professor Tarek N. Saadawi

Professor Joseph Barba

Professor Svetislav Maric

Dr. Joseph Garodnick

Supervisory Committee

**THE CITY UNIVERSITY OF NEW YORK**

## Abstract

# Microcellular Planning for a 2.0 GHz, Direct Sequence Spread Spectrum (DS-SS), Code Division Multiple Access (CDMA) Personal Communication Network (PCN) in a Dense Urban Environment

by

**Maxwell M. Taylor**

**Advisor: Professor Donald L. Schilling**

Good cell planning is a critical component of the emerging Personal Communication Networks if the expected user capacity and service quality are to be achieved. In addition, service providers require careful metrics about the network in order to develop economic plans. This requires detailed knowledge of channel characteristics and communication principles so that the most efficient networks may be developed.

This investigation looks at microcellular planning for a Direct Sequence Spread Spectrum, Code Division Multiple Access PCN system operating in the 2.0 GHz band. The emphasis is on

high user density service areas, such as the central business districts of large cities. Both the outdoor and indoor environments are considered. Empirical models are found for the signal propagation in these regions and the physical characteristics of microcells and picocells are defined. Different layouts of cells in the service areas are examined and criteria involving easily obtained parameters are established for general layout. Adjacent cell interference and its effects on available channels, mobile transmit power requirements, and cell site densities are determined for these cellular configurations.

## Acknowledgements

I would like to express my profound gratitude to my thesis advisor, Emeritus Professor Dr. Donald L. Schilling, for continuing to support my work after his retirement. His guidance and support throughout this most important phase in my life have been solid and his professional judgement and engineering acumen have been of the highest level, and I can only be better off for having studied with him.

I would also like to extend sincere thanks, first, to Mr. James B. LLewellyn, of the Coca-Cola Bottling Company of Philadelphia, and second, to the City University of New York for the fellowship that supported me throughout most of this work; it would just not have been possible without this support.

For their assistance in field tests and data analyses, I would like to thank Dr. Vinko Erceg and Mr. Saeed Ghassemzadeh; they provided invaluable help. I would also like to thank Dr. Schilling and the staff of InterDigital Communications Corporation for the use of their test equipment and facilities.

Finally, I am indebted to my wife, Jennifer, and my daughters, Yssenia and Martina, who suffered long and hard in

order that I could accomplish this task. Besides, none of this would be on paper without the superb typing skills of Yssenia.

Thanks Jennifer, you believed in me, even when I didn't. You stood with me all the way to the end, against all odds, and so I dedicate this work to you.

## Table of Contents

## List of Tables

## List of Figures

# Introduction

Personal Communications Systems (PCS) are at the forefront of current research activity in communications engineering today. Since the mid 1980s, considerable much interest has been generated in industry, academia and government about the promise of these systems for future communication. This has resulted in much discussion in the technical literature and trade journals as well as in the news media. The concepts, issues and concerns have been set forth in entire editions of many publications devoted to the subject. The Institute of Electrical and Electronic Engineers (IEEE) Communication Society's Magazine of February 1991 is one such edition that has given a very clear overview of the concepts and issues involved. Articles on pages 30 through 66 [1-7] have explored the broad commercial and regulatory issues of these systems. The broad technical issues have been dealt with by other articles from that same edition [8-11], as well as from similar publications [12-15].

This intense focus in PCS is due to two main reasons: first, there is the vision that these systems will provide not only advanced communication services for the future; but will be universal, ubiquitous and un-tethered as well. Second, the present mobile communications systems have reached their capacity limits and have to be replaced or upgraded. When

these new systems are implemented, communication access will be provided for large sections of the population. People will then be able to use very small lightweight equipment, such as pocket communicators and portable computing equipment, to communicate to anyone from anywhere, at anytime. This equipment will be universal and the systems will be transparent to the users. The types of services to be provided consist of those now available in the regular telephone system, plus many more advanced features such as multiple and high data rates, and data encryption.

The central feature of PCS is the Personal Communications Network (PCN). This concept has emerged in Europe as a means of providing portable communication services in cities, and in North America as a solution to the overgrowth of the present cellular system. The original concepts, technical issues and descriptions of PCN are due to pioneer researchers such as Steele in the UK and Cox in the USA among others [16-21].

A generally accepted description of a PCN is that it is a network in which many portable (pedestrian) and mobile (vehicular) users with small lightweight equipment communicate with numerous limited range stations covering a large region. These stations are very simple in design and are interconnected by coaxial cables, optical fiber cables, or point-to-point microwave links. The network is in turn

interconnected with other networks via satellites or the public telephone networks to serve a much larger geographic region, or perhaps a global region. The region serviced by a single station is usually called a **microcell** if the service area is outdoor, and a **picocell** if indoor. These names arise due to the physical sizes of the areas covered.

The major issues in the design of a PCN; which are at the foci of current research activities; are **spectrum utilization, user capacity, signalling** and **access** schemes, and **cell planning**. Spectrum utilization is concerned with the frequency bands that PCN will use and how much bandwidth is required to effectively operate the system. At present no firm decision has been made by the regulatory bodies concerned with spectrum allocation, but many researchers and potential system operators believe the 2.0 GHz band will be set aside for PCS. Signalling and access schemes relate to the communication techniques to be used. At present there are two candidate technologies for PCS, **Time Division Multiple Access (TDMA)** and **Code Division Multiple Access (CDMA)**. These are third generation technologies intended to supersede the present **Frequency Division Multiple Access (FDMA)** used in the current cellular mobile radio systems. FDMA ia an analog technology whilst TDMA and CDMA are digital technologies. Research to date has shown that the digital technologies will increase the system capacity by as much as cn order of magnitude while

providing the advanced capabilities expected of PCS. Cell Planning is concerned with locating the fixed stations in a service area and the selecting transmitting power, frequencies and bandwidth to provide acceptable signal coverage. This dissertation deals with cell planning for a dense urban environment. The system considered here is assumed to operate in the 2.0 GHz frequency band using **Direct Sequence Spread Spectrum (DS-SS)** CDMA technology.

## Statement of Work

The biggest problem in cell planning, and especially so for PCN systems, is that the topography of the service area is very irregular. Therefore site specific measurements are usually carried out to determine radio signal propagation characteristics in these areas. This amounts to large expenditure of resources (time, personnel, money and equipment). In cellular mobile radio communications system, empirical models exist for cell planning and these are used to provide fairly good estimates of system requirements. When an actual system is to be laid out, only limited site data is required then, for use with the models.

Since the PCN is a relatively new concept, no such models are available and potential operators are forced to either commission detailed site measurements or make approximations from the cellular models. The drawback with the former is the cost as pointed out earlier; but the latter, if not expertly done, can result in significant mis-estimate of requirements. This obviously means costlier designs in the long run. Because the speculation period of PCN is coming to an end and many potential players are queuing up to provide PCS service, there is a definite need to develop fairly good cell planning models. The aim of this work, at the very least, is to present one such model for the typical business district of a large

urban area.

Using the results of an extensive set of site measurements [22-24] undertaken in the greater New York urban area, and published results from similar studies elsewhere, empirical models for signal propagation are developed. From the resulting models, certain average characteristics are determined. These are taken as typical of the service areas involved and can be obtained with minimum measurement or from available data. Cell planning models are then constructed using these characteristics, and analyses are carried out to derive system parameters providing useful design metrics for systems operators. These include:

**Microcell dimensions**

**Physical Topology of Network**

**Cell Site Density**

**Number of Available Channels**

## Organization of Dissertation

The material presented in this dissertation is organized as follows:

Section 1 presents a brief description of the PCN and reviews the concepts and communication variables involved. Section 2 summarizes the signal characteristics in the micro- and picocellular channels and Section 3 uses the inherent average propagation models for the typical area to define the dimensions of the cells. Section 4 investigates particular configurations of microcells and picocells in the service area based on the results of Section 3. Sections 5 and 6 analyses adjacent cell interference in microcellular and picocellular networks respectively.

# 1 The PCN Concept

Figure (1.1) shows a fairly typical representation of the PCN concept in a dense urban environment. The network consists of a number of fixed communication stations called **base stations** and mobile communicating users called **mobiles**. The pedestrian users are often called **portables**, especially when reference is made to indoor areas. The location of a base station is called a **cell site** and the region it covers is called a **microcell**. Cell sites will be located on buildings and on lamppost-type structures along the sidewalks.

In order to limit interference to external systems and provide uniformly good coverage in the service area, the microcell radius is small, usually less than 1 km, and the cell site antenna is very low, typically less than 10m. These factors require very low the transmit power levels in the microcells, much lower than levels used in the present cellular FDMA systems. The very low power levels coupled with low antenna heights, and large building penetration losses due to high operating frequency, result in inadequate coverage inside building from external microcells. Therefore large, tall buildings or any indoor locations well away from the microcell cell site will have internal cell sites. The regions

covered by these indoor base stations are called **picocells**[1], due to their smaller physical sizes. Figure (1.1) shows picocells in the service area. The cell sites may be suspended from the ceiling above passages and aisles, or located in other unobstructed area free of interference from occupants. Much of the concepts on indoor cells, alluded to here, are handled in much greater detail by Cox [18] in his now classic tutorial on Universal Digital Portable Radio.

Because of the small effective radius of the microcell, many cells will be required to service a given area. The cell site equipment, however, can be made fairly small and simple. If the control functions are removed from most of these units and located in some centralized units, then the resulting base stations are merely signal relay stations. For the remainder of this thesis, the cell sites with control functions are referred to as **Base Stations** and those without as **Repeaters**. Base stations are more complex and expensive than repeaters and have to be sited at secure locations. Repeaters, however, are cheap and robust and are the units mounted on lampposts. Base stations and repeaters are interconnected by co-axial cable or optical fiber systems. The resulting network is in turn connected to the public telephone network.

---

[1]The concept of indoor picocells pre-dates the PCN idea. They have been proposed previously for wireless PBXs and indoor LANs.

Figure (1.2) illustrates how a microcell may be used to provide coverage to indoor areas. On the exterior of the building, there is one or more primary repeaters that receive signal from the microcell. These primary repeaters are then connected by cable through distributing networks to the secondary repeaters of the picocells[2]. The antennas of the primary repeaters can be placed in locations of good signal reception and made highly directive. This would reduce the gain required in the distribution network. Moreover, since the antenna location is fixed, fading effects would be greatly reduced, thus requiring a smaller fade margin in the system.

The communication channel from mobile to base station is called the **uplink**, reverse or **multiple access channel**. Base stations communicate with mobiles through repeaters by broadcasting signals in the microcell; this channel is the **downlink**, forward or **broadcast channel**. In a Spread Spectrum CDMA system, each mobile in the microcell is assigned an unique code called the spreading sequence or simply, the access code. If the total number of available codes is small, then the codes are allocated to the microcells in a re-use pattern, similar to the frequency re-use pattern of FDMA. Since the codes are distinct, the mobiles can all use the same carrier frequency and bandwidth at the same time (An excellent

[2]This arrangement is typical of CATV antenna distribution to large residential apartment buildings and of cable TV distribution networks.

tutorial in Spread Spectrum technology by Pickholtz, Schilling and Milstein covers these concepts [25]). Even though the mobiles can communicate simultaneously, they interfere with each. However, the interference due to a single user is small; it is a function of what is called the **processing gain** of the system. This in turn is a function of the length of the access code. As the number of users in the system increases, the total interference approaches some value that begin to degrade the service quality. Systems such as these are said to be interference limited as opposed to noise (thermal) limited systems. In contrast to FDMA and TDMA, there exists what is called a "graceful degradation of service"; additional users to a system at "maximum" capacity can be carried with a Signal to Noise Ratio (SNR) penalty. This is impossible for either of the others; once all the channels are allocated, no further user can access the system. This thesis investigates the effect of service area topography on the amount of interference adjacent cells generate on neighboring cells.

As the mobile moves about the network, its signal is received at more than one cell sites and conversely it receive signal from more than one cell sites. This situation has an advantage and a disadvantage. The advantage is that signals received over independent paths can be used for **diversity gain** in the system; that is, if one or more of the signals are unusable, then communication can still be maintained, because

it is highly unlikely that all paths will be simultaneously unusable. The disadvantage is that this situation causes additional interference, adjacent cell interference, in the system. If the cell site layout is optimal, then the above effects are minimal when the mobile is fairly close to its cell site. However, when it approaches the cell boundary, they become more pronounced. If there are m cell sites serving the particular location of the boundary and the propagation paths are similar, then the interference experienced by the mobile increases by a factor of m. Likewise, the diversity gain is increased by the same factor.

When mobiles cross into new microcells, **hand-off** is said to occur. In the hand-off process, control of the call is passed from the old microcell to the new microcell. The success or failure of this process depends on two factors; the relative signal strengths (from both microcells) at the cell boundary and whether the new microcell has an available channel. Both factors are influenced by the network topography. The second factor is quite critical, since if the microcellular dimensions are fairly small, vehicle speed high, and the number of users large; then the hand-off rate may be greater than the system can cope with. Thus good planning is required in order to determine optimal dimensions for the microcells.

CDMA systems have a unique hand-off feature, which results from its tolerance to additional amounts of interference (discussed earlier). In this feature, all the diversity paths are used during hand-off, providing the participating cell sites have available channels. That is, the call is carried by one or more cell sites until the signal quality of the principal one is reliable enough. This is called **soft hand-off**; it is not available in TDMA and FDMA systems.

The above overview has revealed the factors that influence the cell planning design of a PCN. It is seen that permissible transmit power, adjacent cell interference and hand-off rates and consequently hand-off success are all dependent on the network topography. That is, the sizes and shapes of the microcells and the locations of the cell sites all have profound impact on the system performance. These effects are investigated in subsequent Sections.

The effects on, and co-existence of the PCN system with external networks such as fixed microwave services (and vice-versa) is not investigated here. These are discussed in [13].

# 2 The PCN Radio Channel

Proper planning of a PCN requires a good understanding of the characteristics of the physical communication channel in which the system must operate. This is a very demanding radio environment, where certain rigid design criteria have to be met. Usually these criteria are trade-offs, for example, minimizing interference to external systems on the one hand and providing adequate signal coverage on the other hand. In addition, there are certain regulatory and environmental factors that impinge on the system design and must translate directly into careful physical planning. One such factor is the expected need to limit the maximum transmit power due to health safety concerns.

From the overview in Section 1, it is seen that the topography of the service area has a very significant effect on the characteristics of the radio signal propagating therein. The two physical channels outlined were the microcellular channel, outdoors, and the picocellular channel, indoors. Their gross topographical characteristics were described. This Section investigates the relationships between the topographic parameters and the communication variables, and defines the physical dimensions of the microcells and picocells.

The communications variables considered here to be critical to an analysis of the system are the propagation path loss, the distribution of the received signal envelope and the rms delay spread. The average path loss directly determines the permissible transmit power for a given receiver SNR. The probability distribution of the envelope indicates the effect of fading in the channel and has impact on the receiver signal output quality. It defines the SNR penalty (fade margin) that must be paid in order to get acceptable communication quality. The rms delay spread of the received signal determines the effect of multipath interference on the communication quality. It is shown later that the effect of multipath in a Spread Spectrum CDMA system is equivalent to additional users.

In the microcellular channel the parameters that influence these variables are the relative heights of the antennas; the street spacings, slopes, widths and orientation; and the level of congestion in the streets. In the picocellular channel, the number of floors and walls, materials in them, furnishing, and occupant traffic all influence signal propagation. In addition factors such as large window areas and buildings close by have significant influence.

## 2.1 Signal Characteristics in the Microcellular Channel

In the dense urban outdoor areas, the microcellular channel is made up of streets congested with pedestrian and vehicular traffic and tall buildings lining these streets. As previously mentioned the cell site antenna is relatively low, 20-40ft high. The buildings that line the streets are very closely spaced leaving very few gaps, and are highly reflective due to their steel frameworks. The combined effect of the buildings and the low antenna height results in the transmitted signal being largely confined to the streets. The highly reflective nature of the buildings results in large transmission losses to signal penetrating them.

Signal propagation measurements have been made in this type of environment by a number of researchers. The vast majority been done for large antenna heights and for narrow-band signals. It is only recently that researchers have begun to investigate low antenna height and wideband propagation. The results and analyses that follows below are due to an extensive set of wideband measurements conducted jointly with Dr. Vinko Erceg (principal investigator) in the greater New York City area [23]. The propagation measurements were done at 1.96 GHz using a 24 Mcps, 255-chip PN sequence giving a test signal of approximately 48 MHz bandwidth. The test equipment and measurement conditions are described in [22]. What is

presented below is a summary of the significant features of the data gathered.

There are two distinct regions, with different signal characteristics, in the dense urban environment. In the street on which the cell site is located, there is usually line-of-sight (LOS) condition between the transmitter and receiver and in the streets crossing the LOS street there is non-line-of-sight (NLS) conditions. In regular cellular mobile communications, the antenna is very far from the area the signal is received and is usually hundreds of feet high. As a result all streets have approximately the same signal characteristics.

**LOS Channel**

Figure (2.1.1) shows the average propagation path loss over a typical LOS run. The solid line plot consisting of two linear regions is the average path loss as determined by linear regression. This dual slope characteristic is predicted by the Friis model [37]. The approximate distance between these regions is called the breakpoint and it marks the change in slope of the characteristic. The variations of the path loss about the average are fairly small and constant throughout the run.

The pre-breakpoint loss was found to depend on the level of "urbanization". The slope exponent varied between 1.8 and 2.2. For runs on narrower street with tall buildings, it was greater than 2.0. The breakpoint and the post breakpoint loss for a given mobile antenna height and operating frequency were found to be functions of cell site antenna height $h_b$ and traffic density. The breakpoint was found to be close to the value predicted by the Friis model. It is proportional to $h_b$ and is given by equation (2.1.4). The loss at the breakpoint was also found to be fairly close to the predicted value. It differed from the predicted value [equation (2.1.3)] by about 1 dB for 10 ft antenna height to about 4 db for 20 ft antenna. The post breakpoint loss decreased with increase in $h_b$ and depended on the traffic density. Values for the slope exponent between 3.5 and 5.1 were observed at 20 ft height and between 3.2 and 3.7 for 10 ft high antenna. The larger values were associated with the busier streets. From the plots of path loss, it was seen that the average path loss was related to distance by a simple empirical formula. The average path loss $L_{LOS}$ is given by

$$L_{LOS} = \begin{cases} [L_0 + 10n_1(\log_{10} d - \log_{10} d_0)] \; ; & d_0 \le d < d_k \\ [L_k + 10n_2(\log_{10} d - \log_{10} d_k)] \; ; & d > d_k \end{cases} \qquad (2.1.1)$$

where d is the linear separation between the transmitter and receiver positions. $d_0$ is some close-in reference distance to the transmitter, here taken to be 10 m from the latter and $L_0$ is the loss at that location. $d_k$ is the breakpoint and $L_k$ is

the loss at the breakpoint. n1 and n2 are the slope exponents in the pre- and post- breakpoint regions respectively. $L_0$, $L_k$ and $d_k$ are given by the theoretical formulas with offset factors used to represent the effect of traffic conditions.

$$L_0 = -20\log_{10}\left(\frac{\lambda}{4\pi d_0}\right), \qquad (2.1.2)$$

$$d_k = \frac{4h_b h_m}{\lambda} \qquad (2.1.3)$$

and

$$L_k = -20\log_{10}\left(\frac{\lambda^2}{8\pi h_b h_m}\right) \qquad (2.1.4)$$

where $\lambda$ is the carrier wavelength, $h_b$ the transmitter antenna height and $h_m$ the receiver antenna height. $d_k$ is the breakpoint.

No significant correlations were seen between the parameters in equation (2.1.1) and the street width, so the average path loss given a fixed mobile antenna height and fixed carrier frequency depends on the cell site antenna height and the linear separation between antenna positions. The standard deviation of the path loss was found to be typically 3.0-5.0 dB. Again there was no marked correlation with street width, but very heavy blockage due to tall vehicles were found to cause significant increase.

**NLS Channel**

Figure (2.1.2) shows the propagation path loss found over a typical run that included NLS conditions. The solid line represents the average path loss. The structural features shown here that are typical of all such runs are (1) a fairly rapid increase in path loss occurring after the transition from LOS to NLS conditions and (2) an increase in path loss slope in the NLS region. The increase in path loss in the transition region is termed the corner loss; it was found to increase with distance of the turning corner from the cell site. The NLS slope was also found to increase with turning corner distance. Table (2.1.1) gives average values, determined from the plots, for the corner loss and the NLS slope exponent as functions of the turning corner distance. This distance is in multiples of standard street blocks, taken to be 275 ft, and is measured from transmitter position to turning corner. At the transmitted power used for the measurements, 1W effective radiated power (ERP), the path loss exceeded the receiver sensitivity in the NLS region after the sixth turning corner. Therefore, the values for the slope exponent and corner loss beyond 1900 ft are extrapolated from those below.

| Distance of Corner from Cell Site, (ft.) | Path Loss Slope exponent | Corner Attenuation (dB) |
|---|---|---|
| 275 | 4.90 | 14.0 |
| 550 | 6.30 | 18.5 |
| 825 | 7.71 | 21.5 |
| 1100 | 9.11 | 23.0 |
| 1375 | 10.51 | 24.5 |
| 1650 | 11.92 | 25.5 |
| 1925 | 13.32 | 26.5 |
| 2200 | 14.72 | 27.0 |
| 2475 | 16.12 | 28.0 |
| 2750 | 17.52 | 29.0 |

**Table (2.1.1) Path loss slope exponent and corner attenuation with LOS distance from "cell site".**

The simple empirical relationships between path loss exponent, corner loss and turning corner distance as represented in the table have been determined from average values over many runs. If $L_{ci}$ is the corner loss, $n_{ci}$ the NLS slope exponent and $d_{ci}$ the distance of the ith turning corner, then

$$L_{ci} = L_{ci}[1 + b_c \log_{10} i] \quad ; \quad i \geq 1, \quad 0 \leq b < 1 \qquad (2.1.5)$$

and

$$n_{ci} = n_{ci} + b_n (i-1) \quad ; i \geq 1. \qquad (2.1.6)$$

Parameters $b_c$ and $b_n$ are factors that fit the above relations

to the measured results. For the data under discussion, they have been found to be 1.15 and 1.40 respectively. $L_{ci}$ and $n_{ci}$ are given in the table, and $i=d_{ci}/d_c$, where $d_c$ is the standard block length. Both the corner loss and the NLS path loss slope exponent have shown some variation with street width. This, however, is not critical here, as only large changes in width (not a reality in the city) can cause significant changes in these parameters.

The average path loss is given by the empirical relation

$$L_{NLS} = L_{LOS}(d_{ci}) + L_{ci} + 10n_{ci}[\log_{10}d - \log_{10}d_i] \;;\; d>d_i \quad (2.1.7)$$

where $L_{LOS}$ is the LOS path loss at the corner and is given by equation (2.1.1). d is the distance of the mobile from the cell site measured along the LOS and the NLS streets. $d_i > d_{ci}$ is the approximate end of the transition distance.

Figure (2.1.3) shows the received signal envelope over a 60m section of a run. The dashed line plot represents the local mean and the scatter plot the point variation (instantaneous signal strength). These are equivalent to the long term and the short term fading components of the envelope. Figure (2.1.4) shows the cumulative distribution function (CDF) of the envelope along with plots of Rayleigh and Rician distribution with same mean and variance as the data. It is seen that a Rician distribution with power ratio k=10 dB provides a close fit to the data. Similar data frames

from different runs have shown k to vary between 10 and 13 dB. The local mean was found to have a standard deviation of between 1.5 and 3.5 mV over the set of data. For the variation about the local mean, the standard deviation was 0.14 to 0.24. The envelope statistics were found to be typically the same for LOS and NLS regions within the dynamic range of the receiver. This is a marked difference from regular cellular mobile channels which exhibit Rayleigh envelope statistics. The difference is due to the very low antenna heights and the relatively close proximity of the receiver to the transmitter.

The delay characteristics have shown also been investigated for low antenna heights and wideband signals [26,27]. It is seen that the rms delay spread is less than 500 ns in the LOS channel. It is found to be around 200 ns close to the transmitter and about 300-400 ns far from the transmitter. The value is slightly larger in the NLS region but is still significantly less than that found for narrow band FDMA channels. The reason is the containment of the radio waves in the streets, and the close proximity of the multipath scatterers (buildings, vehicles and people) to the receiver.

## 2.2 Signal Characteristics in the Picocellular Channel

The picocellular channel is defined for indoor locations, typically large office building, malls and other such large enclosed areas. This is a very complicated communication environment in which many factors influence the propagating signals. The architecture of the internal space, the building materials, the furnishing and the occupants are all factors. In addition, the external environment sometimes has an effect on the signals within the buildings. Because of this wide variety of contributing factors, detailed site measurements have to be carried out many times to identify and quantify the significant ones. Such investigations have been the subject of extensive research effort over a long period of time. The propagation, multipath and fading characteristics have been measured and simulated under both narrowband and wideband conditions, and many empirical site dependent models have been developed and refined over time to describe this communication channel. However, from the vast number of published results, a few factors have appeared consistent and can be used to derive fairly successful generalized empirical models.

There is much similarity in the results of propagation and fading studies, and the kinds of generalized conclusions that can be drawn are typical of the conclusions of these [24,28-32]. From the reported results, the following can be

clearly ascertained: (1), the path loss depends on the number of floors separating the transmitter and the receiver, and (2), the path loss slope exponent is greater measured through rooms than along straight corridors and aisles. The increase of path loss with floor separation is not constant, but diminishes with every floor crossed. This unusual occurrence (diminishing differential loss) is due to diffraction of waves through windows from one floor to near adjacent floors. This hypothesis has been supported in all the works referenced above. Measurements with the transmitter close to windows have shown much smaller differential floor loss than with the transmitter in the middle of the floor. The variation of the path loss exponent with direction across a floor is due to the loss resulting from walls and partitions. Along a corridor there is line-of-sight condition and free space (or better) conditions exists. However as the signal line deviates from the corridor axis, an increasing number of walls and partitions come between the transmitter and receiver. Since each such obstacle result in some loss, the path loss exponent is a function of direction.

Researchers have tried to isolate the effects of walls and floors and have given empirical formulas that account for the differential losses. The formulas of LaFortune and Lecours [31], have parameters that are derived to fit the data, whilst those of Seidel and Rappaport [32] have been derived from

phenomenological considerations and have physical bases. The models to be used here tend to follow the former. Certain values that are common to all studies are used in conjunction with parameters that require minimal site investigation for evaluation. In fact certain average properties are assumed for buildings in the subsequent analysis, and if actual buildings meet these specifications then no modification is required for the parameters. The critical values for the model are the initial differential floor loss (through first floor from transmitter floor) and the minimum and maximum slope exponents across the zeroth floor (the transmitter floor).

From the published results, the initial differential floor loss, $L_{f1}$, varies between 10 and 30 dB. The lower value is obtained for plain concrete floors and the upper bound for concrete floor with steel sheetwork. For ordinary steel reinforced concrete the loss is about 20dB. The path loss slope exponent, $n_o$ varies between 1.8 and 4.5. The value 4.5 occurs for areas well removed from the main corridors and 1.8 results for areas along main corridors. The upper limit is taken to represent 45° from the axis of the main corridor in a symmetrically laid out floor and the lower limit to represent the corridor axis. The loss through i floors, $L_{fi}$, may be given by

$$L_{fi} = L_{f0}\frac{(1-b^i)}{(1-b)} \quad ; \quad i \geq 1, \quad 0 \leq b < 1. \qquad (2.2.1)$$

This particular form is chosen for the function as it can be made to match nearly all the reported results. The parameter b depends primarily on the transmitter location. It is smaller for centrally located transmitters than for those located near external walls. Typically, a value of 0.75 is used for average conditions. The loss exponent over the zeroth floor may also be given by

$$n(\theta) = n_{01} + \frac{4(n_{02}-n_{01})}{\pi}\theta \quad ; \quad 0 \le \theta \le \frac{\pi}{4}. \qquad (2.2.2)$$

This function for the exponent is just chosen to uniformly distribute the change through $\pi/4$ radians; no serious errors result from this choice. The average propagation average path loss in the picocell with negligible contribution from the microcell is given by

$$L_i(\theta) = L_{0i} + L_{fi} + 5[n_0(\theta)][\log_{10}(d^2+h_i^2) - \log_{10}(d_i^2+h_i^2)] \; ; d \ge d_i \qquad (2.2.3)$$

where $L_i(\theta)$ is the path loss along the ith floor (from the transmitter floor) in direction $\theta$ and d is the distance of the receiver from the vertical axis through the transmitter. $h_i$ is the vertical separation between transmitter and receiver antennas. $d_i$ is the reference distance, taken to be 1 m from the vertical axis and $L_{0i}$ is the loss at the reference distance. $h_i$ is given by

$$h_i = \begin{cases} h_c - h_b + h_m & ; i\text{th floor above zeroth floor} \\ h_c + h_b - h_m & ; i\text{th floor below zeroth floor} \end{cases} \qquad (2.2.4)$$

where $h_c$ is the inter-floor distance and $h_b$ and $h_m$ are the

heights of the transmitter and receiver antennas above the zeroth floor respectively. $L_{0i}$ is given by

$$L_{0i} = -10\log_{10}\left[\left(\frac{\lambda}{4\pi}\right)^2\left(\frac{1}{d_i^2+h_i^2}\right)\right]. \qquad (2.2.5)$$

Figures (2.2.1), (2.2.2) and (2.2.3) show the calculated path loss on the cell site floor and on the first and third floors from the cell site floor.

As many studies have been done to determine the fading and multipath characteristics of the received signal as have been done for propagation characteristics. Although the majority of these were conducted at 880-950 Mhz, the results are quite applicable to 2.0 GHz. These studies have studies [22,28-29] have all shown that the received signal envelope is Rician distributed with k values ranging from 6 to 15 dB. The lower limit is usually observed in areas that are significantly shadowed; that is the path between transmitter and receiver is obstructed by thick walls and equipment. The upper limit is observed in locations close to corridors.

Devasirvatham [33-35] has extensively studied the multipath characteristic of the indoor channel. He has found that the rms delay spread varied very widely depending upon the size and construction of the building and the proximity of neighboring buildings. Values as low as 20 ns were obtained close to the transmitter and up to 400 ns maximum for very

large buildings. Other researchers (Saleh and Valenzuela [36]) have shown similar results. For average size buildings with reinforced concrete floors and concrete walls, a maximum rms delay spread of 300 ns is not uncommon.

Having summarized the propagation, fading and multipath characteristics in the outdoor and indoor channels, the next Section develops models for the microcells and picocells. The propagation models just discussed serve as the generators of these cell models. Once the cell models are developed, possible configurations of these into networks are explored.

# 3 Physical Planning for PCN

The concepts of the microcell and picocell were discussed in Section 1 and the signal characteristics in these channels summarized in Section 2. In this section, the physical characteristics of microcells and picocells are explored. Their shapes, sizes and other factors that influence these are determined. Different placements of the cell sites are investigated to determine the influence this has on signal coverage in the cell. The contours of equal path loss are then determined and the cell coverage area, defined by the region within the contour of maximum permissible loss, is found.

## 3.1 The Physical Microcell

As was shown in Section 1, the microcell is principally defined by the regions between the buildings in the dense urban area. Thus the streets and sidewalks primarily comprise the microcell. There is some penetration of buildings, but this is only significant close to the microcell cell site. In order to ascertain the shape and size of a microcell, the average path loss around an isolated cell site is investigated. Figure (3.1.1) shows a section of a hypothetical street grid in a dense urban area. The avenues are labelled using lower case letters and the street labelled using numbers. The intersections are labelled using upper case letters, thus (d,4) defines the coordinates of intersection B.

There are two possibilities in locating the cell site at low antenna heights. The cell site may be placed at an intersection or mid-block between intersections. It is readily observed in the figure that a cell site located an intersection can 'see' in four directions from the intersection. Thus an omnidirectional antenna may be used at this cell site to provide coverage in these directions. A cell site placed mid-block, however, can 'see' in only two directions. Therefore it illuminates a smaller region than the cell site located at an intersection. A directed antenna may be used in this location.

The figure shows a cell site located, for purpose of illustration, at the center of a square. In reality the actual site will probably be on one corner of the square. The cell site is placed in the square so as to maximize the area served by it. This arrangement also lends itself well to cell sectorization. The signal transmitted by the cell site will propagate out from it in four LOS directions . Along each LOS path the signal scatters in crossing streets, propagating in NLS modes. The LOS and NLS regions are illustrated in the figure. From a knowledge of the signal propagation mechanism, discussed in Section 2, it can be readily seen from the figure that there is one significant equivalent propagation path to each location in the LOS region and at most two significant equivalent paths to locations in the NLS region. These

equivalent paths are illustrated in the figure for two intersections, A and D. Path 1 is an LOS path from the cell site at B to intersection A. Path 2 from B to intersection D comprises an LOS segment, BC, and an NLS segment, CD. Path 3 also from B to D comprises LOS and NLS segments BE and ED respectively. The shape of the microcell is now investigated by observing the path loss to the intersections and mid-blocks around the cell site.

The average power received at an observation point due to propagation over equivalent path i may be written as (see Appendix A)

$$\begin{aligned} P_i &= \mu_i P_0 \\ &= \overline{m_i^2}\,\overline{\beta_i^2} P_0 \end{aligned} \qquad (3.2.6)$$

where $\mu_i$ is the average path power attenuation (or gain) at the observation point and $P_0$ is the effective radiated power (ERP) over the path. $m_i$ is the path local mean (voltage) attenuation in the vicinity of the observation point and $\beta_i$ is the variation about the local mean. The random variable $m_i$ is log-normally distributed, typically; its mean value is a function of distance between transmitter and observation point. The gain variation, by definition [38], has unity mean and is Rician distributed for the microcellular channel.

For two paths contributing to the average power, it can be shown that for Rician distributed variations with high power gain ($k \geq 10$), the average attenuation, $\mu$, is given by

$$\mu = (\overline{\beta_1^2}\overline{m_1^2} + \overline{\beta_2^2}\overline{m_2^2}) + (2\overline{m_1^2}\overline{m_2^2})^{\frac{1}{2}}. \qquad (3.2.7)$$

In Section 2, it was seen that the received signal distributions were all Rician with high k. Thus, if the paths are fairly similar (in length and topography), then the gain variations may be assumed identically distributed. Making this assumption and noting that the mean square is approximately equal to the square of the mean for high k, equation (3.1.2) may now be re-written as

$$\begin{aligned} \mu &= (\overline{m_1^2} + \overline{m_2^2}) + (2\overline{m_1^2}\overline{m_2^2})^{\frac{1}{2}} \\ &= (\mu_1 + \mu_2) + (2\mu_1\mu_2)^{\frac{1}{2}}. \end{aligned} \qquad (3.2.8)$$

In the above equation, the mean square of the local mean is also assumed approximately equal to the square of its mean. The average path loss, L, is defined as

$$L = -10\log_{10}(\mu). \qquad (3.2.9)$$

The average path power attenuation over a single equivalent path may be determined from equations (2.1.1) and (2.1.2) in Section 2, and is given by

$$\mu = \begin{cases} \mu_0\left(\frac{d_0}{d}\right)^{n_1} & , d_0 \leq d < d_k \\ \mu_k\left(\frac{d_k}{d}\right)^{n_2} & , d > d_k \end{cases} \qquad (3.2.10)$$

for an LOS path, where $\mu_0$ is the attenuation at the reference distance $d_0$ and $\mu_k$ is the attenuation at the breakpoint $d_k$. For an NLS path

$$\mu = \mu_{LOS}\,\mu_{c1}\left(\frac{d_1}{d}\right)^{n_{c1}} \quad , \quad d > d_1 \qquad (3.2.11)$$

where $\mu_{LOS}$ is the attenuation corresponding to the LOS path loss at the turning corner, $\mu_{c1}$ is the attenuation corresponding to the corner loss and $n_{c1}$ is the path loss exponent along the ith NLS street from the cell site. A path comprising both LOS and NLS segments as path(1) or (2) in figures (3.1.1), has ith path attenuation factor in the NLS region given by

$$\mu_1 = \begin{cases} \mu_0\left(\frac{d_0}{d_{c1}}\right)^{n1}\mu_{c1}\left(\frac{d_{c1}}{d}\right)^{b1} & ; \quad d_{c1} \le d_k\,,\ d > d_{c1} \\ \mu_k\left(\frac{d_k}{d_{c1}}\right)^{n2}\mu_{c1}\left(\frac{d_{c1}}{d}\right)^{b1} & ; \quad d_{c1} > d_k\,,\ d > d_{c1} \end{cases} \qquad (3.2.12)$$

i = 1,2.

Using equations (3.1.5) and (3.1.7) and the table (2.1.1) in Section 2, the path loss is found at the intersections and mid-block positions around the cell site. Figure (3.1.2) shows these values for a cell site located at an intersection, such as B in figure (3.1.1). A consequence of equation (3.1.3) is that the attenuation at an intersection (in the NLS region) is smaller than at a mid-block position the same distance from

the cell site. Thus in figure (3.1.2), nearly all the NLS intersections show smaller path loss than the surrounding mid-block positions. Only one quadrant, with respect to the cell site axes, is shown due to the symmetry of the grid.

The effects of both LOS and NLS propagation are clearly observed. There is 30 dB signal power loss over a distance of 6 blocks along the LOS region,; but for just the first transversal street (into the NLS region), the loss is the same as the above after just only 1 block. For each transversal street, the loss gets bigger fairly quickly into the street and reaches values of 40-60 dB (at 6 blocks) larger than in the LOS street. Regions with average path loss within certain limits are also illustrated in the figure. The chosen limits represent the maximum permissible path loss (appendix C) for defined maximum transmit power levels. Figure (3.1.3a) plots contours of equal path loss passing through intersections and figure (3.1.3b) shows contours through mid-block positions. The selected contours are the maximum permissible loss and a 10 dB bound on either side. The region enclosed by the maximum permissible loss represent the practical coverage area of the microcell and the region within the 10 dB bounds indicates the hand-off and uncertainty regions.

The shape of the microcell, as defined by the maximum loss contour, is approximately a square with diagonals along

axes through the cell site . An important observation is that the boundary of the microcell is much smaller than the LOS range of the cell site; this has significant implications for hand-off and adjacent cell interference in the LOS region (discussed later). The radius of the microcell is defined as the distance to the cell boundary in the LOS region. This (radius) is determined by the loss in the NLS region and is confined to just a few blocks from the cell site (6 blocks in the figure), because of the power limitation in the microcell. Table (3.1.1) gives values of microcell radius and maximum path loss as functions of maximum permissible transmit power in the cell.

| Maximum permissible transmit power, mW | Cell radius, m | Boundary Path Loss, dB |
|---|---|---|
| 0.15 | 168 | 100 |
| 1.0 | 251 | 110 |
| 4.0 | 335 | 117 |
| 25.0 | 419 | 124 |
| 100.0 | 503 | 129 |

**Table (3.1.1) Microcell radius and maximum path loss for selected maximum mobile transmit power level in the microcell.**

Figure (3.1.4) shows path loss values around the cell site, when located at a mid-block position. As was mentioned earlier, the coverage provided by this cell site location is

less than that for intersection located cell site. The shaded regions in the figure have poor coverage; the average path loss in these blocks is on the average 15 dB higher than for similar blocks when the cell site is at an intersection. Figures (3.1.5a) and (3.1.5b) show the path loss contours through intersections and worst case mid-block positions respectively. From the contours and the maximum power limits in figure (3.1.4), it is seen that the radius of the microcell with this cell site location is less than that with cell site at an intersection. If the cell boundary is defined by the worst case maximum path loss, then there will be regions beyond the cell boundary with much path loss. This would result in significant overlap of microcells in a practical network. Alternately if the boundary is defined by the maximum path loss through intersections, then the microcell will have almost the same radius as the intersection cell site microcell; but there will be regions of higher losses within the cell. This is depicted in figure (3.1.4), if the power limits are taken to represent the cell boundaries.

The urban street grid sections illustrated in the figures (3.1.2) and (3.1.4) consist of hypothetical standard city blocks. These street segments are of uniform length and width. In a real city, blocks have varying length and street have varying widths. For example, in mid-town Manhattan, New York City, the avenues are typically 85 ft wide (including

sidewalks) and the streets 55 feet wide. The block lengths are approximately 275 feet (center-to-center) between streets and 1100 feet between avenues. A section of grid from a city area like this has fewer blocks and intersections but typically the same loss contours. Figures (3.1.6) and (3.1.7) show the path loss values around the cell site for a grid section with 4 to 1 block ratio for intersection and mid-block cell sites respectively. Figure (3.1.6) is identical to figure (3.1.2) except for the length of the blocks, so this grid will have the same path loss contours. The mid-block case in figure (3.1.7), however, appear quite similar to the intersection case, figure (3.1.6). This situation results because the blocks that were poorly covered in figure (3.1.4) have now been eliminated by the greater than unity block ratio.

Figure (3.1.8) illustrates the microcell for a 1:1 block ratio, intersection located cell site. This will be called a type Omni-I microcell. When the cell site is located mid-block, the microcell will be called type M microcell. Except for variations due to the different location of the cell site and the difference in power levels, the Omni-I and the M type microcells have the same shape. As mentioned earlier, the Omni-I microcell may be sectored four ways. Figure (3.1.9) depicts such a 4-sector microcell, showing the areas covered by the sectors. For the 1:1 block ratio Omni-I microcell, there are four identical sectors and each overlaps 2 adjacent

sectors. The overlap area for each adjacent sector is one half of the sector area. The overlap of the sectors has important implications for hand-off operation and for adjacent sector interference (see Section 4). For m:1 ratio Omni-I microcells or for M type microcells, there are only two sectors per microcell and there is no sector overlap. The path loss contours for sectored microcells are the same as those for the non-sectored ones.

### 3.2 The Physical Picocell

The picocellular communication scenario was described in Section 1 and the signal propagation and statistics evaluated in Section 2. As for the physical microcell, the path loss contours are determined for typical locations of cell site in the physical area; and the picocell coverage area determined by the maximum permissible path loss.

Figure (3.2.1) shows the plan of a hypothetical floor in a typical high rise office building. A worst case topography is considered, where there are banks of totally enclosed offices separated by a grid of average size corridors. Other floors in the building with the exception of the ground floor are assumed to be replicas of the illustrated floor. In such a symmetric topography, the cell site may be located at the intersection of the main corridors. This, as described in

Section 2, provides good signal coverage in the corridors, enhancing the signal received in adjacent offices.

In the figure, a cell site is located in position A and the path loss is found over a measurement plane above the floor for the cell site floor and those above and below. The height of the measurement plane corresponds to the approximate height of the portable unit in use. Using equation (2.2.3), the average path loss along the ith floor from the cell site floor (the zeroth floor) is calculated for locations around a vertical axis through the cell site . For the purposes of the analysis, the floor dimension is taken to be 100 m square; thus the building is assumed to be about 1 block wide. In addition, the path loss exponent is assumed constant around the axis, as the width of the corridors is small compared to office dimensions. Thus the calculated contours are all circular; this is a very typical situation for the office building. The use of a variable slope exponent does not significantly change the path loss because of the relatively small dimensions of the building. Also, whatever change that (changing slope) would make, would be less evident on floors beyond the zeroth floor. The figure also reveal that contours of equal loss have smaller radii as the floor number increases. Contours of equal path loss are plotted for different floors, as shown in figure (3.2.2). As for the microcellular case, the contour levels are for maximum

permissible path loss and for 10 dB bounds about the maximum. The contours show the losses for floors below the zeroth floor; these are chosen because the losses are greater on these than on the upper ones due to greater distance from the cell site.

It is clearly obvious from the contours that the zeroth floor and the first floors from it are all entirely within the maximum loss contours. It is also noted that radius of the maximum path loss contour decreases as the number of floor increases. The picocell may be considered to consist of a 'stack' of circular regions centered on an a vertical axis through the cell site. These regions have diminishing radii as the floor number increases from the cell site. Figure (3.2.3.) shows the representation of the picocell, as defined by the maximum permissible path loss. The latter is actually a region in 3-dimensional space, but since the portables are most likely located along the measurement planes, the picocell is reduced to an array of 2 dimensional regions. The radius of the picocell is defined as the radius of the maximum loss contour on the zeroth floor and the height as the distance from the zeroth floor to the floor where the coverage area falls below some set value. Table (3.2.1) gives radius and height of the picocell as a function of permissible transmit power in the picocell. The coverage that is used to define the height is 25 percent that of the zeroth floor; that is if the

coverage area a floor is less than 25 percent of the coverage on the zeroth floor, it is deemed outside of the cell. This factor corresponds to a contour radius of one half the cell radius. An immediate consequence of the unequal coverage area on different floors is the need for more than one cell sites to adequately cover the picocell volume. This is explored in Section 4.

| Maximum permissible transmit power, dBm | Maximum path loss, dB | Picocell radius, m | Picocell height, floors from zeroth floor |
|---|---|---|---|
| 10.00 | 115 | > 75 | 4 |
| 0.00 | 105 | > 75 | 2 |
| -3.01 | 102 | > 75 | 2 |
| -10.00 | 95 | 60 | 1 |
| -20.00 | 85 | 25 | 1 |

**Table (3.2.1) Picocell radius and height as functions of maximum permissible transmit power in the picocell.**

# 4 Cellular Configurations

Having determined the physical characteristics of microcells and picocells, this section now investigates the possible arrangement of these cells to provide coverage to a large area. At the outset, the factors that influence the suitability of a particular configuration are the cell site density, adjacent cell interference and hand-off rate. The cell site density is a direct factor in the cost of the network, so the aim is to minimize this factor. Adjacent cell interference and hand-off rate are directly related to the number of users the network can support. As these factors increase, the number of users must be decreased. Thus the network revenues decreases. Therefore, the arrangement of the cell is very important, not only for technical reasons but for economic ones as well. This section determines suitable layouts of cells and find the cell site densities; adjacent channel interference and hand-off rates are dealt with in subsequent sections.

## 4.1 Microcellular networks

The shapes and sizes of the microcells are dependent on the topography and composition of the service region. If the region is isotropic and regular, then the microcells have the same properties and a single size and shape can be used to populate the region. However, if the region is not isotropic

and regular, then different parts will have microcells of different shapes and sizes. For this type of region, an apriori analysis is not possible, except in some average sense, as the properties of the different localities are very variable. These properties have to be investigated by site inspections and the information used in Sections 2 and 3 used to determine the physical properties of the microcells for the different localities. This analysis is for the former type of region, which is typical of the central region of dense urban environments.

The basic shape of the microcell for the regular isotropic region is seen in figures (3.1.8) and (3.1.9). This region as discussed previously is a rectangular grid and the microcell is a square region with diagonal lying along the LOS axes. The square is one of the few shapes that can be tesselated in a region so there will be no geometric gaps in the layout of the region. Figure (4.1.1) shows a section of the service region laid out with the basic microcell. For convenience, the radius of the microcells shown is 2 blocks; but can be up to 6 blocks as shown in Section 3. As seen in the figure, there is no geometric overlap of the cells. Each is surrounded by eight nearest neighbors as denoted by the cells labelled 0 to 8 in the figure. The cell 0 is the reference cell and cells 1 to 8 are the nearest neighbors. Cells 1,3,5 and 7 are adjacent on the vertices of the

reference cell and cells 2,4,6 and 8 are adjacent on the sides. Thus, the vertex neighbors only share a common intersection, whilst the side neighbors share the total boundary of the microcell.

The unequal common areas with the neighboring means that interference due to the vertex neighbors will primarily be LOS in nature, whereas that due to the side neighbors will be NLS. In Section 3, it was shown that the cell radius is much smaller than the LOS range, which implies that the effect of the vertex adjacent cells extends well within the reference cell. The effective LOS range of a cell is 20 blocks (5500 ft) at 20 dBm transmit power and about 5 blocks (1375 ft) at -10 dBm power level. Therefore at maximum cell radius (6 blocks), a cell will interfere with up to 4 cells along the LOS axis! This is an inevitable consequence of this layout, about which more is said later.

The bulk of the hand-off transfers will be with the side neighbors as these share the entire boundary of the cell. If the signal overlap due to the vertex adjacent cells is allowed to exist in the network, then hand-off between vertex neighbors occur only infrequently. Hand-off rates and adjacent cell interference are dealt with in subsequent sections.

Let the radius of the cell be denoted as $r_c$ meters or $n_c$ blocks, the area as $A_c$ and let R and w represent the standard block length and average street width (inclusive of sidewalks) respectively. Then the gross cell area $A_I$ is given by

$$A_I = 2r_c^2 = 2R^2n_c^2. \qquad (4.1.1)$$

The effective cell area, that is the region contained in the streets, is quite smaller; but cannot be used to determine cell site density. The latter, denoted by $\sigma_I$, is

$$\sigma_I = \frac{1}{A_I}. \qquad (4.1.2)$$

Table (4.1.1) gives microcell radii, areas and cell site densities as functions of maximum permissible transmit power.

| Maximum permissible transmit power, dBm | microcell radius, m | Microcell area, x $10^3$ $m^2$. | Cell site density, $km^{-2}$ |
|---|---|---|---|
| -8.24 | 168 | 56.45 | 17.71 |
| 0 | 252 | 127.01 | 7.87 |
| 6.02 | 336 | 225.79 | 4.43 |
| 13.98 | 420 | 352.80 | 2.83 |
| 20 | 504 | 508.03 | 1.97 |

**Table (4.1.1) Microcell area, radius and cell site density for different transmit power level for Omni-I microcell.**

The omni-M and the 4-sector microcells have identical areas to the omni-I microcell; thus the above table applies to these cells as well. The differences between these cells exist in the adjacent cell interference and the hand-off rates.

Earlier it was seen that the LOS range of the cell site exceeded the cell radius, and in Sections 2 and 3 it was shown that entering the NLS region the average path loss was on the average 15 dB greater than in the adjacent LOS region. Therefore, if the transmit power levels are reduced sufficiently, then the it is possible to "confine" the signal to the LOS region. The microcells that results are then linear in dimensions; these are referred to as linear or L type microcells. Figure (4.1.2) shows the L-type microcells that are obtained from the intersection (I-type) and the mid-block (M-type) microcells. The type LI consists of four LOS regions (arms) extending from the cell site and the type LM 2 arms. Some the signal does extend to the NLS region, but this is well below the boundary value and may be ignored in cell with radii less than 6 blocks. These microcells, particularly the LM type, are very useful in areas of the service region that do not conform to the basic grid structures.

Figure (4.1.3) shows the most obviously way of arranging the cell sites in a network of LI-type microcells. They are located on diagonals through intersections spaced $2n_c$ blocks apart and each microcell is overlapped by $2(n_c-1)$ adjacent cells. For the network in the figure, $n_c$ is two there are two overlapping cells; microcells 3 and 4 overlap 2 as shown. There are also four microcells abutting the four limbs of any cell resulting in total of $2n_c+2$ nearest neighbors.

The effective area, $A_{LI}$, of the microcell is given by

$$A_{LI} = 4r_c^2w^2 - w^2 = w^2(4r_c^2 - 1) \qquad (4.1.3)$$

where $r_c$ and w are the cell radius and the average street width respectively. To determine the cell site density, a square region enclosing one complete microcell is chosen. This region encloses $(2n_c-1)$ cell sites, and shares four others with adjacent regions. The cell site density $\sigma_{LI}$ then is

$$\sigma_{LI} = \frac{2n_c}{(2r_c)^2} = \frac{1}{2n_cR^2}. \qquad (4.1.4)$$

Table (4.1.2) gives these values in for different permissible transmit power levels in the network.

| Maximum permissible transmit power, dBm | Microcell radius, m | Microcell area, x $10^3$ $m^2$. | Cell site density, $km^{-2}$ |
|---|---|---|---|
| -22 | 168 | 13.86 | 35.44 |
| -18 | 252 | 21.02 | 23.62 |
| -13 | 336 | 28.18 | 17.71 |
| -8 | 420 | 35.34 | 14.17 |
| -5 | 504 | 42.50 | 11.81 |
| -2 | 588 | 49.66 | 10.12 |
| 1 | 672 | 56.82 | 8.85 |
| 3 | 756 | 63.98 | 7.87 |
| 5 | 840 | 71.14 | 7.08 |

**Table (4.1.2) Microcell radius, effective area and cell site density for different transmit power levels for the LI microcellular network.**

For a microcell radius of 10 blocks, the signal level will be above the threshold for about 2 blocks into the first NLS

street from the cell site. These blocks will result in significant interference to the adjacent cells of which these blocks belong. The number of these interfering blocks decreases as the cell radius decreases; for 5 block radius there are no such interfering blocks.

Comparisons of tables (4.1.1) and (4.1.2) reveal three significant facts. First, the radius of the I-type microcell is limited to six blocks (due to acceptable power levels) and that of the LI-type can be as high as ten blocks. Second, the power levels in the former are a minimum of 25 dB higher than for the latter for the same radius. And third, the cell site density is five times larger at 6 blocks radius in the LI-type network than in the I-type network. Thus for the same coverage areas, the I-type network uses a fifth of the cell sites the LI-type uses but at 25 dB more power requirement. The cost of the network depends on the number of cell sites and the connectivity between them. The factor of 5 for the LI-type network represents a significant increase in the number of cell sites over the I-type network; but the required power levels are very much lower and the cell sites can be made extremely small and cheap. It is not certain, at this time, however, that the cost savings from the cheaper cell sites can offset the cost of additional units and the additional connectivity costs; it is very doubtful that it will. So the I-type network may be the choice for the microcellular PCN.

Another factor that enhances the suitability of the I-type network is that continuity will be required in moving from outdoor to indoor locations. Since the coverage of the I microcell extends well into the NLS region, the penetration of buildings will be greater than for the L microcell and better transition regions will be provided.

As will be discussed in the next section, maximum adjacent cell interference to mobile occurs at intersections where four microcells meet. It is possible to arrange LI-type microcells in other configurations to eliminate this effect. Figure (4.1.4) shows one possible arrangement (for a 2 block radius microcell). Different configurations are obtained by displacing the cell sites in either the horizontal or vertical the grid lines in figure (4.1.2) so that four-way intersections are eliminated. The optimal layout criterion is to arrange the cell sites so that at any intersection, the difference in the distances to the two incident cell sites is not large. This is necessary, since if the difference in distances is large, the difference in received power may be large enough to force a hand-off even if the mobile is not changing cells. This is similar to the "ping-pong" effect that occurs at cell boundaries in cellular mobile radio. The mobile hands-off to the new cell site, then back to the old one and to the new one again, as the signal level varies with shadow fading. For this case illustrated, an intersection is either

equidistant from the two cell sites or is at the boundary of one cell; this is only possible for $n_c=2$.

Another way of minimizing four-way interference is to use M-type microcells. This however is effective only for small radii microcells. The cell site density for the network configuration is the same as that for the configuration in figure (4.1.3) because the cell site are merely rearranged.

The number of users the network can support is directly related to the cell site density. The cost also increases with the density. Therefore the system may use larger radii microcells to provide service in its early stages and as the user base increases, reduce the size of the cells to increase the cell site density. The cell radius reduction may also be carried out in areas with dense user population to provide increased support. This technique is termed cell splitting and is widely used in mobile cellular technology. Figure (4.1.5) shows a network as that in figure (4.1.1) with one of the microcells split into smaller microcells. The original microcell labelled A has a radius of eight blocks and is split into four smaller microcells B,C,D and E. One of the resulting microcells C is then split into four more microcells F,G,H and J. At each subdivision, the cell site of the cell being split is removed after the new cells are formed. For the I-type network, cell splitting is only possible when the radius of

the cell is a multiple of four blocks. This technique is not necessary for the L-type cells, as the type LM can be arranged in any size to fit a particular area.

## 4.2 Picocellular networks

In the previous section, picocells were investigated for typical high-rise building environments in the dense urban area. Under the assumptions of symmetric floor plan and isotropic conditions over the floor area, the picocells were determined to be circular in shape. It was seen that the radii of equal path loss decreased as the number of floors between the cell site and the portable increased. This means that the coverage area is unequal on the different floors, a potential problem in providing total coverage to a building. The typical high-rise can occupy up to a square block, which is about a 50m square region. The equal path loss contours as seen in table (3.2.1) show that up to 4 floors from the cell site can be adequately covered by 10 dBm and at -20 dBm transmit power only the next floor can be covered. At the height of the picocell, defined as the floor that has 25 % of the coverage area of the cell site floor, additional coverage has to be provided. This is not a trivial matter as is subsequently shown.

Figure (4.2.1) shows the cell site boundary on the farthest floor of the picocell; figure (3.2.3) shows the 3-dimensional representation of the picocell. If the zeroth floor is assumed to be entirely covered by the threshold path loss contour, that is the cell radius $r_c$ is greater that $w/\sqrt{2}$; then by the definition of the picocell height, the coverage radius on the farthest floor is $w/(2\sqrt{2})$. In the diagram, contour 0 represents the radius of coverage region on the zeroth floor and contour n the radius on the farthest floor, floor n. The square represents the floor area and the central shaded region, the coverage area provided by the cell site on the zeroth floor. Therefore, the area outside the central circle is the region that has to covered; this is by definition 75 % of the coverage area on the zeroth floor.

Four smaller (lower power) cells sites shown by A,B,C and D are used to illuminate the deficient region. Besides overlapping each other, the central region is completely overlapped by the boundaries of the new cell sites. Then for two reasons, the old and new cell sites have to use the same set of channels. First, since the old cell (region) is completely enclosed in the new cells, there will be high levels of interference to users in the old cell. Second, users in the old cell close to the cell boundary will strongly interfere with the new cell site; this is a case of the near-far problem in CDMA. As the diagram shows, the central region

boundary is very close to the new cell sites, therefore users communicating with the old cell site are received very strongly at the new site because they have to transmit at higher levels to reach their own cell site. The result is that different sets of channels cannot be used, unless the hand-off control system is sophisticated enough to detect the event and hand-off immediately to the new cell sites. If the same set of channel is used as suggested, then the overlapping region provide diversity paths for the communicating users.

From the above it is implicit that one high power and eight low power cell sites are required to cover (2n+1) floors. The high power transmitter provides coverage to zeroth and much of the (n-2)th floors from the zeroth floor; and at each end of the picocell, four low power cell sites provide coverage to the (n-1)th and nth floors. As an example, table (3.2.1) gives the height of the picocell as 4 floors for 10 dBm transmit power level in the picocell. Therefore, the latter covers nine floor using nine cell sites. The difference between this coverage and that of the microcellular networks is that no additional users are added to the system with the eight additional cell sites. Thus if no distinction is made of the cell sites, the picocellular network has a lower capacity than the microcelluar network. For a building with many more than nine floors, a number of these basic picocell units are used in such a manner that the farthest floors of each are distinct.

Figure (4.2.2) shows a vertical plane through a high-rise building illustrating the cell site layout. With the type of layout, adjacent picocells can use different channel sets. Since the cell boundaries are on different floors, the near-far problem mentioned earlier does is not significant then. However, adjacent cell interference still exists. If the maximum transmit power is -10 dB, the picocell covers three floors only. At -20 dB, even though the same number of floors are covered, the cell radius is down to less than half of the value used for the 10 dB case. This requires additional cell sites on the zeroth floor; these are added in the same manner as shown earlier for improved coverage on the farthest floor. The cell site density for the picocellular network may be defined as the ratio of the number of cell sites to the number of floors covered by the picocell. Table (4.2.1) gives typical cell site densities for the transmit power levels used in table (3.2.1).

| Maximum transmit power, dBm | Picocell radius, m | Picocell height, floors | Cell site density, per floor |
|---|---|---|---|
| 10.00 | >50 | 4 | 1.00 |
| 0.00 | >50 | 2 | 1.80 |
| -3.01 | >50 | 2 | 1.80 |
| -10.00 | 60 | 1 | 3.00 |
| -20.00 | 25 | 1 | 4.33 |

**Table (4.2.1) Cell site density in Picocellular network**

# 5 Adjacent Cell Interference in PCN

In a cellular CDMA system, the same carrier frequency and the same transmission bandwidth is used by all transceivers; so each user must interfere with every other user in a given cell. This is an intrinsic property of the Spread Spectrum systems and the resulting interference, termed multiple access interference (MAI), is usually treated as added noise. In appendix A, it is shown that the amount of interference to any user is directly proportional to the number of users in the cell, for given conditions. The effect of the interference on communication quality is derived in appendix B. The measures used to define the signal quality, the signal to noise ratio (SNR) and the bit error rate (BER), are shown to be directly related to the MAI. Thus, the number of users that the cell can support is dependent on the interference levels that can be tolerated.

When cells are configured into networks, it is impossible to confine the signals, from a given cell site or from the mobile users, within the cell's boundary. Furthermore, as a result of area topography or desired configurations, cells may overlap physically. Then, as outlined in the previous paragraph, the result of this interaction between cells is additional MAI. So in determining the maximum number of users per cell, not only the internal MAI, but the adjacent cells

MAI must be considered. Within a given cell, the users powers are controlled to the same level so the internal MAI is constant for all local users. The external MAI, however, depends on the relative positions of the adjacent cell sites and interfering mobiles to the given cell.

This section determines the adjacent cell interference at a given cell due to neighboring cells in the microcellular network. In arriving at the adjacent cell interference, the average interference is found. This is a function of the location of the adjacent cell sites and the probable locations of the mobiles. Two quantities are determined, the ***user reduction factor*** $\eta$ and the ***quality reduction factor*** $\gamma$. Both quantities are related to location probabilities in the microcell. If the adjacent cell interference is to be counteracted then this can be effected by reducing the permissible number of users by the factor $\eta$. It is to be noted that reduction in permissible transmit power cannot reduce interference since by assumption all users in the network must use the same transmit power. If design constraint forces the system to operate with the adjacent cell interference, then $\gamma$ expresses the fraction of the cell in which mobiles experience sub-quality communication.

To arrive at adjacent cell interference in both microcellular and picocellular networks, the interference in the uplink and in the downlink is found and the limiting interference in the system is taken as the larger of the two. The downlink is the channel from the cell site to the mobile. Thus the interference experienced is from adjacent cell sites to mobile. The uplink is from the mobile to cell site so the adjacent cell interference is from neighboring cell sites to the mobiles in a given cell. Both types of interference are dependent on the network geometry, the cell site positions and locations of the mobiles at any given time. It is easily seen that highest values of interference occur when the mobiles are at the cell boundaries.

## 5.1 Adjacent Cell Interference in Microcellular Networks

The adjacent cell interference scenario, in both uplink and downlink in the microcellular network[3], is depicted in figure (5.1.1). The diagram illustrates two cell sites $B_0$ and $B_i$ and two mobiles $m_0$ and $m_i$ in the cells covered by $B_0$ and $B_i$ respectively. $B_0$ and $m_0$ are may be taken as references and $B_i$ and $m_i$ as the interferers. $m_0$ is located at X, a distance of $r_0$ from $B_0$ and $m_i$ is at Y, a distance $r_i$ from $B_i$. The cells have radii $r_{c0}$ and $r_{ci}$ respectively. Let the controlled power in the

[3]The analysis in this section applies equally well to the picocellular network.

cells be $P_{c0}$ and $P_{ci}$ respectively. Then from appendix A, the interference at cell $B_0$ due to mobile $m_i$ at location Y is

$$U_i = \rho \frac{\mu(y_i)}{\mu(x_i)} P_{ci} \qquad (5.1.1)$$

and the interference to mobile $m_0$ at location X due to cell site $B_i$ is

$$D_i = \rho K_i \frac{\mu(x_0)}{\mu(x_{ci})} P_{ci}. \qquad (5.1.2)$$

$y_i$ is the distance between the $m_i$ and $B_0$ and $x_0$ is the distance between $B_i$ and $m_0$. $K_i$ is the number of users in cell i. $\rho$ is a constant that depends on the Spread Spectrum parameters involved in the signalling, and on the channel delay spread. The function $\mu$ is the average path power attenuation between mobile and cell site, as determined in Section 3. Since this function was shown to be at least a fourth power decreasing exponential function over large distances, the interference diminishes rapidly so that only the nearest neighboring cell sites contribute significantly to the total interference.

The locations of the mobiles in the cell are changing all the time, hence total interference is averaged over all possible locations. Then, if there are N nearest neighbors for any chosen cell site, the total interference, D, in the downlink is

$$D = \rho \int_{x_0} p(x_0) \sum_{i=1}^{N} K_i \frac{\mu(x_{0i})}{\mu(x_{ci})} P_{ci} \, dx_0 \qquad (5.1.3)$$

and the total interference, U, in the uplink is

$$U = \rho \sum_{i=1}^{M} \sum_{j=1}^{K_i} P_{ci} \int_{x_{ij}} p(x_{ij}) \frac{\mu(y_{ij})}{\mu(x_{ij})} \, dx_{ij}. \qquad (5.1.4)$$

p(x) is the probability of the mobile being at location X at a distance x from its cell site.

If the PCN is in a fairly isotropic environment, all the cells will use the same controlled transmit power and will support the same number of simultaneous users. Therefore in equations (5.1.3) and (5.1.4), D and U may be written as $D=n_D(\rho P_c K_c)$ and $U=n_U(\rho P_c K_c)$ respectively. $P_c$ is the controlled power, $K_c$ the number of simultaneous users and n is a function of the network. Let $I_0$ be the total interference in an isolated cell and $I_N$ be the total interference in a cell in the network. Then assuming the same controlled power, $I_0 \propto P_c K_0$ and $I_N \propto (P_c K_N + n P_c K_N)$, where $K_0$ and $K_N$ are the number of users in the isolated cell and in the network cell respectively. If the signal quality is to remain constant, then the interferences must be the same and

$$\begin{aligned} K_N &= \frac{1}{1+n} K_0 \\ &= \eta K_0. \end{aligned} \qquad (5.1.5)$$

Since n is greater than zero, $K_N$ is always less than $K_0$ and $\eta$ is called the user reduction factor.

The quality reduction factor $\gamma$ is determined by finding the fraction of the cell in which users experience significant interference. This factor is shown later to be a function of the location probabilities of the users in the cell.

Within a given cell, a mobile is subject to significant interference only at certain locations. The same is also true for interfering mobiles in adjacent cells; they can cause significant interference at the reference cell site from only certain locations within their local cells. This coupled with the fact that the cells are represented by regular geometric shapes allows the interference to be analyzed at discrete locations so replacing the integrals in equations (5.1.3) and (5.1.4) by discrete sums. The locations chosen for the analysis are the intersections and the mid-block positions. With this simplification, the location probabilities are given in terms of the probability of the mobile at an intersection and the probability of the mobile at mid-block. These probabilities are determined next.

## 5.2 Mobile Location Probabilities in microcells

The probabilities of locating a mobile on a given block position or at an intersection are denoted as $P_B$ and $P_I$ respectively. These quantities are directly related to the average times spent on a block or at an intersection and can

be derived by considering all paths in the microcell and averaging over these times.

Consider a path that includes n intersections. Then there are (n-1) segments (blocks) included in the path. Assume that path segments are homogeneous as are intersections and that all intersections are similar. Let $t_s$ be the time taken to travel a segment and $t_I$ be the time spent at the intersection, clearing time plus the waiting time. Then the total time, T, to travel the path is given by

$$\begin{aligned} T &= \sum_{i=1}^{n-1} t_{si} + t_{Ii} \\ &= \sum_{i=1}^{n-1} \frac{l_{si}}{v} + p_{Li} t_{Li} \end{aligned} \qquad (5.2.1)$$

where $P_{Li}$ is the probability of being stopped by the traffic lights at the ith intersection and $t_{Li}$ is the time spent at the intersection. In order to simplify the analysis, the traffic lights along a given path are considered independent of each other; heavy traffic congestion may justify this assumption. Thus $P_{Li} = 1/2$ for all intersections. Furthermore $t_{Li}$ is random and is assumed uniformly distributed over $T_{Li}$, the duration of the light. Therefore the average time for the path is

$$\bar{T} = \frac{1}{v} \sum_{i=1}^{n-1} l_{si} + \frac{n-1}{4} T_L. \qquad (5.2.2)$$

For m paths in the microcell,

$$\begin{aligned} T &= \sum_{k=1}^{m} T_k \\ &= \frac{1}{v} \sum_{k=1}^{m} \sum_{i=1}^{n_k-1} (l_s)_{ki} + \sum_{k=1}^{m} \frac{(n_k-1)}{4} T_L \\ &= T_s + T_I \end{aligned} \tag{5.2.3}$$

where $n_k$ is the number of segments in the k path.

Define $q_B$ = probability of being on a segment

$q_I$ = probability of being at an intersection

$P_B$ = probability of being at a particular segment

$P_I$ = probability of being at a particular intersection

then

$$q_s = \frac{T_s}{T} = \frac{4 \sum_{k=1}^{m} \sum_{i=1}^{n_k-1} (l_s)_{ki}}{4 \sum_{k=1}^{m} \sum_{i=1}^{n_k-2} (l_s)_{ki} + vT_L(n_k-1)} \tag{5.2.4}$$

and

$$p_s = \frac{L}{L_s} \frac{q_s}{N_s} \tag{5.2.5}$$

where L is the length of the given segment, $L_s$ is the standard segment length and $N_s$ is the number of standard segments.

$$q_I = \frac{vT_L \sum_{k=1}^{m} (n_k-1)}{4 \sum_{k=1}^{m} \sum_{i=1}^{(n_k-1)} (l_s)_{ki} + vT_L \sum_{k=1}^{m} (n_k-1)} \tag{5.2.6}$$

and

$$P_I = \frac{q_I}{N_I} \qquad (5.2.7)$$

where $N_I$ is the number of intersections.

For a homogeneous isotropic network, as assumed for the networks in section 4, any path can be chosen in the network to give the location probabilities. Therefore assuming a 1:1 block ratio microcell and a path over one block and 2 intersections, equations(5.2.4) and (5.2.6) reduce to

$$q_B = \frac{4l_s}{(4l_s + vT_L)} \qquad (5.2.8)$$

and

$$q_I = \frac{vT_L}{4l_s + vT_L} \qquad (5.2.9)$$

respectively. For a block ratio other than 1:1, $P_B$ and $P_I$ are arrived at as follows. Let $N_{B1}$ and $N_{I1}$ be the number of segment and intersections respectively for the network for block ratio **b=1** and $N_{Bb}$ and $N_{Ib}$ be the respective numbers for **b≠1**. Also let $P_{B1}$, $P_{I1}$, $P_{Bb}$ and $P_{Ib}$ be the respective probabilities, then

$$P_{Bb} = \frac{N_{B1}}{N_{Bb}} P_{B1} \qquad (5.2.10)$$

and

$$P_{Ib} = \frac{N_{I1}}{N_{Ib}} P_{I1}. \qquad (5.2.11)$$

The quantities $N_B$ and $N_I$ are determined in the analyses for the different network configurations subsequently. The previous analysis did not take into account the fact that some thoroughfares in an actual network may have unidirectional traffic flow. This was not necessary as the assumptions of homogeneity and isotropism predict similar conditions in each flow direction. Typical values of **v=10** mph, $T_L$**=45** seconds and $l_s$**=275** feet are used in equations (5.2.8) to (5.2.11).

## 5.3 Adjacent Cell Interference in I-type network

The Omni-I network is shown in figure (4.1.1). In this network, each microcell has eight nearest neighbors as shown for microcell 0. Four of these are adjacent on the sides and the other four are adjacent at the vertices. Figure (5.3.1) is a reproduction of figure (4.1.1) illustrating the region of significant interference. This region is a one block strip on either side of the cell boundary. The labels "0" and "1" show the locations where downlink interference exists. In regions "0", the interference is due to vertex adjacent cells and in region "1" to side adjacent cells. Locations "2" and "3" are regions that generate uplink interference. Locations "3" are in the vertex adjacent cells and locations "2" are in the side adjacent cells.

**Downlink Interference**

In the regions labelled "0", along each semi-axis, there are $n_c$ segments and ($n_c$-1) internal (from cell boundary) intersections receiving LOS interference from one vertex adjacent cell site. There is also one boundary intersection receiving LOS interference from one vertex and two side adjacent cells, and there is the central intersection receiving LOS interference from the four vertex adjacent cell. Therefore using equation (5.1.3), the average downlink interference, $D_0$, in region "0" is

$$D_0 = 4K_c P_c \left[ p_B \sum_{i=1}^{n_c} \frac{\mu(x_{B0i})}{\mu(r_c)} + p_I \sum_{i=1}^{n_c-1} \frac{\mu(x_{I0i})}{\mu(r_c)} \right] + 4(3p_I) K_c P_c + 4p_I K_c P_c \frac{\mu(2r_c)}{\mu(r_c)} \qquad (5.3.1)$$

where $K_c$ is the number of simultaneous users in the cell, $x_{B0i}$ and $x_{I0i}$ are the distances of the ith internal mid-block and intersection respectively from the vertex adjacent cell site. $p_I$ and $p_B$ are the probabilities of location at mid-block and intersection positions respectively.

In region "1", there are ($n_c$-1) intersections on the cell boundary, $n_c$ internal intersections and $n_c$ mid-block positions in each grid direction. Each intersection can receive interference power over two distinct paths from the interfering cell site.

Therefore, the average interference in region 1 is

$$D_1 = 4K_cP_c\left[2p_B\sum_{i=1}^{n_c}\frac{\mu(x_{B1i})}{\mu(r_c)} + 2p_I\sum_{i=1}^{n_c}\frac{\mu(x_{I1i})}{\mu(r_c)}\right] + 4[2(n_c-1)p_IK_cP_c]. \quad (5.3.2)$$

The total downlink interference $D=D_0+D_1$ can be written as $D=n_d(K_cP_c)$, where $n_d$ is

$$n_d = 4p_B\left[\sum_{i=1}^{n_c}\frac{\mu(x_{B0i})}{\mu(r_c)} + 2\sum_{i=1}^{n_c}\frac{\mu(x_{B1i})}{\mu(r_c)}\right] + 4p_I\left[\sum_{i=1}^{n_c-1}\frac{\mu(x_{I0i})}{\mu(r_c)} + 2\sum_{i=1}^{n_c}\frac{\mu(x_{I1i})}{\mu(r_c)} + \frac{\mu(2r_c)}{\mu(r_c)} + 2(n_c-1) + 3\right]. \quad (5.3.3)$$

The user reduction factor $\eta_D$ is then given by

$$\eta_D = \frac{K_c}{K_c+n_dK_c} = \frac{1}{1+n_d}. \quad (5.3.4)$$

The distances, x, are

$$x_{B0i}=(n_c+i-0.5)r_{BB} \quad x_{I0i}=(n_c+i)r_{BB}$$

$$x_{B1i}=(n_c+0.5)r_{BB} \quad x_{I1i}=(n_c+1)r_{BB}$$

where $r_{BB}$ is the length of a standard block.

**Uplink Interference**

Mobiles in the regions labelled "2" and "3" cause interference at the reference the cell site. In the region "3", there are $n_c$-1 intersections and $n_c$ mid-block positions in each of vertex adjacent cells and the boundary intersection is commonly shared by mobiles in the vertex adjacent cell and two side adjacent cells. There are $n_c$ mid-block positions in

each grid direction, $n_c$ internal intersections and ($n_c$-1) boundary intersections in the region "2". In a similar manner to the region "1", at each intersection, mobiles can cause interference along two distinct paths. From equation (5.1.4), the average interference caused by mobiles in the regions "3" is

$$U_3 = 4K_cP_c\left[p_B\sum_{i=1}^{n_c}\frac{\mu(y_{B3i})}{\mu(x_{B3i})} + p_I\sum_{i=1}^{n_c-1}\frac{\mu(y_{I3i})}{\mu(x_{I3i})}\right] + 4K_cP_c(3p_I) \qquad (5.3.5)$$

and for regions "2"

$$U_2 = 4K_cP_c\left[2p_B\sum_{i=1}^{n_c}\frac{\mu(y_{B2i})}{\mu(x_{B2i})} + 2p_I\sum_{i=1}^{n_c}\frac{\mu(y_{I2i})}{\mu(x_{I2i})}\right] + 4K_cP_c[2(n_c-1)p_I]. \qquad (5.3.6)$$

$y_{Bi}$ and $y_{Ii}$ are the distances from the ith mid-block and intersections, respectively, in the interfering cell to the cell site in the reference cell. $r_{Bi}$ and $r_{Ii}$ are the distances from these positions to the local cell site. The total uplink interference is now written as $U=U_2+U_2=n_uK_cP_c$, where $n_u$ is

$$n_u = 4p_B\left[\sum_{i=1}^{n_c}\frac{\mu(y_{B3i})}{\mu(x_{B3i})} + \sum_{i=1}^{n_c}\frac{\mu(y_{B2i})}{\mu(x_{B2i})}\right] + 4p_I\left[\sum_{i=1}^{n_c}2\frac{\mu(y_{I3i})}{\mu(x_{I3i})} + \sum_{i=1}^{n_c}2\frac{\mu(y_{I2i})}{\mu(x_{I2i})} + 2(n_c-1)+3\right]. \qquad (5.3.7)$$

The user reduction factor is then given by

$$\eta_U = \frac{K_c}{K_c + n_u K_c} = \frac{1}{1 + n_u} \qquad (5.3.8)$$

and the lengths, y, are

$$y_{2B1} = (n_c + 0.5)\, r_{BB} \qquad r_{2B1} = (n_c - 0.5)\, r_{BB}$$

$$y_{3B1} = (2n_c - i + 0.5)\, r_{BB} \qquad r_{3B1} = (i - 0.5)\, r_{BB}$$

$$y_{2I1} = (n_c + 1)\, r_{BB} \qquad r_{2I1} = (n_c - 1)\, r_{BB}$$

$$y_{3I1} = (2n_c - i)\, r_{BB} \qquad r_{3I1} = i r_{BB}$$

In appendix D, the number of intersections and blocks in the Omni-I network are derived and these are substituted in equations (5.2.5), (5.2.7), (5.2.8) and (5.2.9) to obtain the probabilities $p_B$ and $p_I$, given by

$$p_B = \frac{r_{BB}}{(4r_{BB} + vT_L)\, N_B} = \frac{r_{BB}}{n_c^2 (4r_{BB} + vT_L)} \qquad (5.3.9)$$

$$p_I = \frac{vT_I}{(4r_{BB} + vT_L)\, N_I} = \frac{vT_I}{(2n_c^2 + 2n_c + 1)\, (4r_{BB} + vT_L)}. \qquad (5.3.10)$$

The values of the user reduction factor are determined later for all the networks.

## 5.4 Interference in 4-Sector I-type Network

A 4-sector microcellular configuration is shown in figure (5.4.1). For the microcells in this network, the interference

analysis is a bit more involved, as there is adjacent sector interference, as well as adjacent cell interference. The figure illustrates two types of intersections, inter-sector and intra-sector. The inter-sector intersections are common to two or more adjacent sectors and the intra-sector intersections are exclusive to a given sector. Within the cell, the adjacent sectors interfere with each other only at intersections, as the signal due to interferers in mid-block position suffers double corner loss and is well below the level at intersections. Each sector is adjacent to one LOS sector from the one vertex adjacent cell and to one NLS sector from each of two side adjacent cells. As in figure (5.3.1), the downlink interference regions are labelled "0" and "1" for LOS and NLS conditions respectively, and the uplink regions "2" and "3". Since a sector is like a self-contained cell, the interference analysis can be carried out for each sector as for the Omni-I network.

**Downlink**

As shown in the figure, region "0" is subject to interference in the mid-block position and intersections, whilst in the region "1", the intersections and only blocks in one grid direction are subject to interference. It is also observed that, boundary inter-sector intersections in region "1" are subject to signal from 4 sectors, and intra-cell intersections receive signal from 2 sectors only.

The total interference per sector in region "0", $D_0$ is

$$D_0 = K_c P_c \left[ p_{sa} \sum_{i=1}^{n_c} \frac{\mu(x_{s0i})}{\mu(x_c)} + p_{sI} \sum_{i=1}^{n_c-1} \frac{\mu(x_{I0i})}{\mu(x_c)} \right] + K_c P_c (3 p_{sI}) \qquad (5.4.1)$$

and the average interference in regions "1" is

$$D_1 = K_c P_c \left[ 2 p_{sa} \sum_{i=1}^{n_c-1} \frac{\mu(x_{s1i})}{\mu(x_c)} + 2 p_{sI} \sum_{i=1}^{n_c-1} 2 \frac{\mu(x_{I1i})}{\mu(x_c)} \right] + K_c P_c p_{sI} [2(2)(n_c-1) + n_{1I}] \qquad (5.4.2)$$

where $n_{2I}$ is the number of internal intersections per sector. Defining D, as for the Omni-I network, as $D=D_0+D_1=n_d K_c P_c$, then $n_d$ is given by

$$\begin{aligned} n_d = {} & p_{sa} \left[ \sum_{i=1}^{n_c} \frac{\mu(x_{s0i})}{\mu(x_c)} + 2 \sum_{i=1}^{n_c-1} \frac{\mu(x_{s1i})}{\mu(x_c)} \right] \\ & + p_{sI} \left[ \sum_{i=1}^{n_c-1} \frac{\mu(x_{I0i})}{\mu(x_c)} + 2 \sum_{i=1}^{n_c-1} 2 \frac{\mu(x_{I1i})}{\mu(x_c)} \right] \\ & + p_{sI} [2(2)(n_c-1) + n_{1I} + 3] \end{aligned} \qquad (5.4.3)$$

and $\eta_d$ is given by equation (5.3.3).

**Uplink**

In the uplink, the analysis is again similar to that for the Omni-I network except for the additional interference due to internal inter-sector interaction. The LOS interference in region "3", $U_3$, due to the vertex adjacent cell is

$$U_3 = K_c P_c \left[ 2 p_s \sum_{i=1}^{n_c-1} \frac{\mu(y_{s3i})}{\mu(x_{s3i})} + 2 p_I \sum_{i=1}^{n_c-1} 2 \frac{\mu(y_{I3i})}{\mu(x_{I3i})} \right] + K_c P_c p_{sI} [2(2)(n_c-1) + n_{1I}] \qquad (5.4.4)$$

and the average interference in regions "2" is

$$U_2 = K_c P_c \left[ 2 p_B \sum_{i=1}^{n_c-1} \frac{\mu(y_{B2i})}{\mu(x_{B2i})} + 2 p_I \sum_{i=1}^{n_c-1} 2 \frac{\mu(y_{I2i})}{\mu(x_{I2i})} \right] + K_c P_c p_{BI} [2(2)(n_c-1) + n_{1I}] . \quad (5.4.5)$$

Writing U as $U = U_2 + U_2 = n_u K_c P_c$, $n_u$ is given by

$$\begin{aligned} n_u = {} & p_{BB} \left[ \sum_{i=1}^{n_c} \frac{\mu(y_{B2i})}{\mu(x_{B2i})} + 2 \sum_{i=1}^{n_c-1} \frac{\mu(y_{B2i})}{\mu(x_{B2i})} \right] \\ & + p_{BI} \left[ 2 \sum_{i=1}^{n_c-1} \frac{\mu(y_{I2i})}{\mu(x_{I2i})} + 2 \sum_{i=1}^{n_c-1} 2 \frac{\mu(y_{I2i})}{\mu(x_{I2i})} \right] \\ & + p_{BI} [2(2)(n_c-1) + n_{1I} + 3 . \end{aligned} \quad (5.4.6)$$

The distances x, y and r are given as in the analysis for the Omni-I network. The number of blocks, $N_{aB}$, and intersections, $N_{aI}$, per sector of the microcell are $n_c^2$ and $(n_c^2+1)$ respectively. Substituting in equations (5.2.5) and (5.2.7)

$$\begin{aligned} p_{BB} &= \frac{4 r_{BB}}{(4 r_{BB} + v T_L) N_{aB}} \\ &= \frac{4 r_{BB}}{n_c^2 (4 r_{BB} + v T_L)} \end{aligned} \quad (5.4.7)$$

and

$$\begin{aligned} p_I &= \frac{v T_I}{(4 r_{BB} + v T_L) N_{aI}} \\ &= \frac{v T_I}{(n_c^2+1)(4 r_{BB} + v T_L)} . \end{aligned} \quad (5.4.8)$$

## 5.5 Interference in LI-type network

Figure (5.5.1) shows the configuration of the LI-type network. In this network, each microcell has four "arms" with $n_c$ intersections and $n_c$ blocks per "arm". Only LOS conditions are assumed to exist in the network. The regions labelled "0" are where mobiles experience downlink interference and the regions labelled "3" are where they cause uplink interference. Because of the topology of the network, there are many more adjacent cells in this network than in the Omni-I network. For each "arm" of the microcell, there are three adjacent cells at the end intersection and two adjacent cells at each inner intersection. Only the end intersection adjacent cells can cause mid-block interference in the cell.

### Downlink

There are $n_c$ mid-block positions (per "arm") in locations "0", each subject to interference from the end adjacent cell and there are $(n_c-1)$ intersections that experience interference due to two side adjacent cells as well as the end adjacent cell. The cell site intersection experiences interference from the four end adjacent cells. Therefore total downlink interference is given by

$$D = 4K_c P_c \left[ p_B \sum_{i=1}^{n_c} \frac{\mu(x_{B0i})}{\mu(r_c)} + 2p_I \sum_{i=1}^{n_c-1} \frac{\mu(x_{I0i})}{\mu(r_c)} \right] + 4K_c P_c p_I \left[ (n_c-1) + \frac{\mu(2r_c)}{\mu(r_c)} + 3 \right] \qquad (5.5.1)$$

and $n_d$, as defined previously, is given by

$$n_d = 4\left[p_B\sum_{i=1}^{n_c}\frac{\mu(x_{Bdi})}{\mu(r_c)} + 2p_I\sum_{i=1}^{n_c}\frac{\mu(x_{Idi})}{\mu(r_c)}\right] + p_I\left[(n_c-1) + \frac{\mu(2r_c)}{\mu(r_c)} + 3\right]. \qquad (5.5.2)$$

**Uplink**

In the uplink, mobiles in the end adjacent cells and at the internal intersections interfere with the reference cell site. There are $n_c$ mid-block positions and intersections in the end adjacent cell and $(n_c-1)$ internal intersections. So the total uplink interference is

$$U = 4K_cP_c\left[p_B\sum_{i=1}^{n_c}\frac{\mu(y_{Bui})}{\mu(x_{Bui})} + 2p_I\sum_{i=1}^{n_c}\frac{\mu(y_{Iui})}{\mu(x_{Iui})}\right] + 4K_cP_cp_I[(n_c-1)+3] \qquad (5.5.3)$$

and $n_u$ is given by

$$n_u = 4\left[p_B\sum_{i=1}^{n_c}\frac{\mu(y_{Bui})}{\mu(x_{Bui})} + 2p_I\sum_{i=1}^{n_c-1}\frac{\mu(y_{Iui})}{\mu(x_{Iui})}\right] + p_I[(n_c-1)+3]. \qquad (5.5.4)$$

x, y and r are defined as for the other networks.

There are $4n_c$ blocks and $(4n_c+1)$ intersections in the microcell. Substituting these for $N_B$ and $N_I$ in equations (5.2.5) and (5.2.7) respectively, give the location probabilities $p_B$ and $p_I$ as

$$p_B = \frac{4r_{BB}}{(4r_{BB} + vT_L)\, N_B} = \frac{r_{BB}}{n_c (4r_{BB} + vT_L)} \tag{5.5.5}$$

and

$$p_I = \frac{vT_I}{(4r_{BB} + vT_L)\, N_I} = \frac{vT_I}{(4n_c+1)\,(4r_{BB} + vT_L)}. \tag{5.5.6}$$

## 5.6 User Reduction Factors for Microcellular Networks

The relations for the location probabilities $p_S$ and $p_I$, the network constants $n_d$ and $n_u$, and the user reduction factors $\eta_D$ and $\eta_U$ have been derived in Sections 5.3-5.5 for the various networks. Substituting the expressions for the location probabilities into the equations for the network constants and evaluating, the values of the latter are found and are used to obtain the user reduction factors. Figures (5.6.1), (5.6.2) and (5.6.3) show plots of the these factors for the Omni-I, the 4-sector I and the LI networks. The user reduction factor $\eta = \max(\eta_D, \eta_U)$ versus cell radius for these networks are given in table (5.6.1).

| Microcell radius, m | User reduction factor | | |
|---|---|---|---|
| | Omni-I network | 4-sector I network | LI network |
| 168 | 0.460 | 0.499 | 0.440 |
| 252 | 0.519 | 0.509 | 0.453 |
| 335 | 0.566 | 0.520 | 0.460 |
| 419 | 0.604 | 0.532 | 0.464 |
| 503 | 0.636 | 0.541 | 0.466 |
| 587 | | | 0.468 |
| 671 | | | 0.470 |

**Table (5.6.1) User reduction factor for three types of microcellular networks.**

## 5.7 Quality Reduction Factor in microcellular networks

If the number of simultaneous users in the microcell is close to the maximum permissible value, then the user reduction factor must be applied to maintain the communication quality constant. Specifically, the maximum permissible number in the network is $\eta N_0$, where $N_0$ is the capacity of the isolated microcell and $\eta$ is the user reduction factor. If the number of users cannot be reduced due to say capacity constraint, then the communication quality in the microcellular network will be reduced in regions subject to adjacent cell (sector) interference.

The quality reduction factor $\gamma$ is defined as the fraction of the cell in which the mobile experiences significant adjacent cell interference. The locations contributing to this factor have been denoted by regions "0" and "1" for downlink communication in the networks. $\gamma$ is then found as ratio of the number of intersections and blocks in these regions to the total in the microcell. Therefore

$$\gamma = \frac{n_I + n_B}{N_I + N_B} \qquad (5.7.1)$$

where $n_I$ and $n_B$ are the number of intersections and blocks in the interference regions and $N_I$ and $N_B$ are the total number of intersections and blocks respectively.

For the Omni-I network $n_I$ and $n_B$ are given by $[12(n_c-1)+1]$ and $[4(3n_c-2)]$ and $N_I$ and $N_B$ are $[2n_c(n_c+1)+1]$ and $4n_c^2$ respectively and $\gamma_I$ is

$$\gamma_I = \frac{24n_c-19}{6n_c^2+2n_c+1}. \qquad (5.7.2)$$

For the 4-I network $n_I$ and $n_B$ are $(n_c^2+1)$ and $(3n_c-2)$ and $N_I$ and $N_B$ are $(n_c^2+1)$ and $n_c^2$ are respectively so $\gamma_4$ is

$$\gamma_4 = \frac{n_c^2+3n_c-1}{2n_c^2+1}. \qquad (5.7.3)$$

In the LI network all the blocks and intersections are subject to significant interference; therefore $\gamma_L$ is 1.0.

Figure (5.7.1) shows plots of $\gamma$ versus microcell radius and table (5.7.1) gives the values as a function of microcell radius for the above networks.

| Microcell radius, m | Quality reduction factor | | |
|---|---|---|---|
| | Omni-I network | 4-I network | LI network |
| 168 | 1.000 | 1.000 | 1.000 |
| 252 | 0.869 | 0.895 | 1.000 |
| 335 | 0.733 | 0.818 | 1.000 |
| 419 | 0.627 | 0.765 | 1.000 |
| 503 | 0.546 | 0.726 | 1.000 |
| 587 | 0.482 | 0.697 | 1.000 |
| 671 | 0.431 | 0.674 | 1.000 |

**Table (5.7.1) Quality reduction factor for different microcellular networks as function of cell radius**

# 6 Adjacent Cell Interference in Picocellular Network

In Section 1 two specific modes of employing picocells were discussed. In the first mode picocells are used as extensions of a surrounding microcell, and in the second as self-contained distinct cells. To minimize poorly covered areas picocells invariably overlap. If extension picocells are employed there is little increase in interference in the network; in fact it was observed in Section 1 that there is a distinct advantage gained from the overlap (possible diversity gain). However, if distinct picocells are used, overlapping leads to significant increase in adjacent cell interference reducing the maximum permissible number of simultaneous users in the picocell. The amount of interference depends on the overlap area of the picocells so there is a trade-off in providing adequate coverage and the interference level tolerated. Improving coverage results in more overlaps and hence more interference. Adjacent cell interference is now evaluated by determining the overlap area for distinct picocells.

The coverage region of a typical picocell was determined in Section 3 and is shown in figure (3.2.3). The areas covered on each floor are circular with decreasing radius from the cell site. The radius of the boundary contour on the cell site

floor, $r_0$, is defined as the radius of the cell. Let $r_i$ and $A_{ci}$ be the radius and area of coverage region on the ith floor, then $A_{ci}=\pi r_i^2$. Normalizing with respect to the coverage area on the zeroth floor, the fractional coverage on the ith floor, $\sigma_{ci}$ is

$$\sigma_{ci} = \frac{A_{ci}}{A_{co}} = \frac{r_i^2}{r_0^2}. \qquad (6.1)$$

The height of the picocell is defined as the floor on which $\sigma_{ci}$ is 0.25. If the transmit power is carefully selected, then one cell site can cover a number of floors on either side and on each of the boundary floors four low power cell sites can provide coverage.

Because the radius $r_0$ can be fairly large for small transmit powers and because the width of the buildings are limited by the street block size, more than one cell site will rarely be required on the zeroth floor. If the scenario, however, requires more than one, then there will be overlap of the contours on each coverage floor, resulting in adjacent cell interference. Figure (6.1) shows a worst case scenario in which a given cell site is adjacent to four cell sites on the zeroth floor. The regions labelled A are exclusive to one picocell and are relatively free of adjacent cell interference, and the shaded regions, B, are intersection (overlap) areas and are subject to significant interference from an adjacent picocell. If $A_0$ is the maximum coverage area

and $A_I$ the area of the intersection region, then $A_0=\pi r_0^2$ and $A_I=0.25(\pi-2)r_0^2$.

Figure (6.2) shows the coverage areas on the farthest floor from the zeroth floor. As discussed in Section 4, an additional four low power cell sites are used to cover the same area as covered by the main cell site. Again the adjacent cell intersection regions are shown shaded and labelled B. In contrast to the zeroth floor, not all the intersection regions are adjacent cell regions and the ratio of the total interference area to the total area is half the value for the zeroth floor.

In arriving at the adjacent cell interference in the network, the assumption is made that the portable users are uniformly distributed over the floors in the building. The interference generated by users in a particular region then is proportional to the area of the region. The interference is investigated here as for the microcellular network. The downlink is considered, followed by the uplink and interference reduction factors are derived. The analysis is carried out in much the same manner as for the microcellular network.

Figure (6.3) shows the worst case adjacent cells scenario. There are eight nearest neighbors to each picocell.

If the picocell is considered to circumscribe a rectangle, as shown, then four of the neighbors are on the diagonals (vertex adjacent cells) and the other four are on the side bisectors (side adjacent cells). Following the approach for the microcellular networks, the interferers will be considered to be concentrated at the mid-points of the sides and the vertices of the rectangle. These will be referred to as vertex interferers and side interferers. In the downlink, as well as for the uplink, regions are considered to be influenced by a particular cell only if adjacent to that cell. Figure (6.4) shows the interference scenario for the farthest floor. The arrangement of interfering cell sites is the same as in figure (6.3) except that coverage area of each cell consists of four overlapping regions. The intervening floors between the zeroth and the farthest floor are considered to be laid out as the zeroth floor.

## 6.1 Downlink Interference in Picocells

In figure (6.3), portables are shown at mid-side and vertex positions. At the mid-side position, the portable is adjacent to five cell sites. One of these shares an overlap region with the reference cell site and the other four are in cells adjacent at vertices and are equidistant from the mid-side position. At the vertex position, the portable is equidistant from three adjacent cell sites, however this

region is comparatively smaller than the mid-side position and is ignored in subsequent analysis. The average interference experienced in the downlink on the zeroth floor, is

$$P_{D0} = 4K_c P_c p_s \left[1 + 4\frac{\mu(x_{s2})}{\mu(r_c)}\right] \qquad (6.1.1)$$

where as in Section 5, $K_c$ and $P_c$ are the number of users in the simultaneous users and the controlled transmit power in the cell respectively. $p_s$ is the location probability at the mid-side positions; this is directly proportional to the area of the region containing the position. $r_{s2}$ is the distance from the equidistant interfering cell sites to the portable at mid-side position and $r_c$ is the radius of the picocell.

On the farthest floor, as shown in figure (6.4), there are eight mid-side positions. For each of these, there are four adjacent interfering cell sites, one of which shares an overlap region with the reference cell site and the other three are in cells adjacent at vertices only. The average adjacent cell interference, $P_{Dn}$, experienced on this floor is

$$P_{Dn} = 8K_c P_c p_{sn} \left[1 + 3\frac{\mu(x_{sn2})}{\mu(r_n)}\right] \qquad (6.1.2)$$

where $r_n$ is the cell radius on this floor and $r_{s2}$ is the distance from the equidistant interferer to the mid-side position. $p_{sn}$ is the location probability at mid-side position on this floor.

The interference reduction factor, $\eta_D$, as defined in Section 5, is given by

$$\eta_D = \frac{1}{1+n_D}. \qquad (6.1.3)$$

Assuming that the interference scenario on the intermediate floors is similar to that on the zeroth floor, then equation (6.1.1) applies to (2n-1) floors and equation (6.1.2) to two floor. Therefore $n_D$ is given by

$$n_D = 4(2n-1)p_s\left[1+4\frac{\mu(x_{s2})}{\mu(x_o)}\right]+16p_{ss}\left[1+3\frac{\mu(x_{ss2})}{\mu(x_s)}\right]. \qquad (6.1.4)$$

## 6.2 Uplink Interference in Picocells

In the uplink, as in the downlink, the bulk of the interference arise from the overlap regions. On the zeroth floor, each cell site gets interfered with by portables from twelve mid-side positions. Four of the interfering mid-side positions are common to the given cell and the remaining eight are in adjacent cells only. This situation is illustrated in figure (6.3). The average uplink interference on the zeroth floor, $P_{U0}$, then is

$$P_{U0} = 4K_oP_op_s\left[1(0.5)+2\frac{\mu(y_{s2})}{\mu(x_o)}\right]. \qquad (6.2.1)$$

Figure (6.4) illustrates the scenario on the farthest floor. Each cell site is interfered with by portables from eight mid-

side positions, four of which are in the overlap region of the cell and the other four in adjacent cells only. The average uplink interference experienced, $P_{Un}$, is

$$P_{Un} = 4K_c P_o p_{vn}\left[4(0.5) + 4\frac{\mu(y_{sm2})}{\mu(r_n)}\right] \qquad (6.2.2)$$

where $p_{vn}$ and $p_{sn}$ are the vertex and mid-side positions location probabilities. $y_{sn}$ is the distance from the mid-side position to the reference cell site and $r_n$ is the radius of the cell site on the farthest floor.

The user reduction factor for the uplink $\eta_U$ is then given by equation (6.1.3), with the subscript U substituted for D. The number, $n_U$, from the equation is given by

$$n_U = 4(2n-1)p_s\left[0.5 + 2\frac{\mu(y_{s2})}{\mu(r_c)}\right] + 8p_{sn}\left[2 + 4\frac{\mu(y_{sm2})}{\mu(r_n)}\right]. \qquad (6.2.3)$$

## 6.3 Location Probabilities in Picocells

The location probabilities are proportional to the fractional areas of the intersection regions. The interference positions M and V are identical and are assumed to be in a region of radius $0.1r_0$. The total area of the picocell, $A_c$ is

$$A_c = r_0^2[(2n-1)\pi + 4] \qquad (6.3.1)$$

and the areas of the interference regions on the zeroth and the farthest floor are $A_{I0}=0.25(\pi-2)r_0^2$ and $A_{In}=0.0625(\pi-2)r_0^2$

respectively. The location probabilities are given by

$$p_s = \sigma_s = \frac{0.25(\pi-2)}{(2n-1)\pi+4} \qquad (6.3.2)$$

$$p_{sn} = \sigma_{sn} = \frac{0.0625(\pi-2)}{(2n-1)\pi+4} \qquad (6.3.3)$$

for the zeroth floor mid-side and the farthest floor mid-side positions respectively.

## 6.4 User and Quality Reduction factors in Picocells

Substituting for the location probabilities in the equations for $n_D$ and $n_D$, the user reduction factors are calculated. Table (6.4.1) gives the values for $\eta = \max(\eta_D, \eta_u)$ as a function of picocell radius.

| Picocell radius, m | User reduction factor |
|---|---|
| 20 | 0.31 |
| 30 | 0.31 |
| 40 | 0.40 |
| 50 | 0.45 |
| 60 | 0.48 |

**Table (6.4.1) User reduction factor as a function of picocell radii**

The quality reduction factor $\gamma$ is simply the fractional areas subjected to interference in the picocellular case.

Therefore $\gamma$ is given by

$$\gamma = 4(2n-1)p_s + 16p_m. \qquad (6.4.1)$$

Table (6.4.2) gives the quality reduction factor as a function of picocell radius.

| Picocell radius, m | Quality reduction factor |
|---|---|
| 20 | 0.320 |
| 30 | 0.320 |
| 40 | 0.340 |
| 50 | 0.348 |
| 60 | 0.351 |

**Table (6.4.2) Quality reduction factor as a function of picocell radii**

It is to be noted that in addition to the interference regions there are fringe reception areas on the intermediate floors, so that even if the number of users are reduced to improve overall communication quality, there will still be areas with poor reception. Improving the reception in the fringe areas results in a trade-off. The coverage areas on the intermediate floors can be increased by raising the power levels, but this will result in an increase in the overlap areas, increasing adjacent cell interference. Additional cell sites, as a solution, is not acceptable, so lower quality reception in the fringe areas must be tolerated.

# Conclusions

This dissertation explored the physical planning required for establishing a PCN in a typical dense urban environment. The primary goals of the underlying research were: (1), to determine suitable criteria for cell site placement in the service area; (2), to find cell site density in the network and determine the factors that influenced this quantity; (3), to quantify the effects of adjacent cells in the network; and (4), to identify general, easily obtained parameters, that defined cellular layouts, thus minimizing the need for extensive in site measurements for future cell planning work. In fulfilling these goals, much experimental work was conducted to investigate the topography of the PCN environment and its effect on signals propagating within it. This resulted in a clear understanding of the requirements of the system that proved very useful in arriving at the cellular configurations and criteria presented in the work.

From the analysis of the physical channels, the empirical formulas extracted to describe the signal propagation were indeed found to depend on simple parameters that could easily be obtained. The main parameter that influenced the propagation characteristics in the outdoor environment was the height of the cell site antenna. For indoor locations, the propagation loss through the floors of the building was seen

to be the critical parameter.

The physical characteristics of microcells and picocells were determined from the empirical models. It was seen that microcells were basically square regions of maximum radius ( along diagonal) of about 500m in the street grid. In the indoor environment, picocells were seen to be approximately circular regions on each floor and covered about 4 floors on either side of the floor with the cell site.

Different configurations of microcells were examined and three fairly representative types were analyzed. These were named the Omni-I type, the 4-sector I type and the LI type networks. The Omni-I network consisted of a tessellation of the basic square shaped cells in which there was both line of sight (LOS) and non-line of sight (NLS) propagation. The 4-sector I network was seen to be an Omni-I network in which the microcells were divided into four adjacent sectors. The LI network consisted of cells in which the propagation was predominantly LOS. The cell site densities were found for the networks and it was seen that the Omni-I network had the lowest density and the LI the highest. The cell site density was calculated to be about 2.00/km at a radius of 500m for the Omni-I network and about 11.80/km for the LI network with the same cell radius. However, the LI network required about 25 dB less transmit power than the Omni-I network. For the indoor

locations, it was shown that in the typical high rise office building, only one configuration of picocells was necessary. The cell site density for this configuration was a function transmit power and was about 1.00/floor at 10 dBm to about 4.33/floor at -20 dBm.

The adjacent cell interference existing in the networks were analyzed and two interference criteria were defined, the user reduction factor (URF) and the quality reduction factor (QRF). The URF factor was used to account for the effect of the interference by reducing the maximum number of simultaneous users each microcell could support. The values of the URF ranged between 0.45 and 0.65, which meant that with adjacent cell interference, the number of simultaneous users dropped to between 45 and 65 percent of the value for the isolated cell. The Omni-I network had the highest URF and the LI network, the lowest. The number of simultaneous users in the isolated microcell was determined to be approximately 387. This, however, was an upper bound. As the processing gain of the Spread Spectrum decreased, then this number decreased also.

The QRF was derived to express the fraction of the cell that was subject to significant interference if it was loaded to its isolated maximum capacity. The LI network had a 100 percent QRF independent of cell radius. This meant that the at

maximum capacity everywhere in the cell experienced adjacent cell interference. The Omni-I network had a 100 percent QRF at 168 m radius and 43 percent at 671 m radius. The QRF values were 100 percent at 168 m and 67 percent at 671 m for the 4-I network. So the Omni-I network is less susceptible to interference than the other networks. In the picocellular network, the URF ranged between 31 percent for 20 m cell radius to about 48 percent for 60 m cell radius. The QRF was 31 percent at 20 m and 48 percent at 60 m radius.

The analyses have shown that a PCN system could be configured in a dense urban area using the Omni-I microcells. No advantage was found to be gained from the use of the sectored microcell network. The number of available channels (simultaneous users), even with a reduction factor of 40 percent, is conceivably more than that required to service the area. Therefore, the recommendation of this work is that the network with omnidirectional cell sites located at street intersections, Omni-I network, be used for a PCN in a dense urban environment.

## Future Work

This work, although having provided significant tools for the physical design of a PCN, is not sufficient in addressing all the design issues involved in such a system. However, it has laid a good foundation for another important area, teletraffic in PCN. This area is concerned primarily with hand-off issues in the network. Therefore a logical extension of this work is to determine the effect of the various network configurations on the teletraffic variables such as blocking probability, hand-off failure rate and channel holding time.

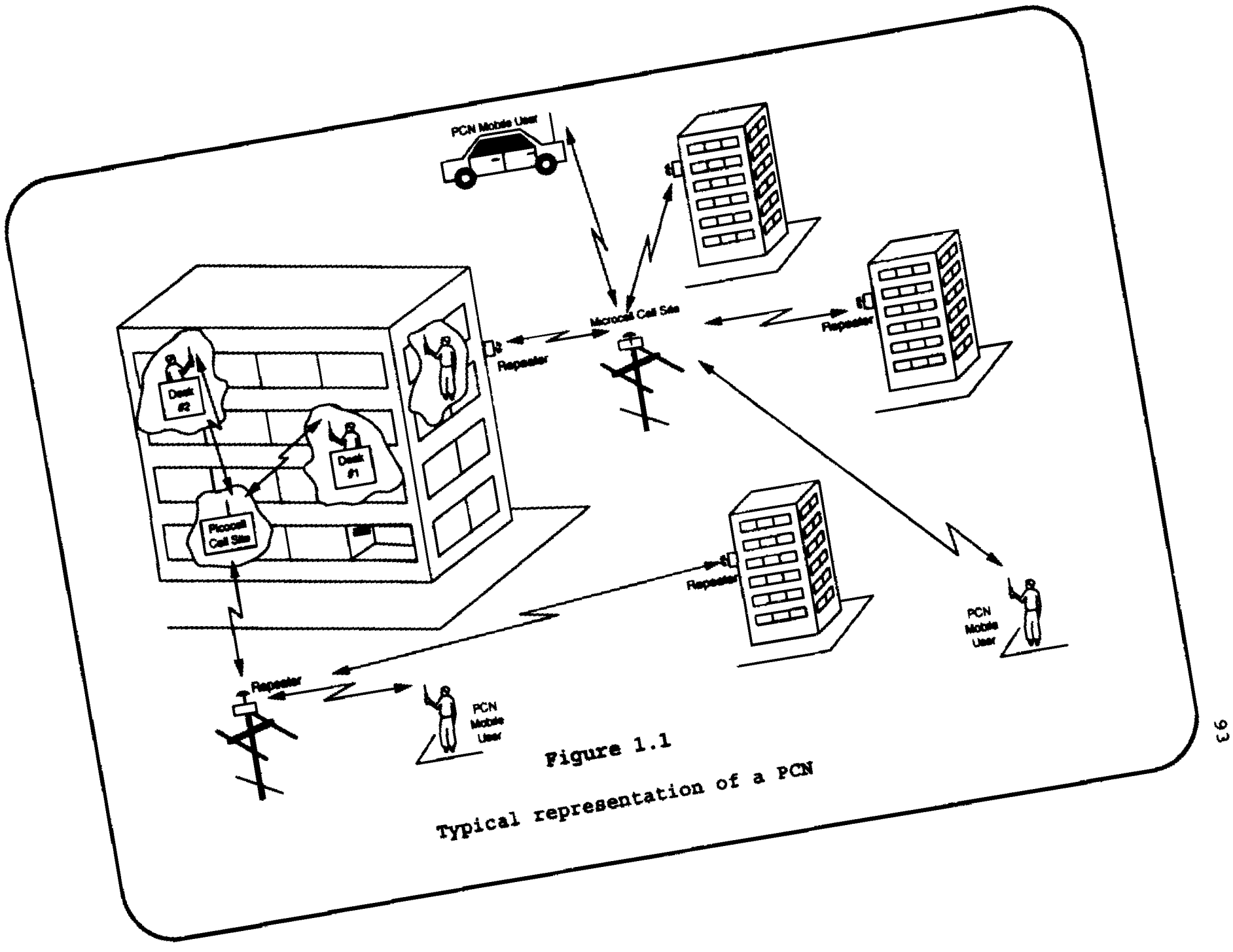


**Figure 1.1**

**Typical representation of a PCN**

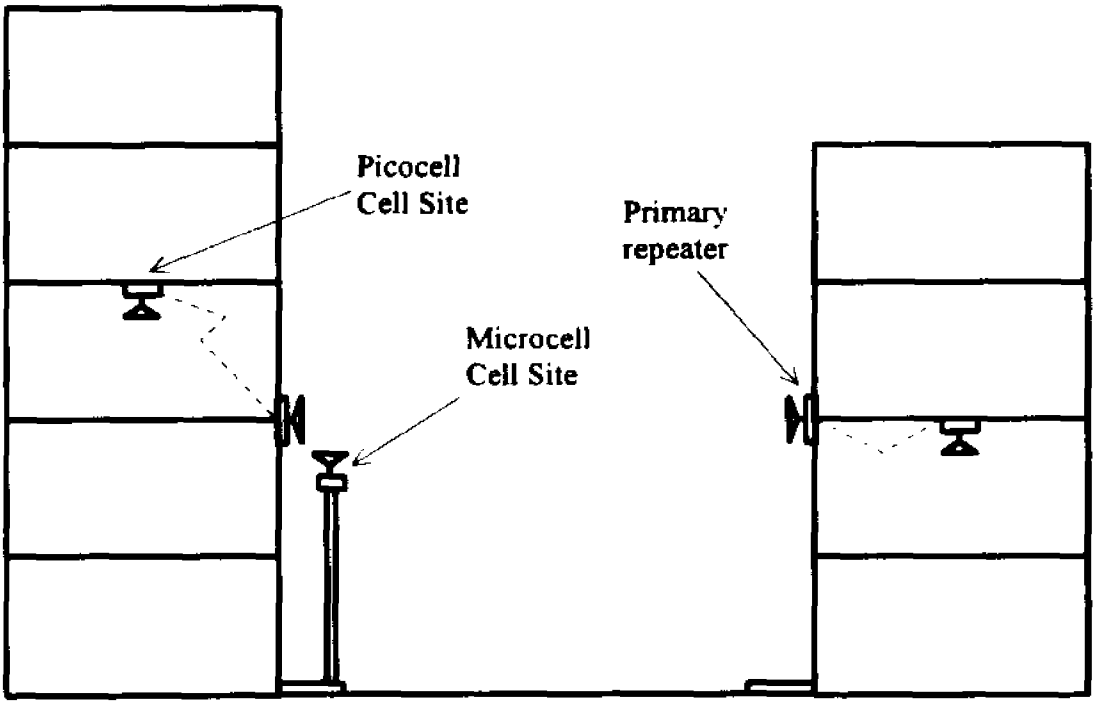


**Figure 1.2**

**Picocells relaying signal from Microcell**

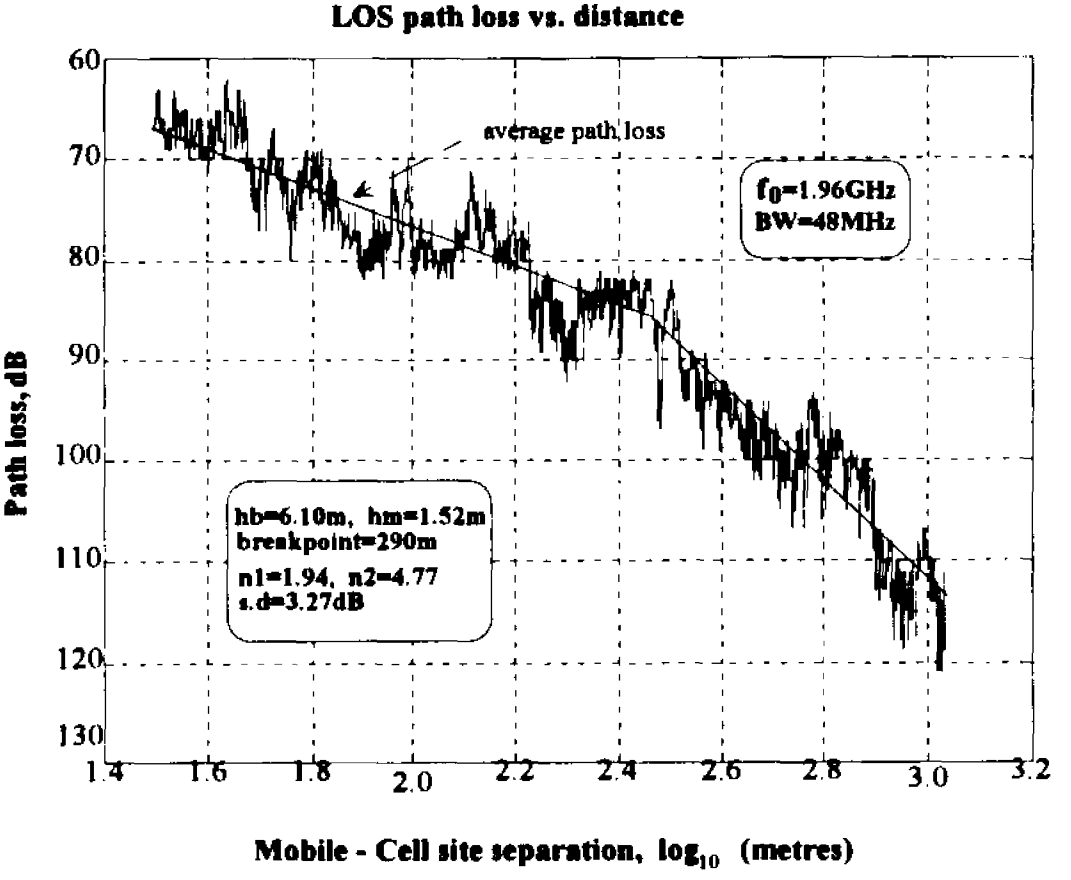


**Figure (2.1.1)**

**Average path loss over typical LOS run**

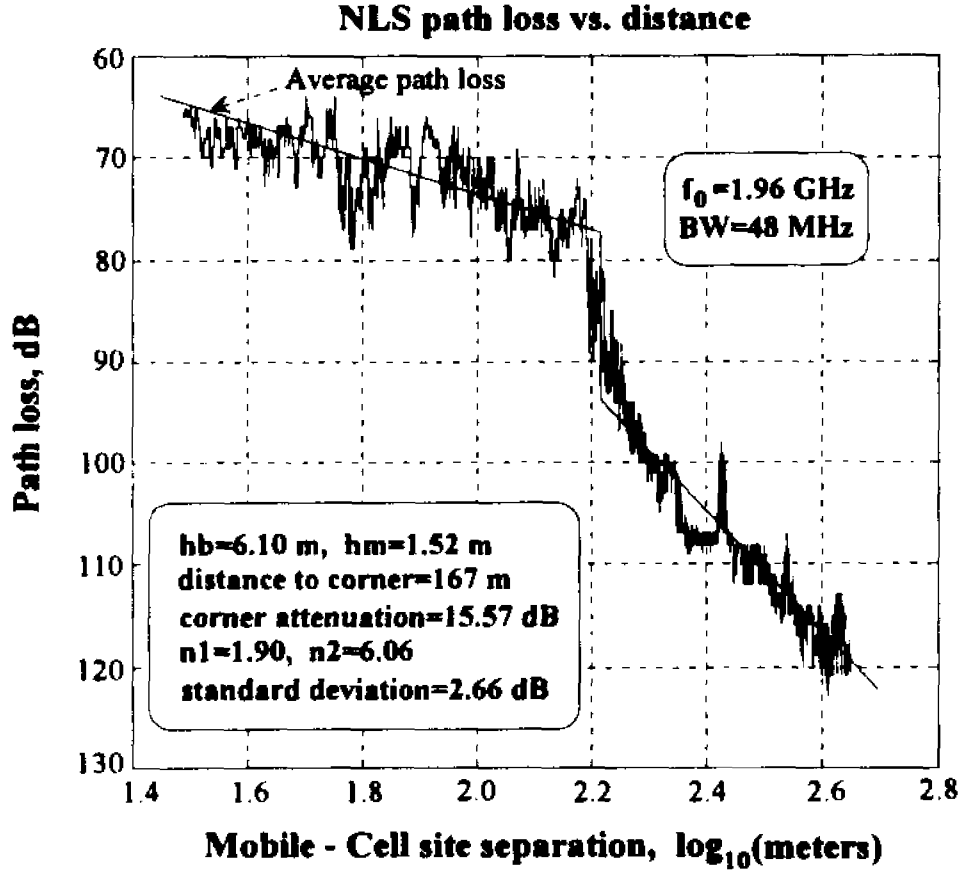


**Figure (2.1.2)**

**Average propagation path loss over run with NLS segment**

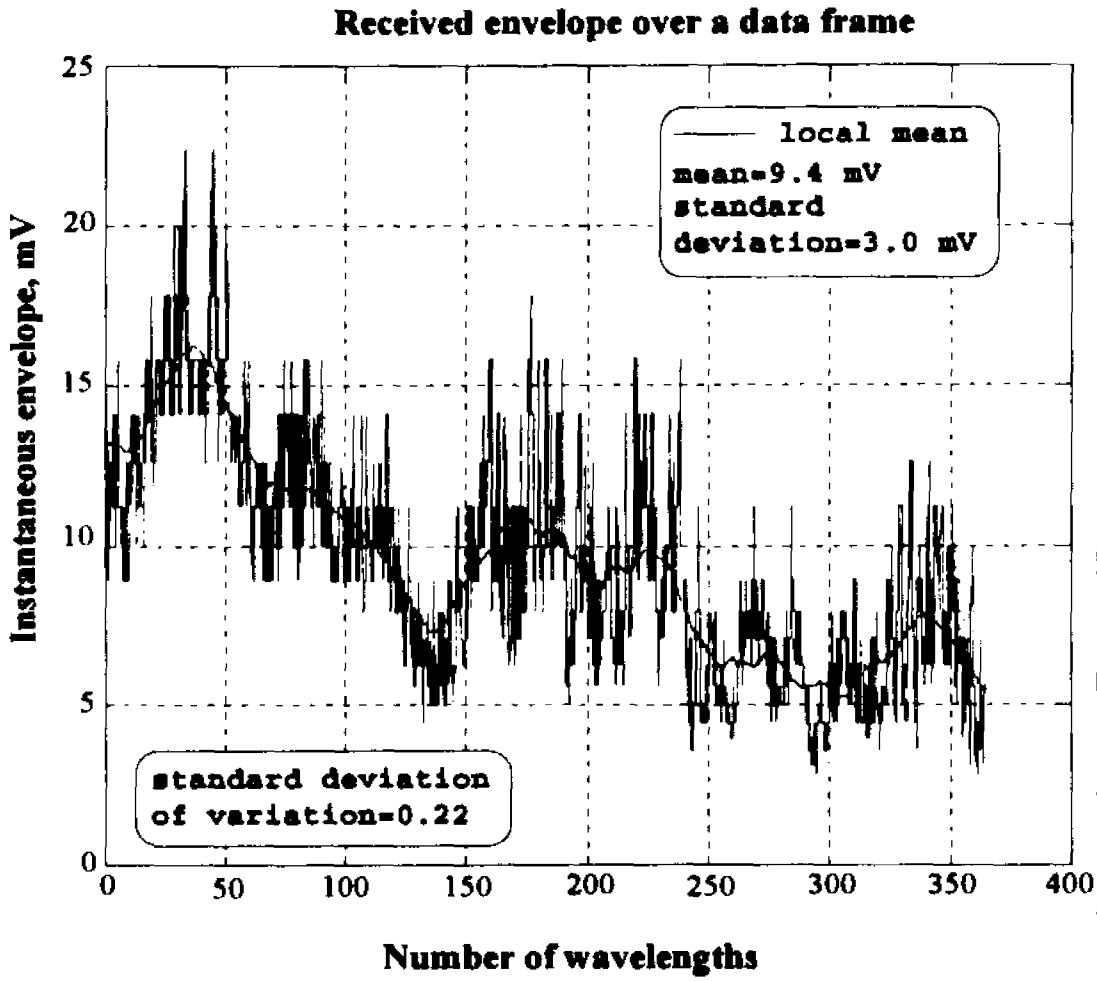


**Figure (2.1.3)**

**Received signal envelope over 60m section of run**

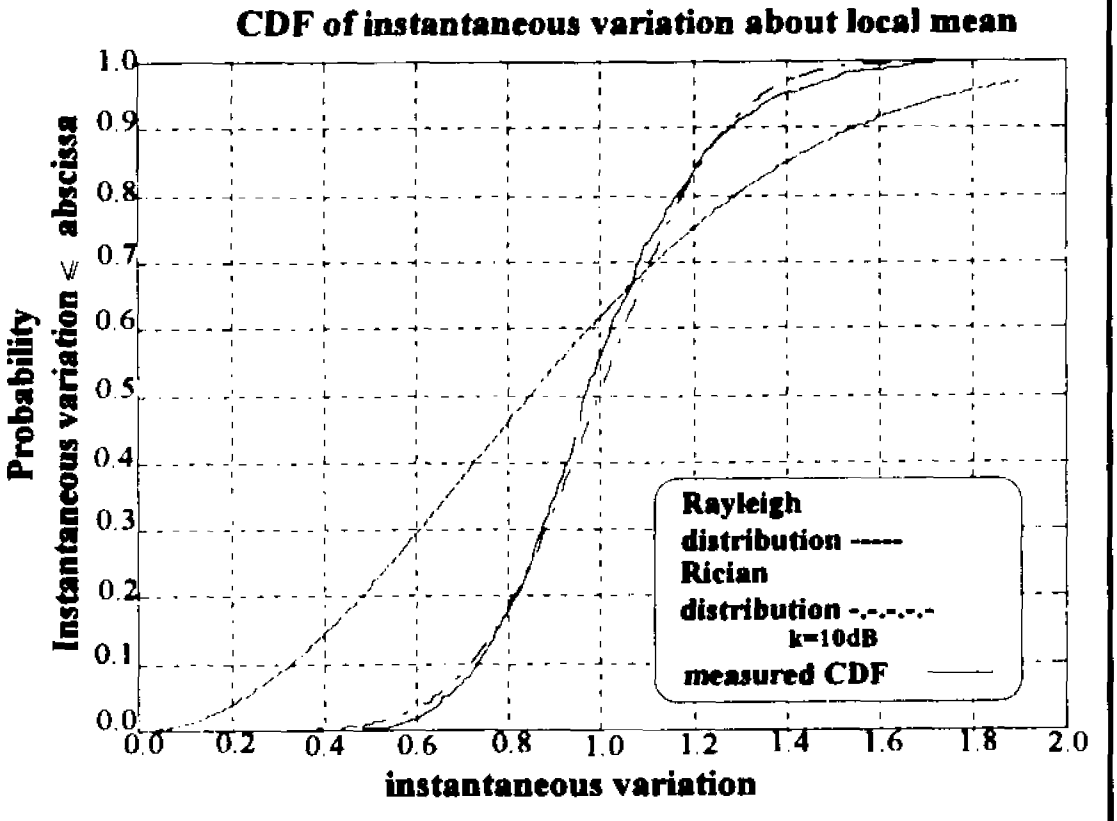


**Figure (2.1.4)**

Cumulative distribution function of instantaneous variation of received envelope about local mean

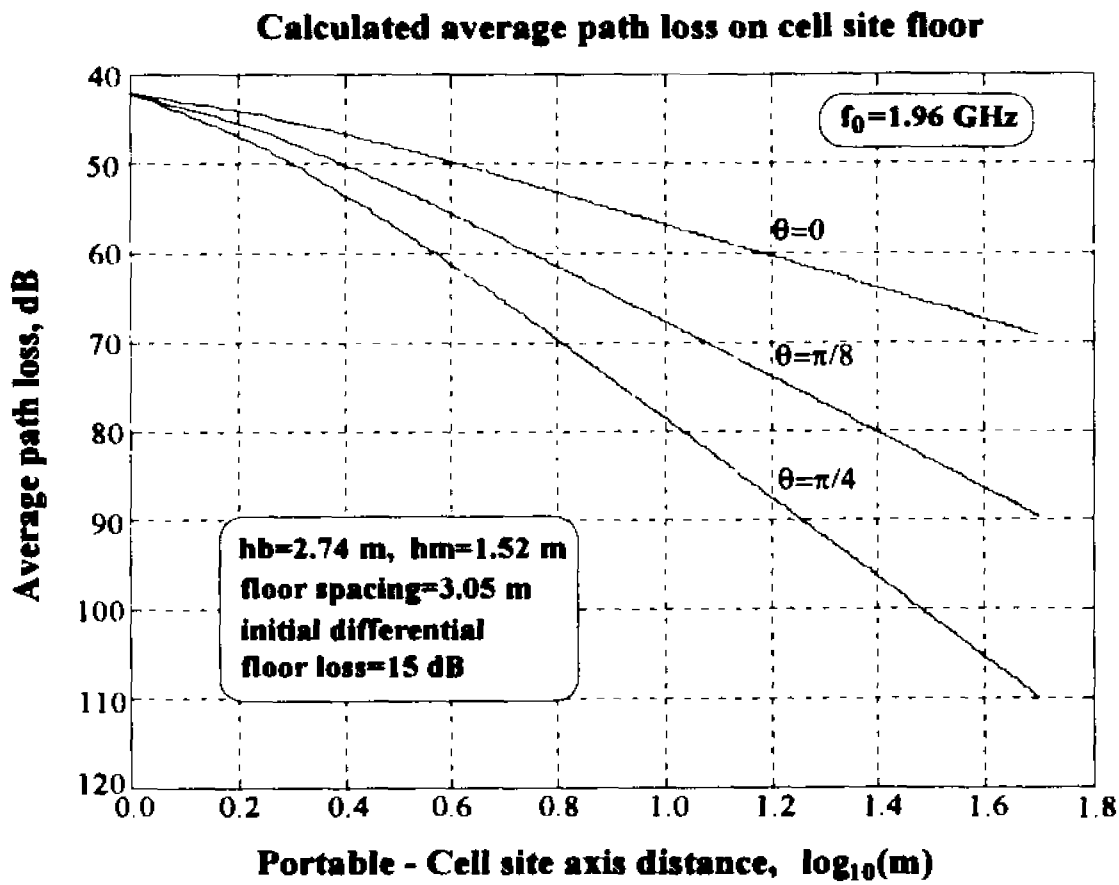


**Figure (2.2.1)**

**Calculated average path loss on cell site floor in typical office building**

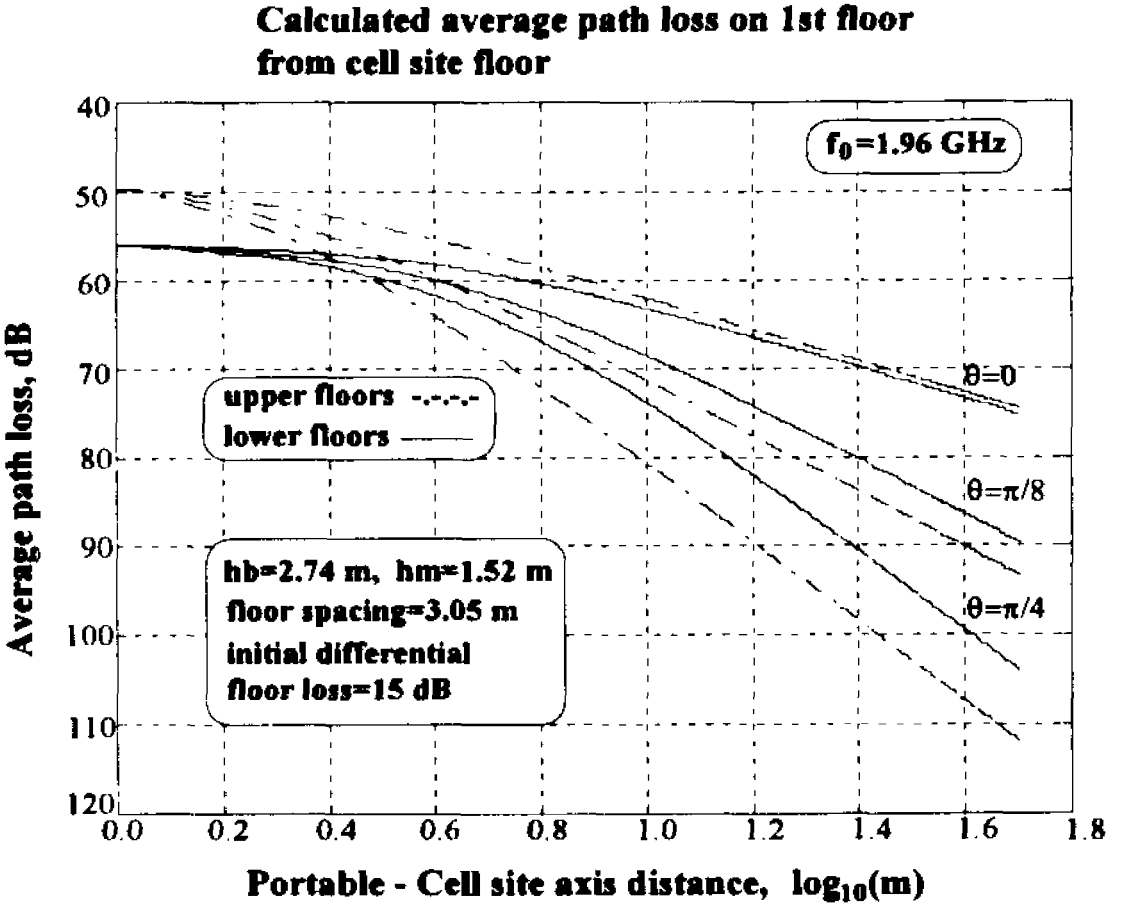


**Figure (2.2.2)**

Calculated average path loss on 1st floor from cell site floor in typical office building

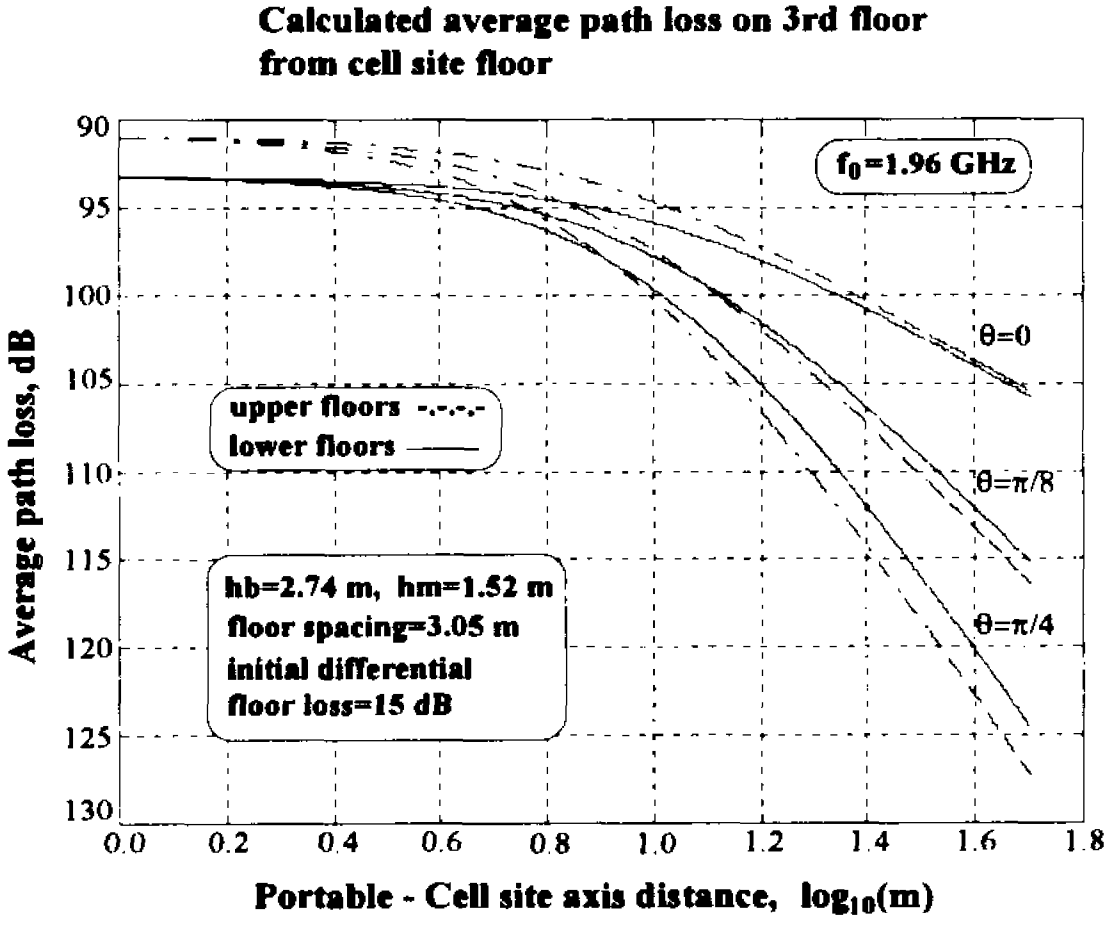


**Figure (2.2.3)**

Calculated average path loss on 3rd floor from cell site floor in typical office building

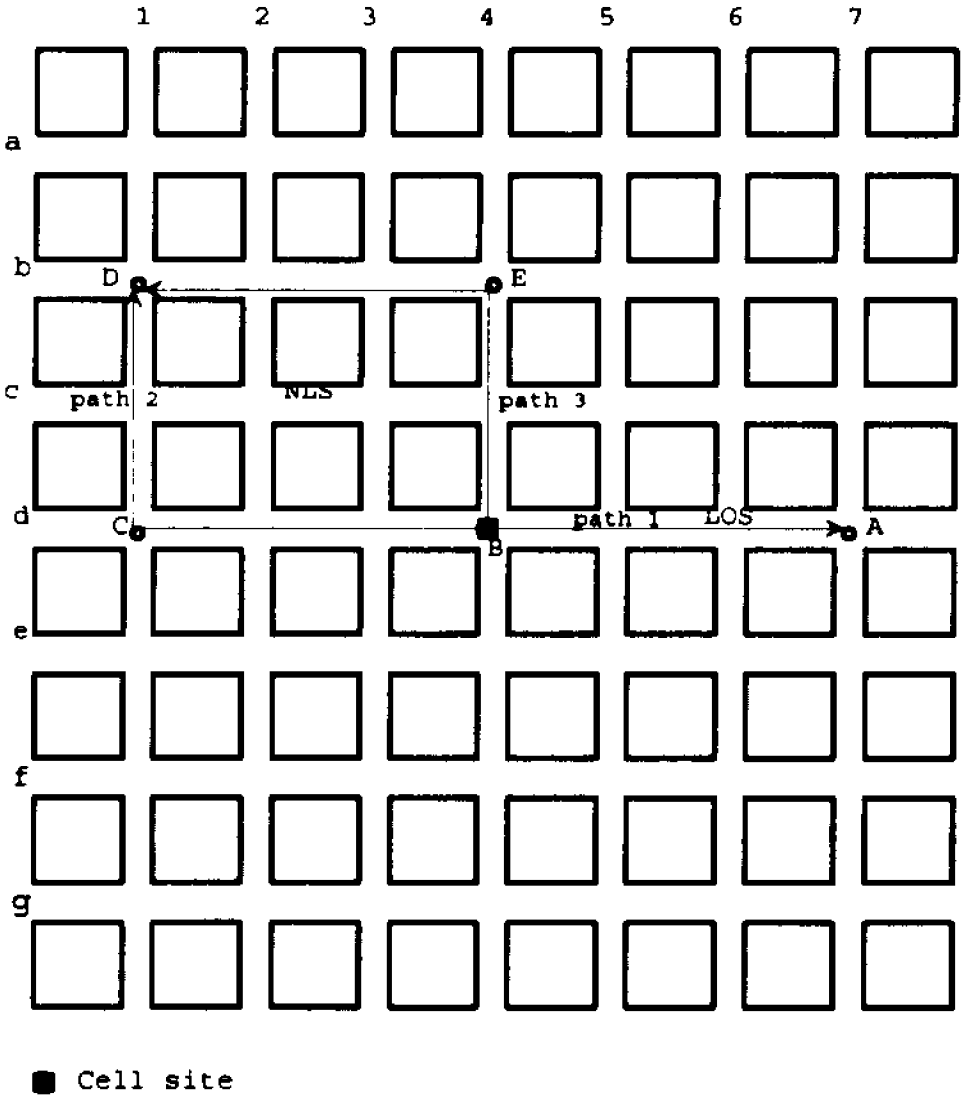


**Figure 3.1.1**

**Section of rectangular street grid showing cell site, 1 LOS path and 2 NLS paths**

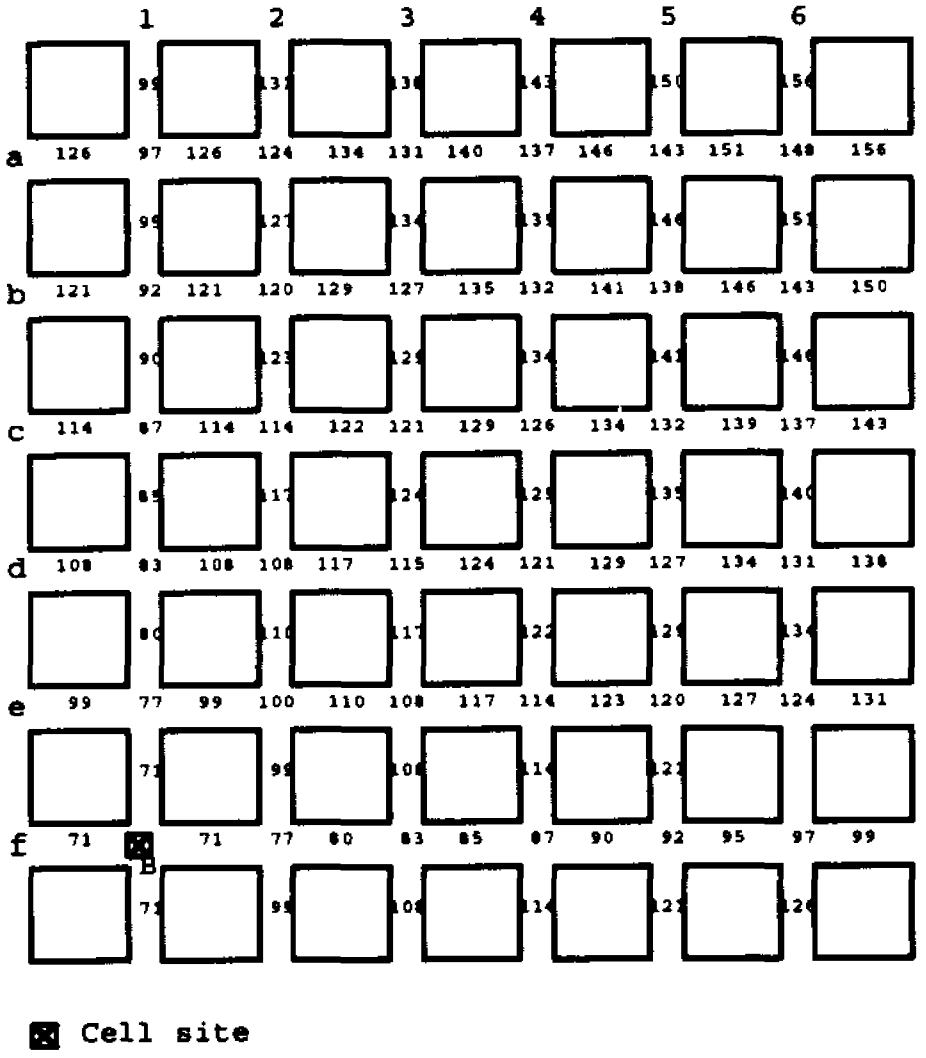


**Figure 3.1.2**

**Section of rectangular street grid showing cell site located at an intersection and path loss at intersections and mid-block positions around the cell site.**

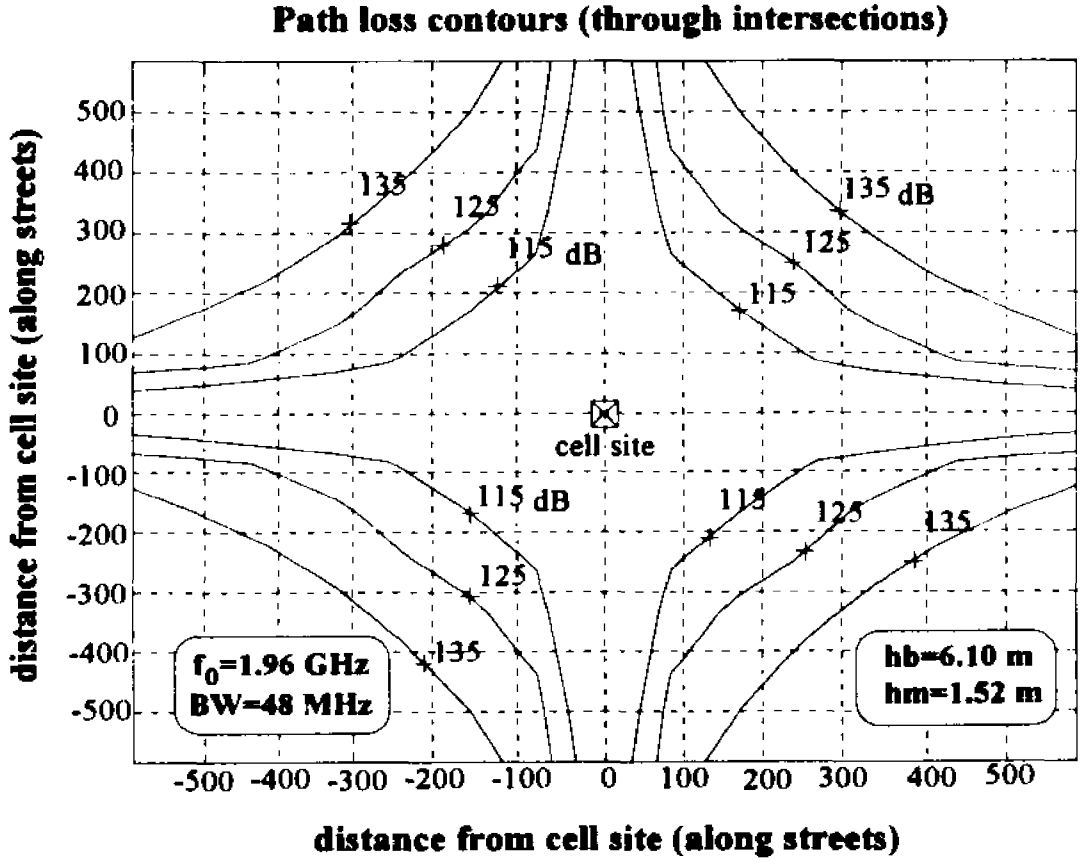


**Figure (3.1.3a)**

**Path loss contours through intersections around cell site located at an intersection**

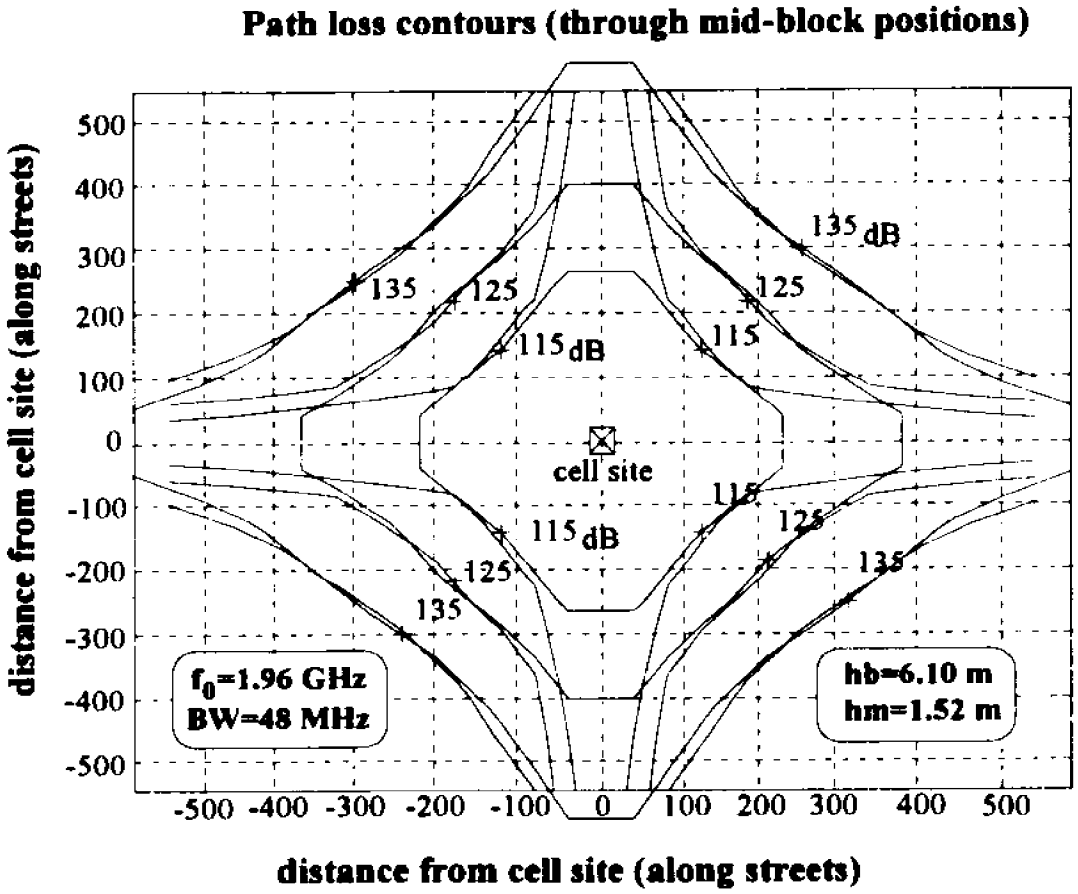


**Figure (3.1.3b)**

Path loss contours through mid-block positions around cell site located at an intersection

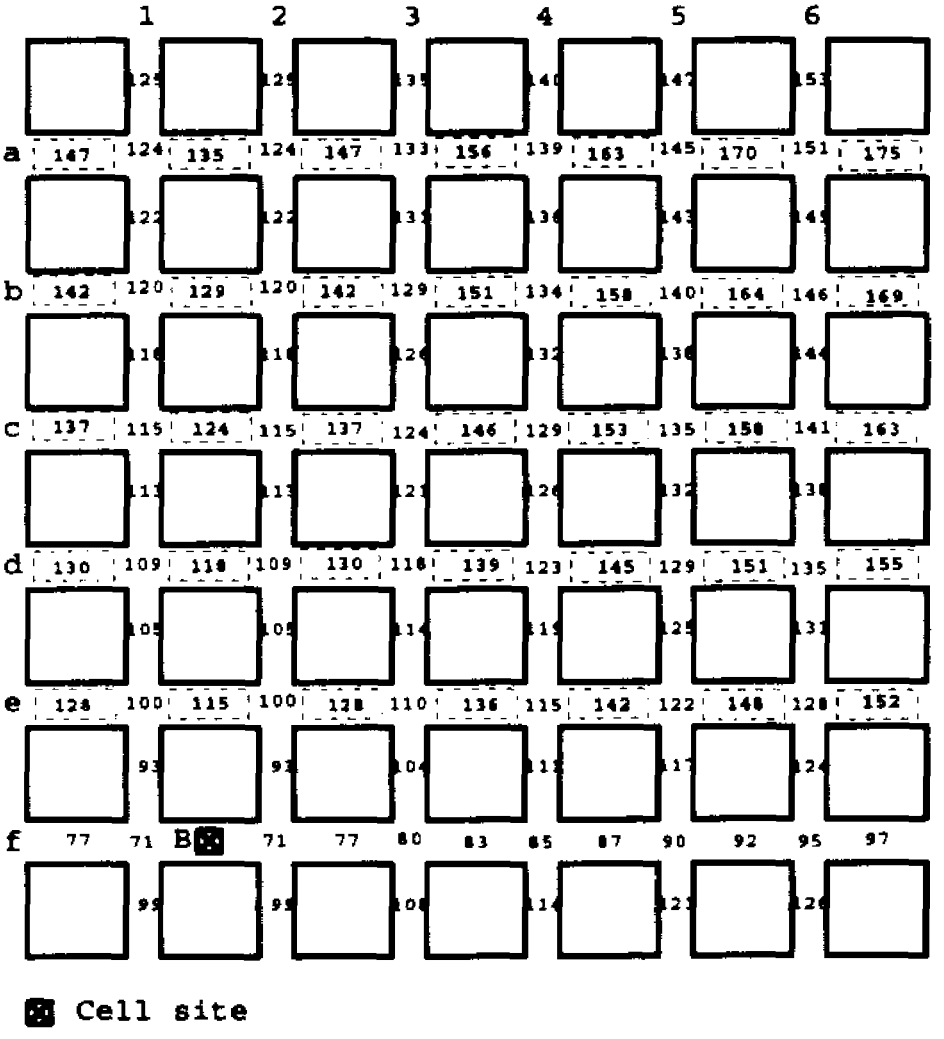


**Figure 3.1.4**

**Section of rectangular street grid showing cell site located at mid-block and path loss at intersections and mid-block positions around the cell site.**

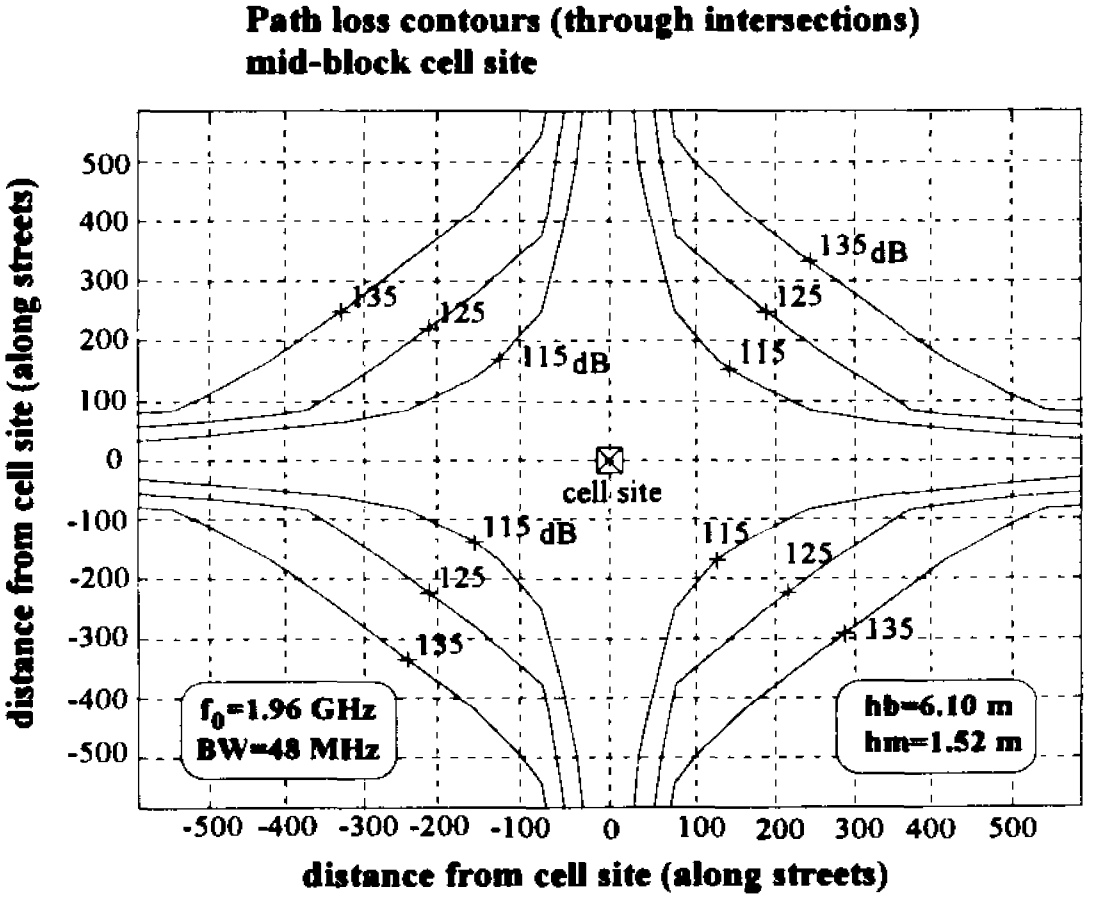


**Figure (3.1.5a)**

**Path loss contours through intersections around cell site located at mid-block**

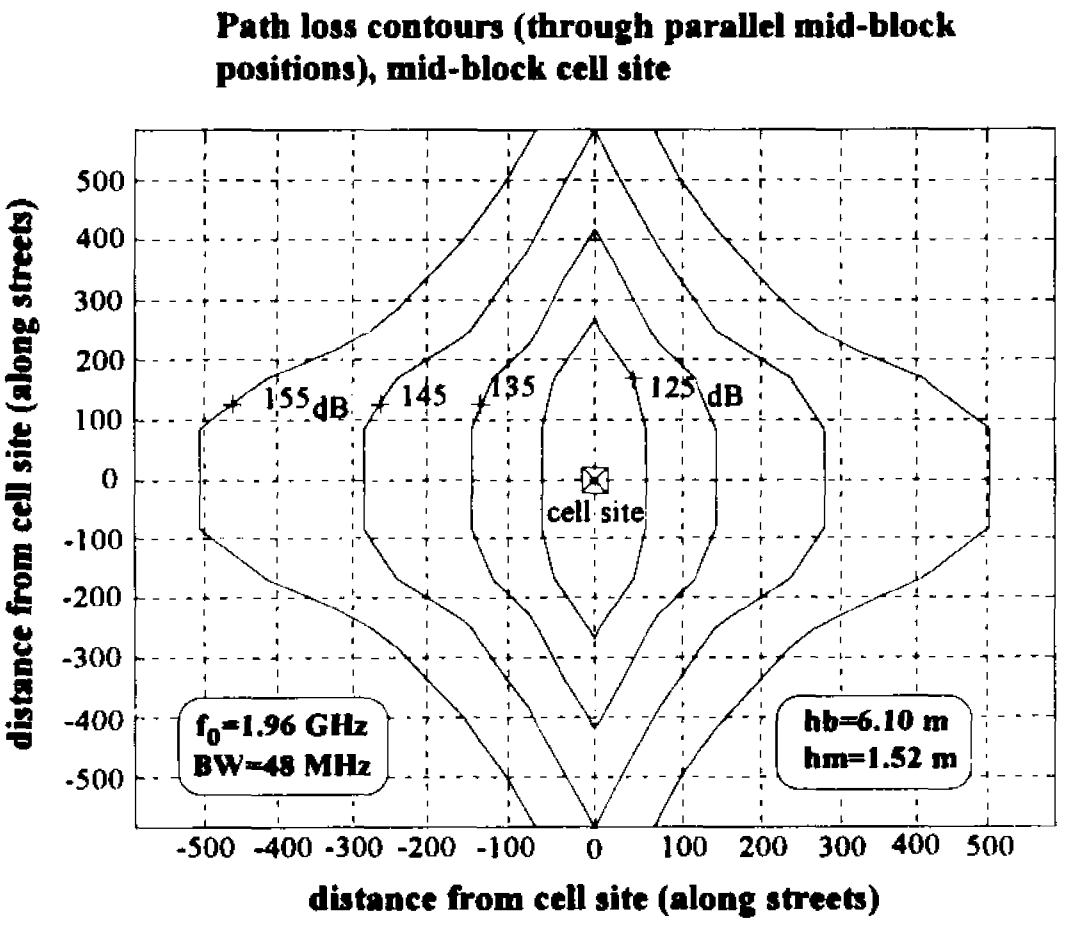


**Figure (3.1.5b)**

**Path loss contours through mid-block positions around cell site located at mid-block**

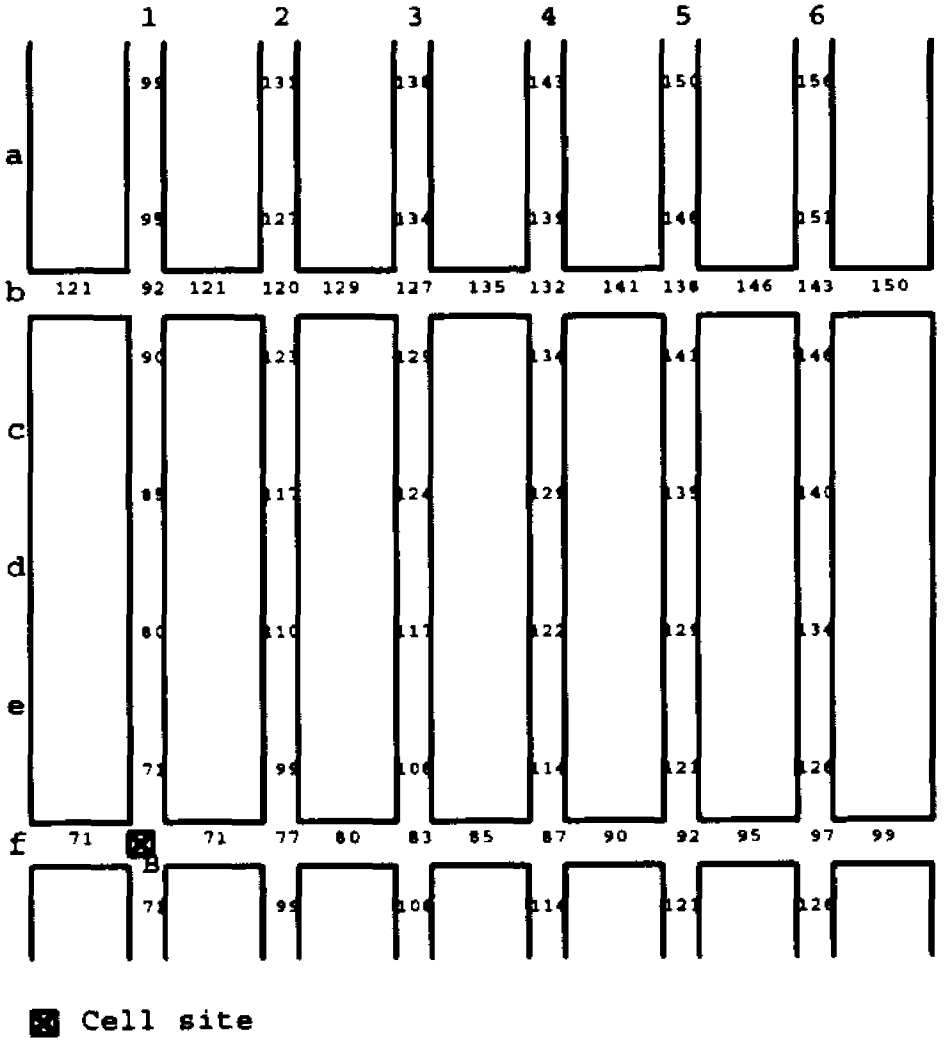


**Figure 3.1.6**

**Section of rectangular street grid, with 4:1 block ratio, showing cell site located at an intersection and path loss at intersections and mid-block positions around the cell site.**

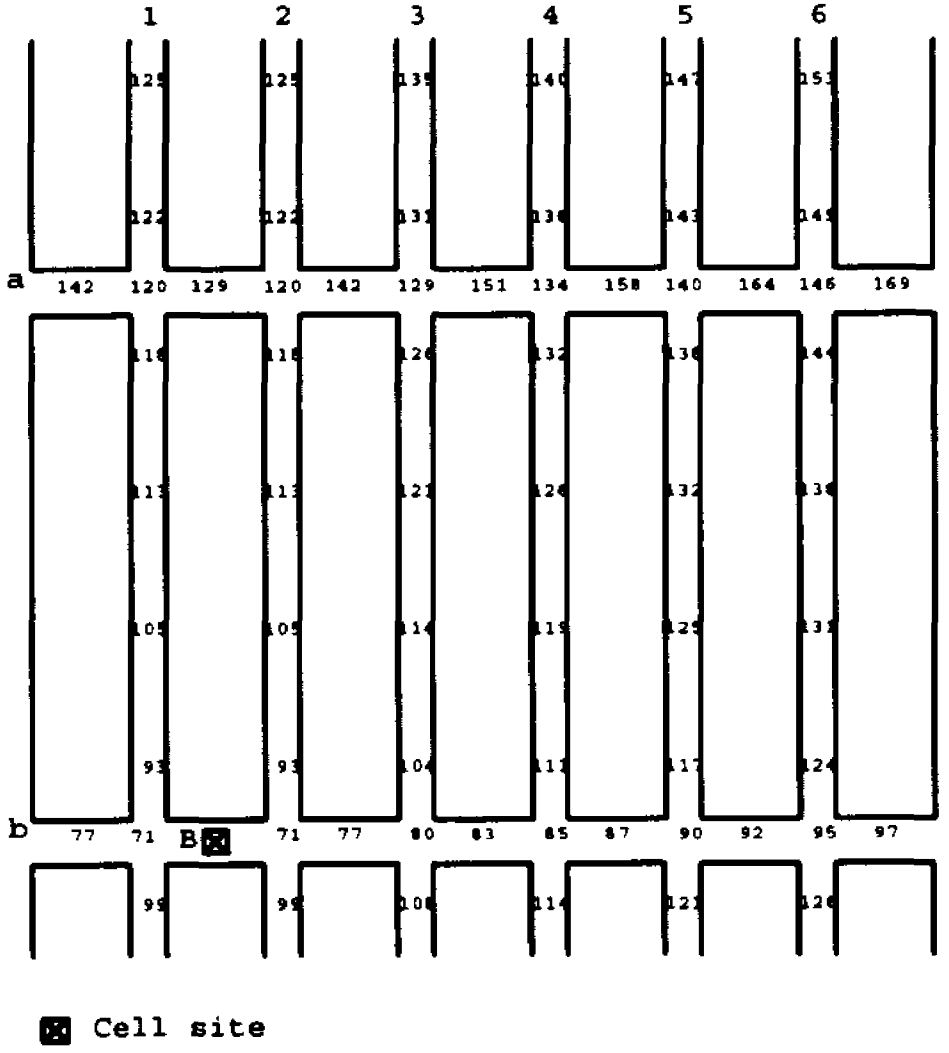


**Figure 3.1.7**

**Section of rectangular street grid, with 4:1 block ratio, showing cell site located at mid-block and path loss at intersections and mid-block positions around the cell site.**

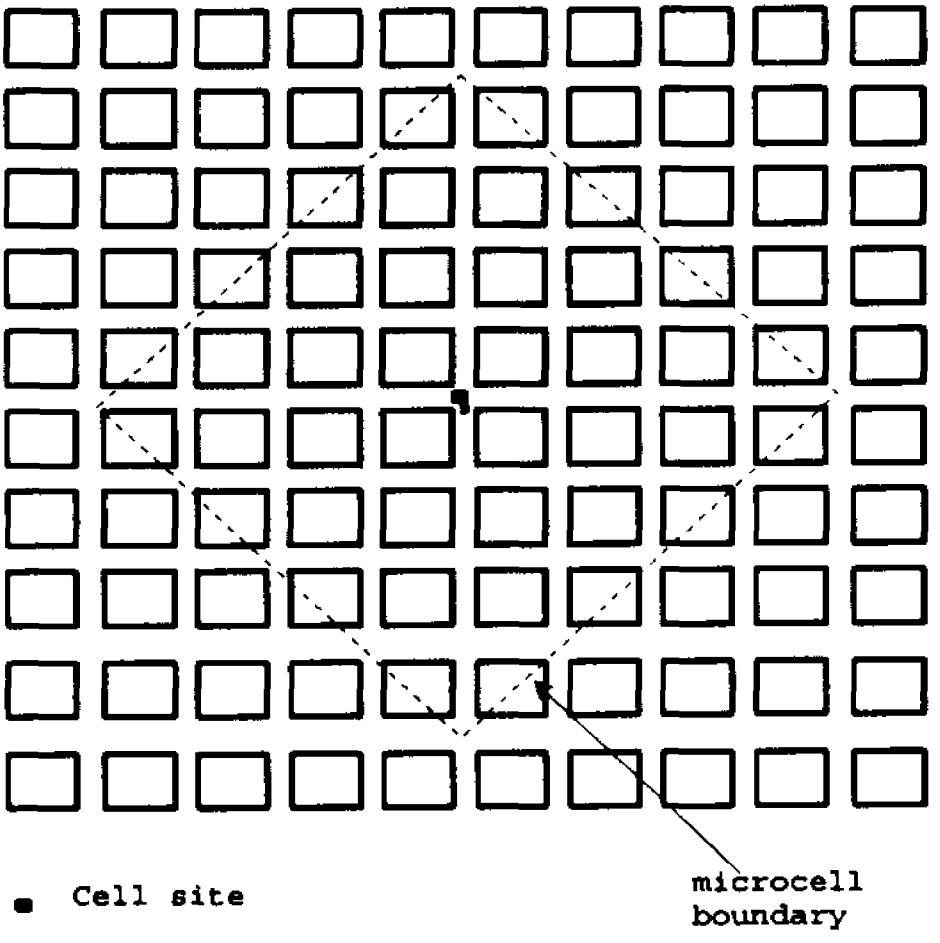


**Figure 3.1.8**

**Omnidirectional, intersection located cell site microcell (type Omni-I).**

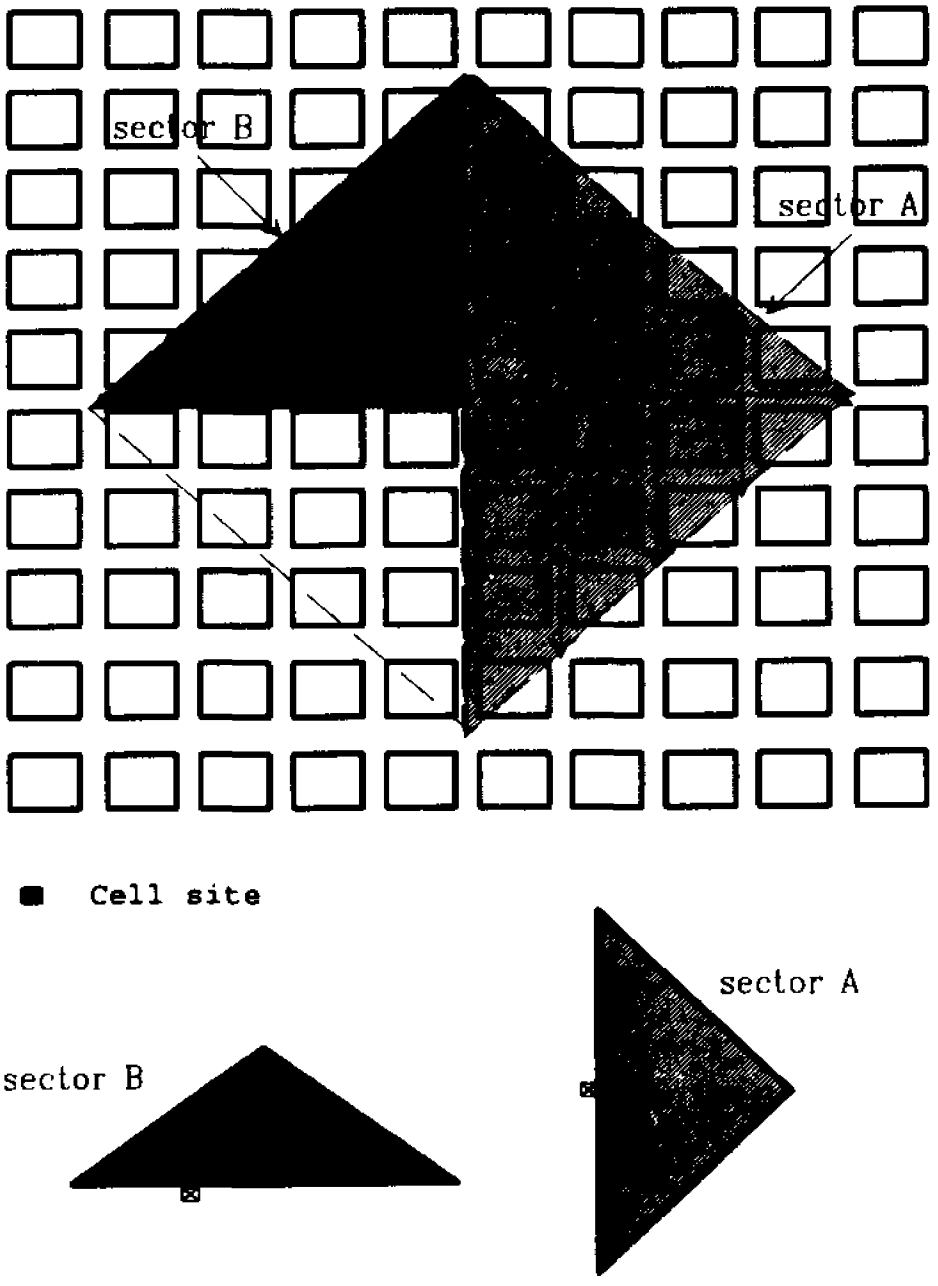


**Figure 3.1.9**

**4-sector I type microcell, (4-I).**

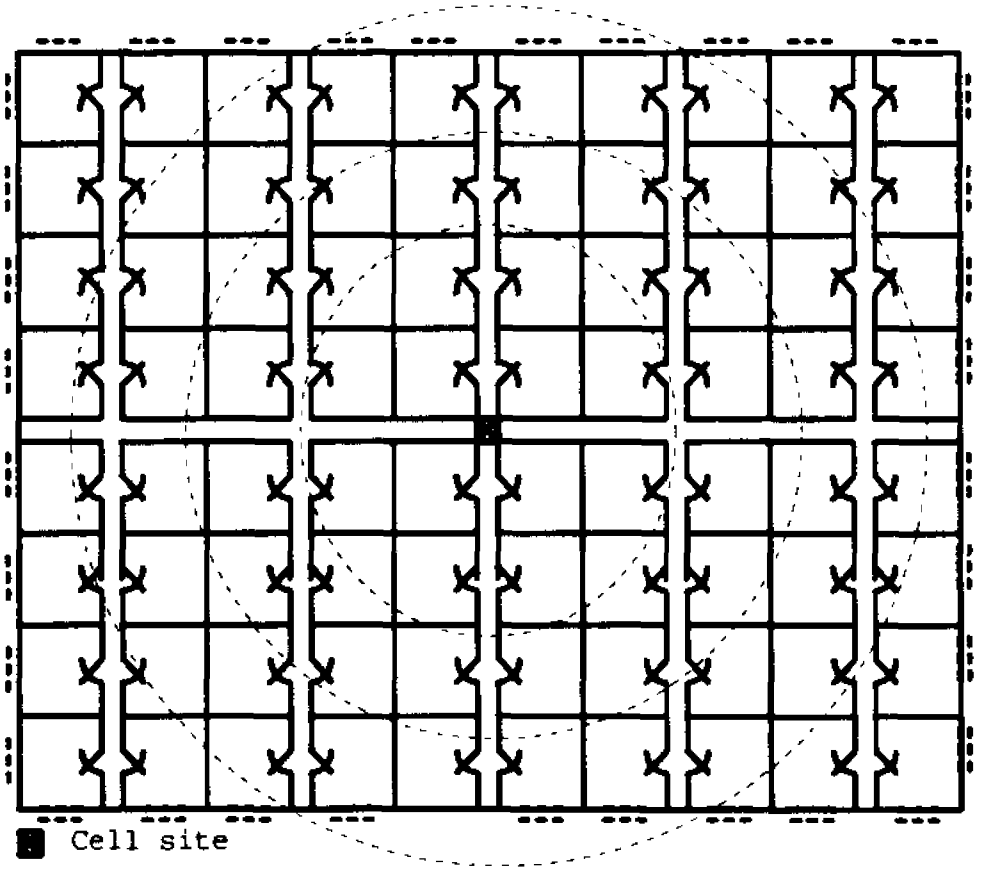


**Figure 3.2.1** Hypothetical plan view of one floor of a high rise building showing cell site and path loss contours.

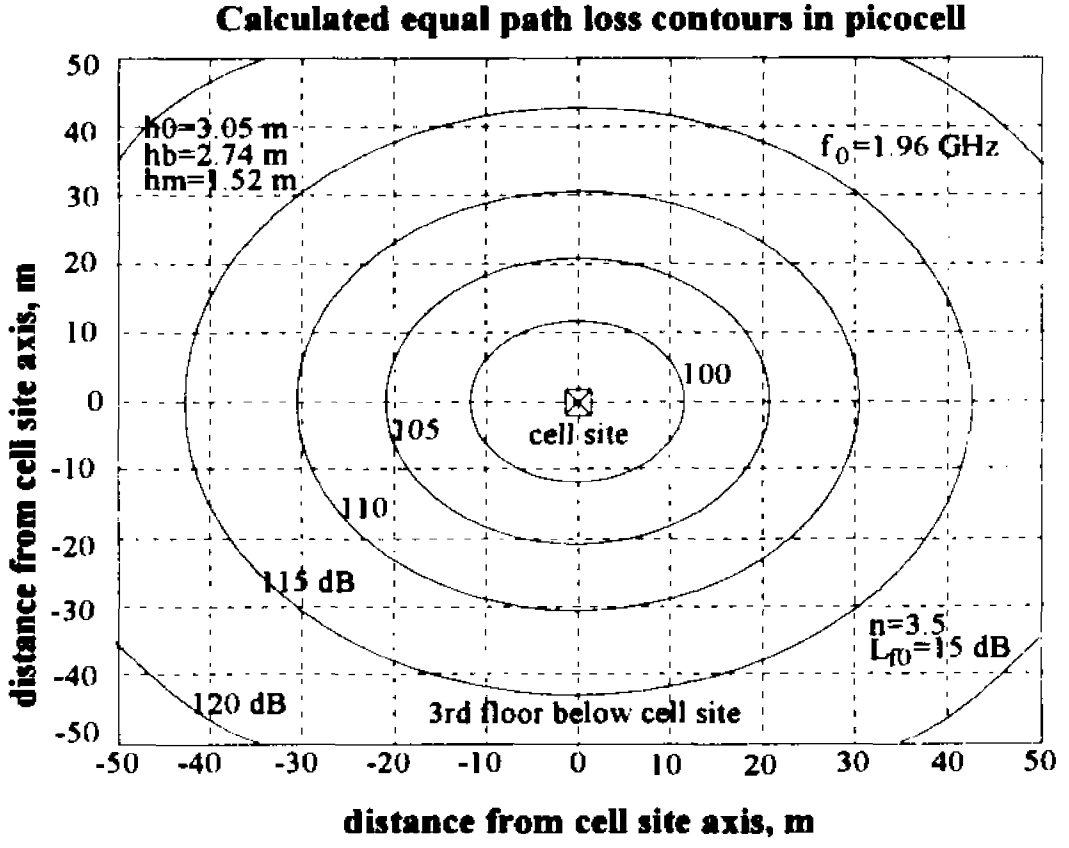


**Figure (3.2.2a)**

**Equal path loss contours on 3rd floor from cell site floor**

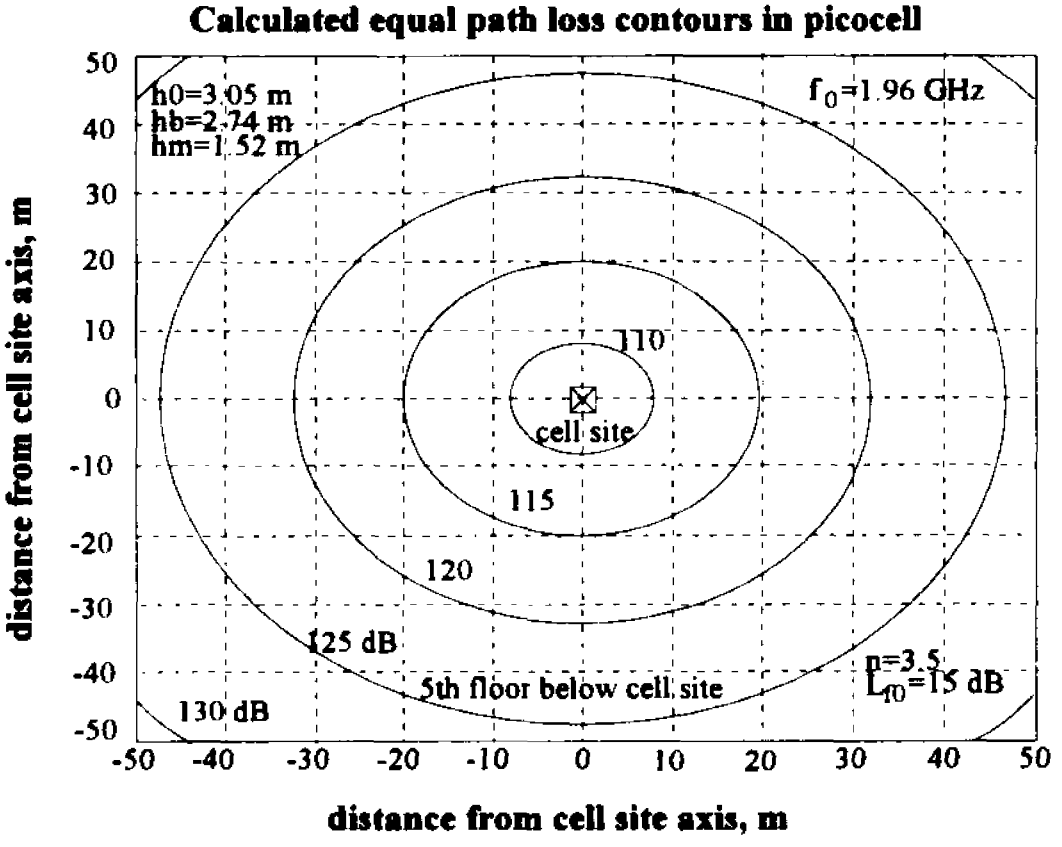


**Figure (3.2.2b)**

**Equal path loss contours on 5th floor from cell site floor**

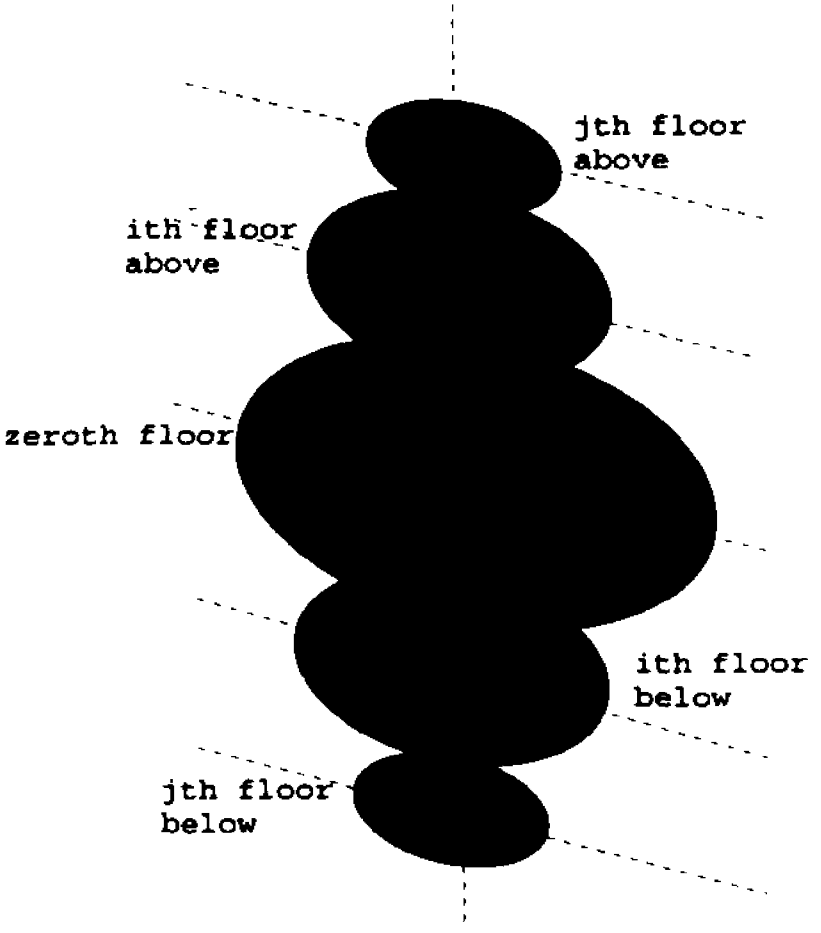


**Figure 3.2.3**

**3-dimensional representation of picocell showing coverage area on different floors from the cell site.**

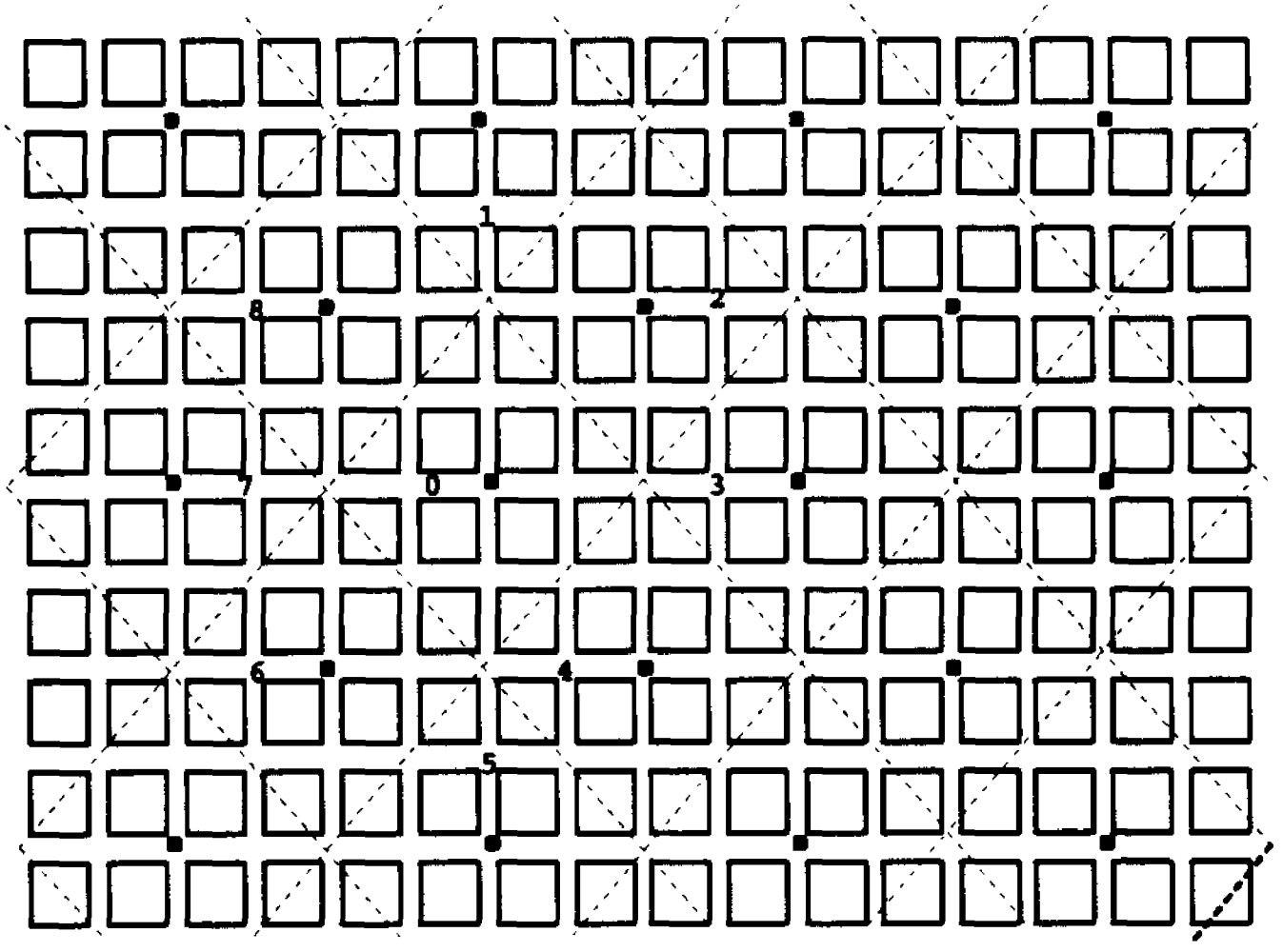


**Figure 4.1.1**

**Section of rectangular street grid showing cell site layout**

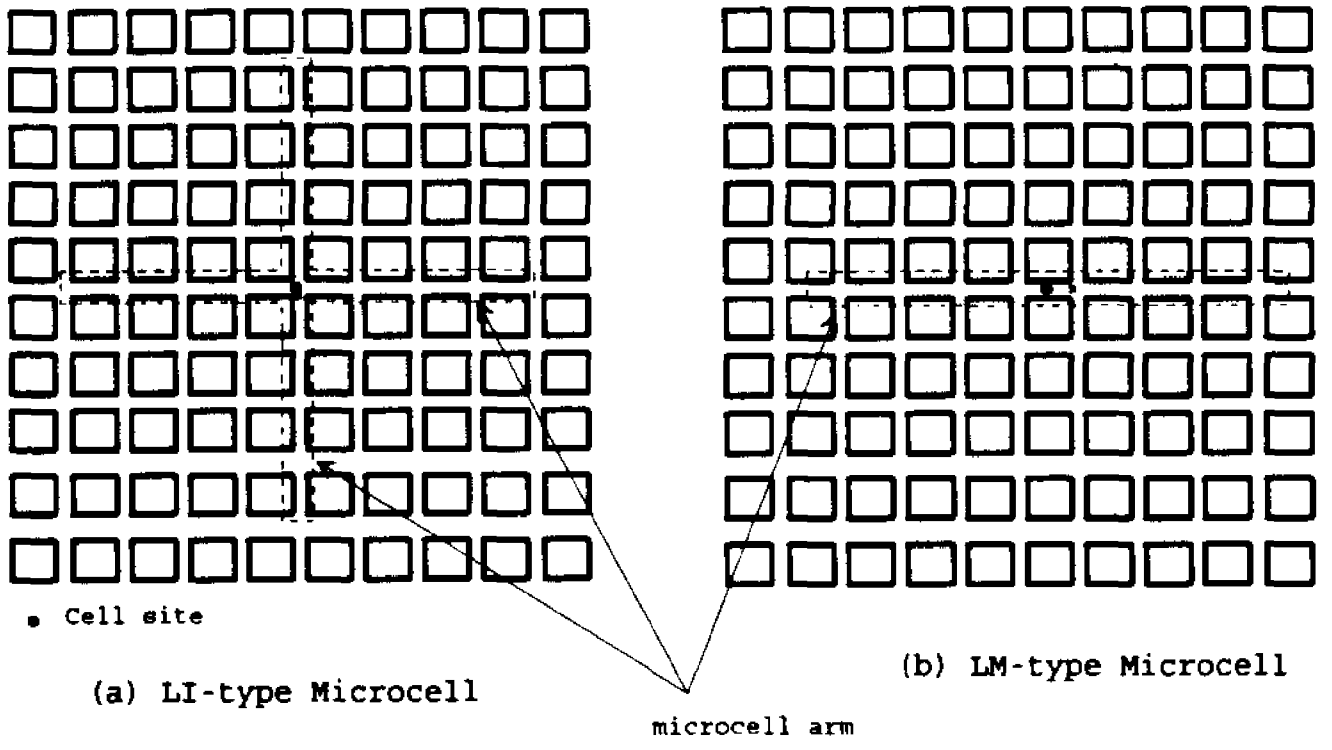


**Figure 4.1.2**

**Linear (L-type) microcells resulting from LOS reduction of I- and M-type microcells.**

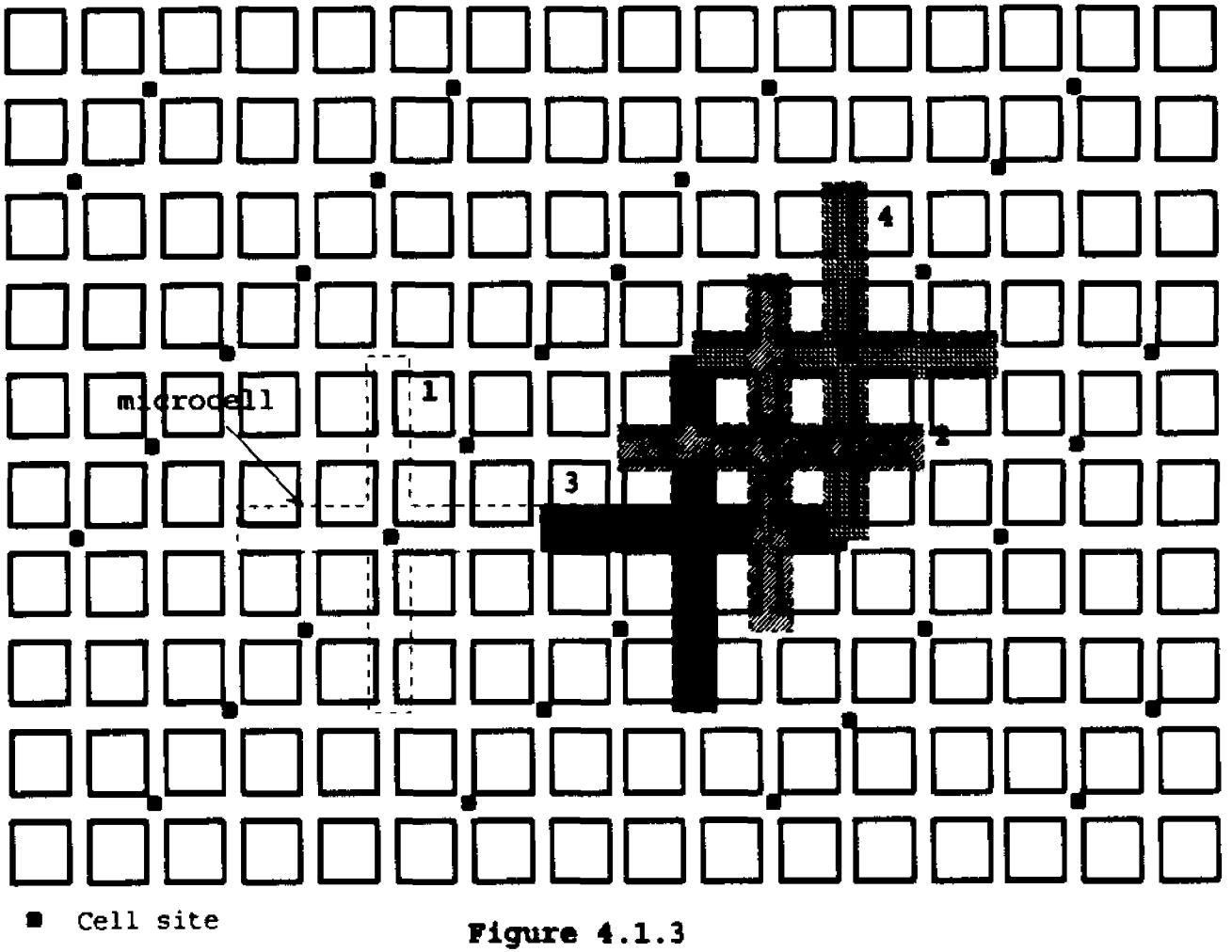


**Figure 4.1.3**

**Section of rectangular street grid showing cell site layout for type LI microcells.**

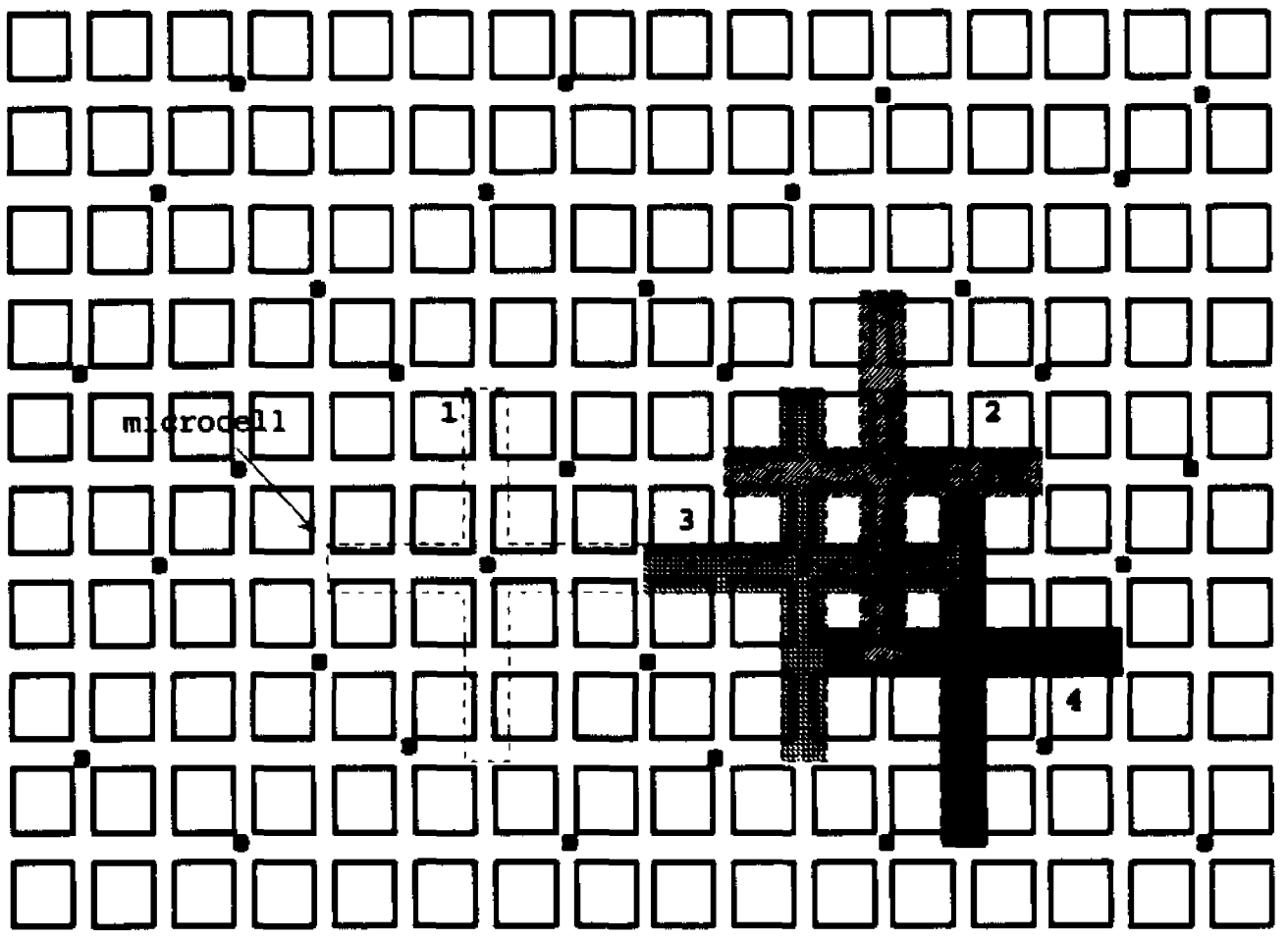


**Figure 4.1.4**

**Cell site layout for LI-type microcells eliminating 4-way intersection interference .**

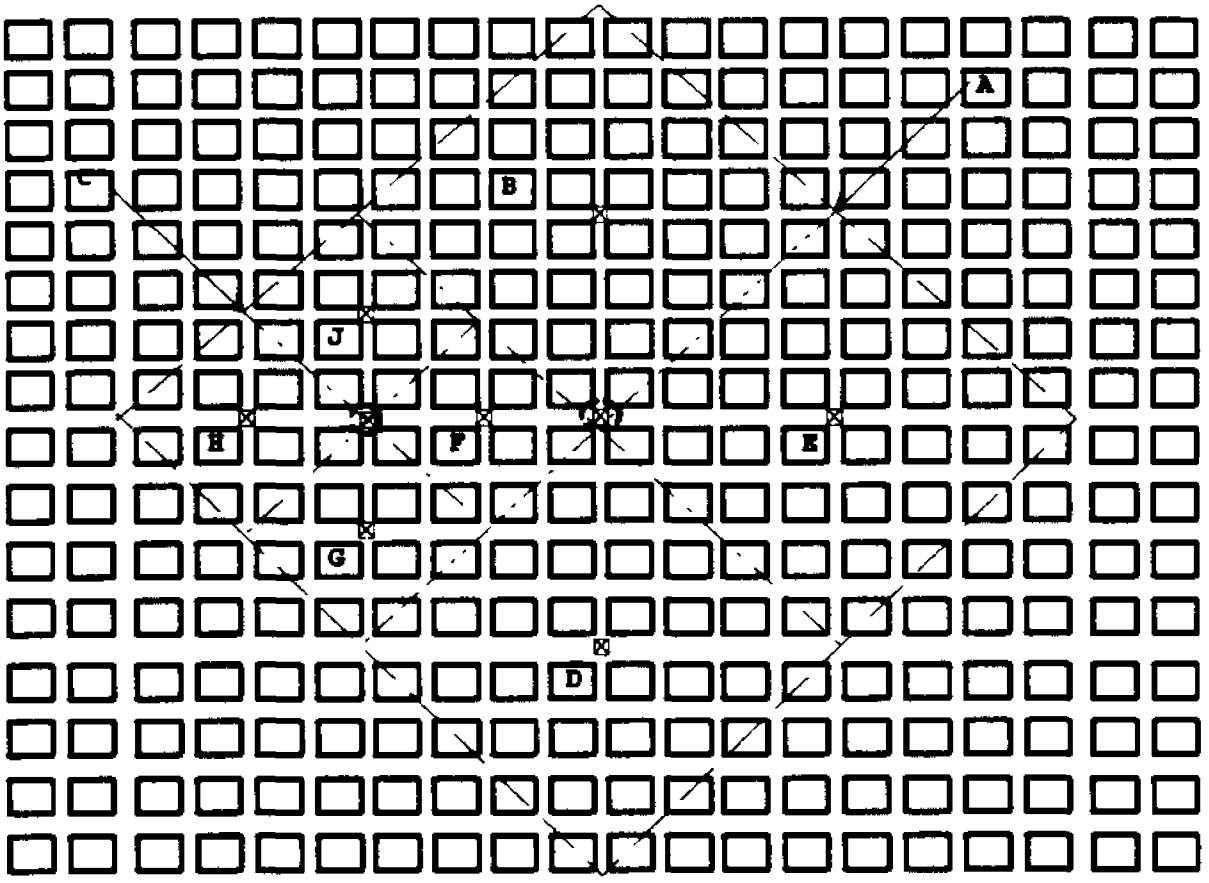


**Figure 4.1.5**

**8 block I cell split into three 4 block I cells and four 2 block I cells.**

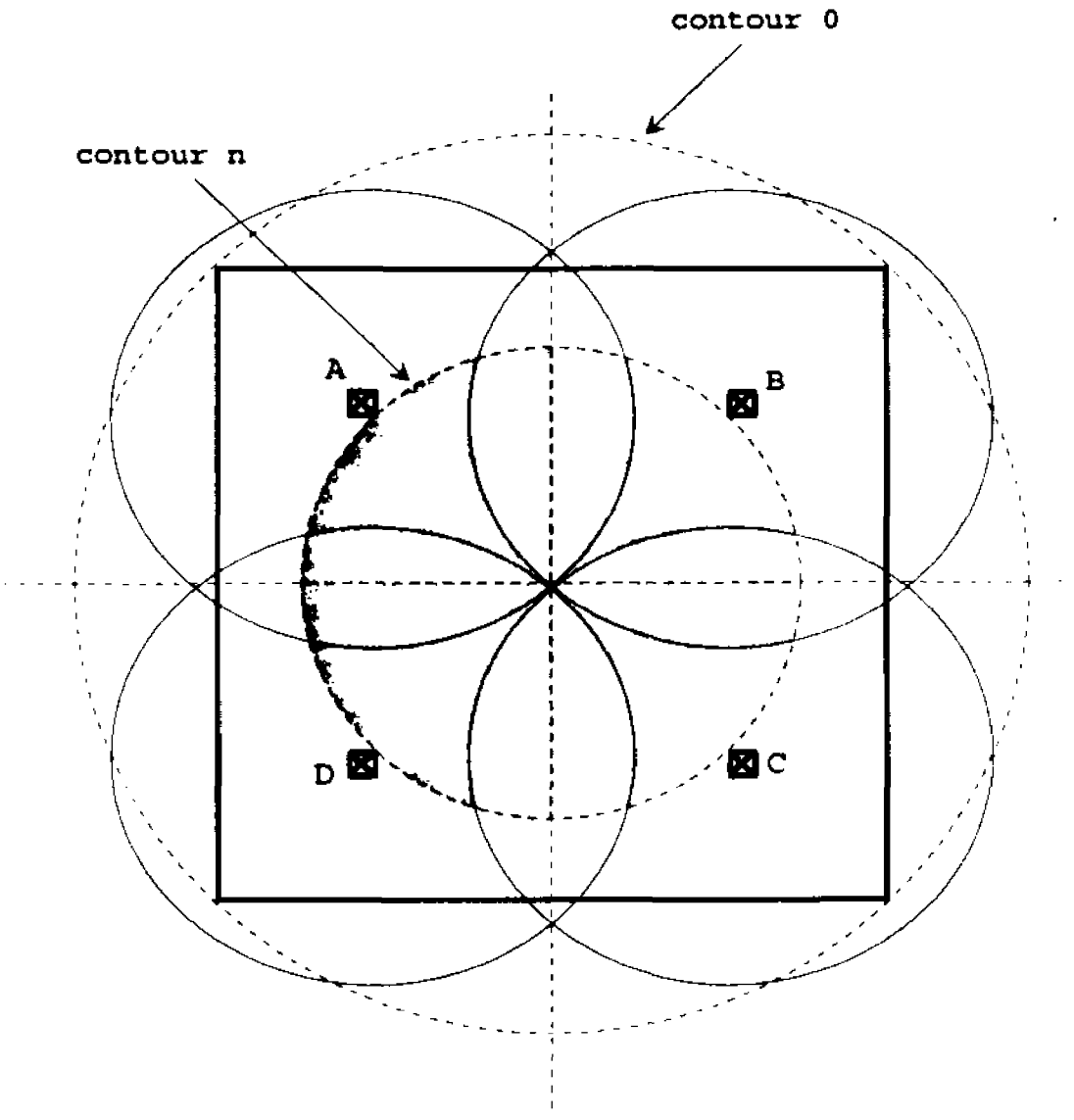


**Figure 4.2.1**

**Picocell coverage on farthest floor from zeroth floor**

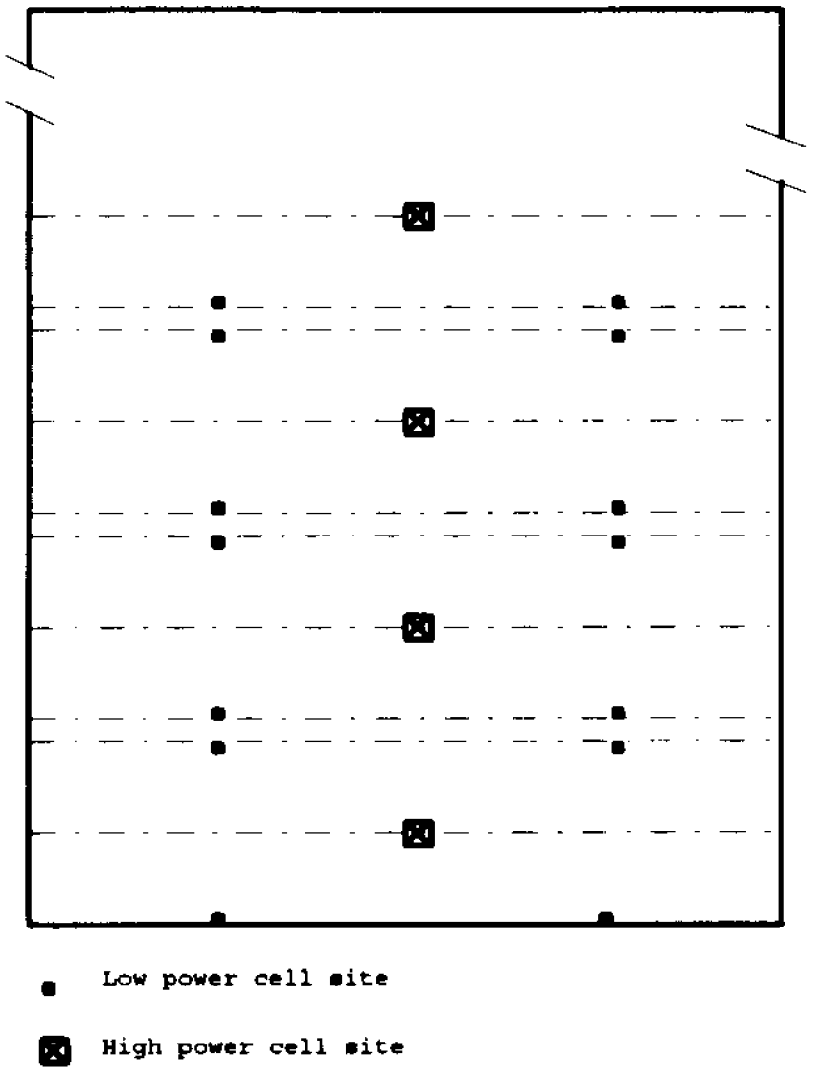


**Figure (4.2.2)**

**Vertical plane through building showing cell site arrangement.**

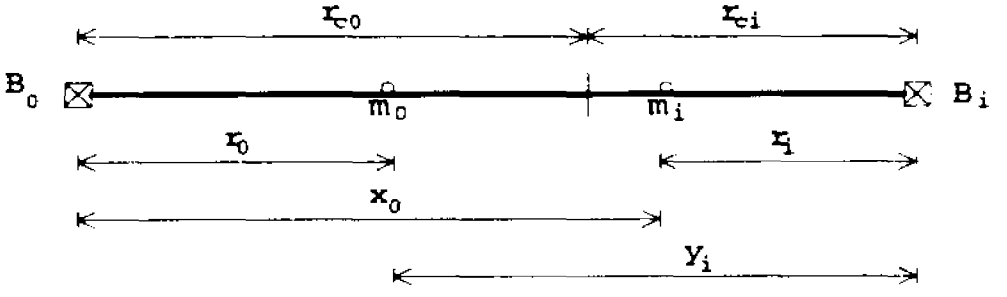


Cell site

mobile

**Figure (5.1.1)**

**Interference scenario between adjacent cell sites**

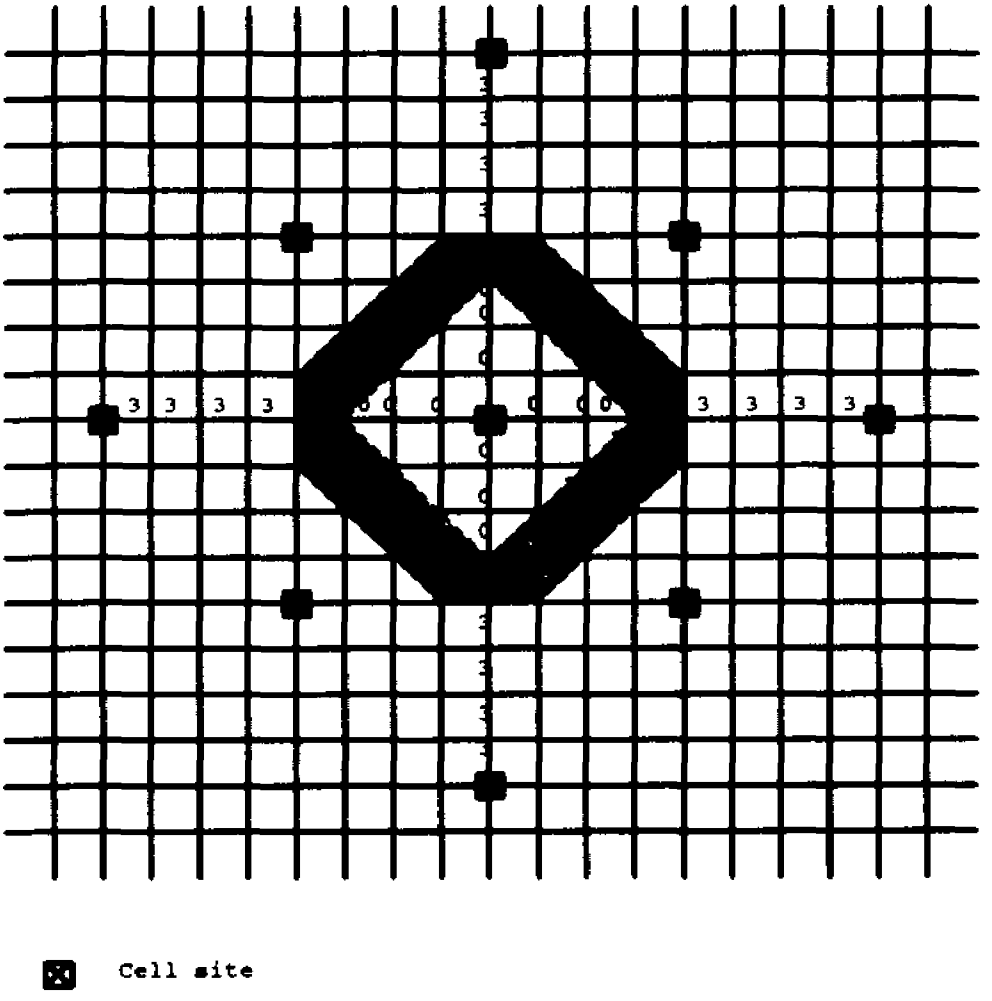


**Figure (5.3.1)**

**I-type microcell with 8 nearest neighbours showing interference regions.**

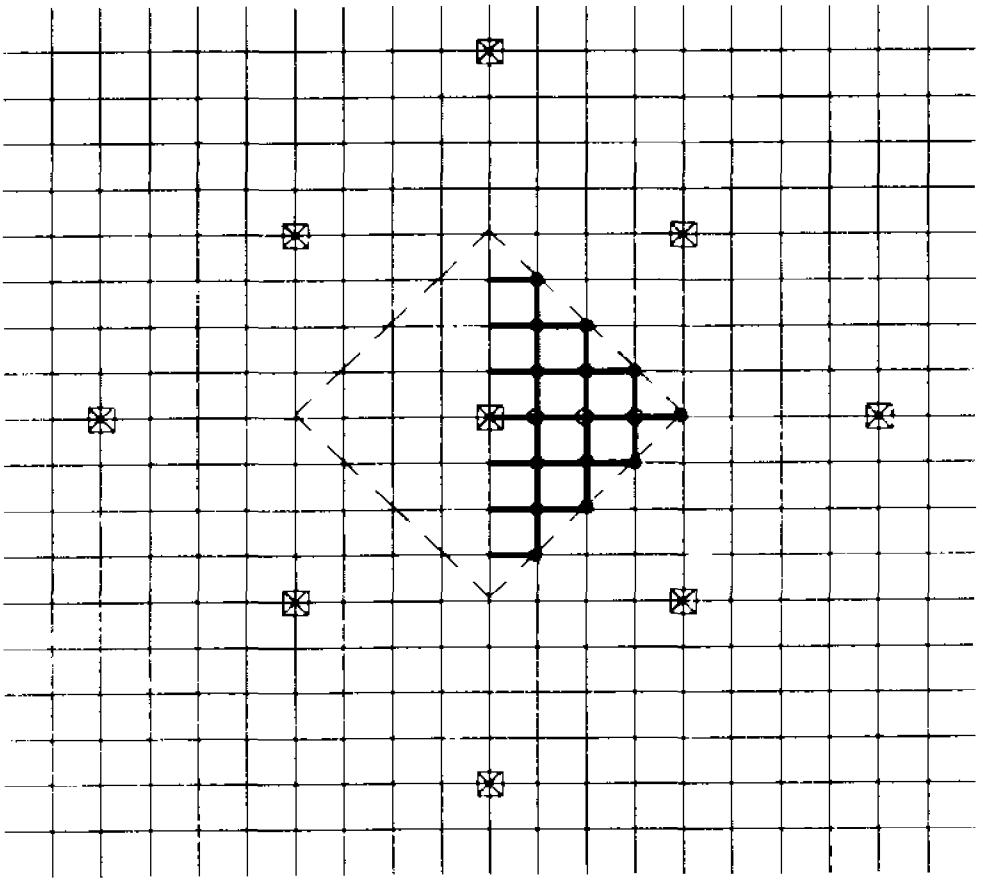

⊠ Cell site

● Inter-sector intersection

○ Intra-sector intersection

**Figure (5.4.1)**

**4-I type microcell showing inter-sector and intra-sector intersections**

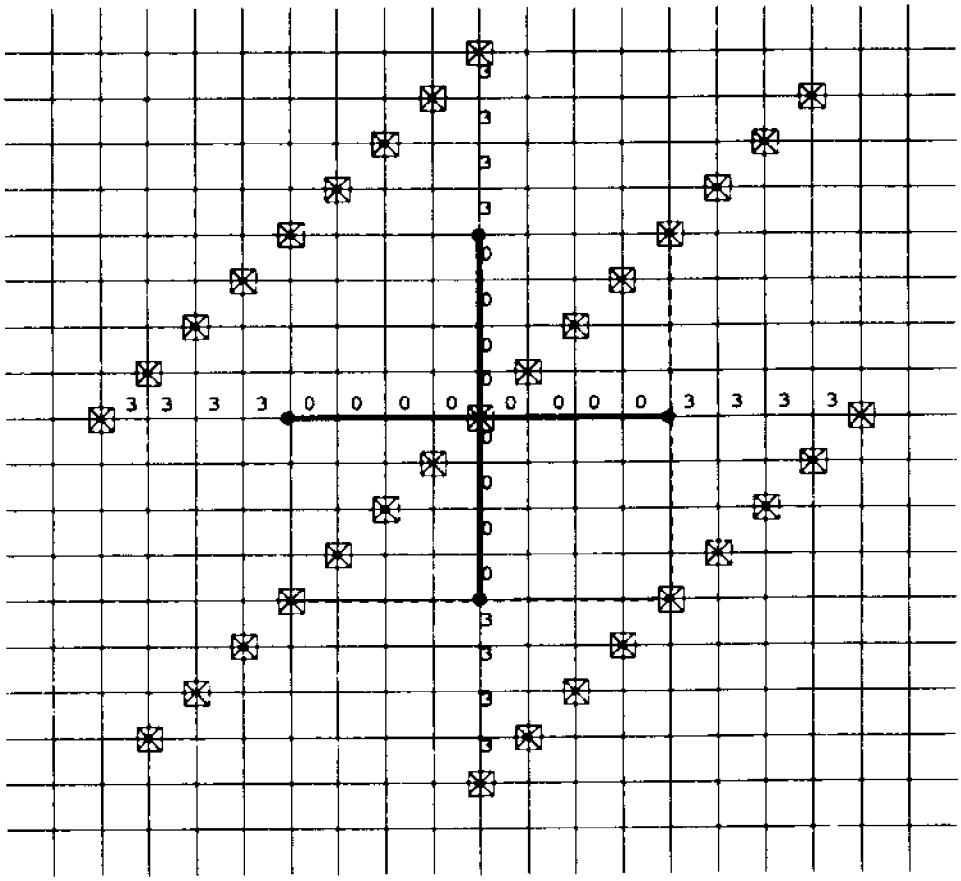


**Figure (5.5.1)**

**LI-type network showing interfering microcells and interference regions with respect to a given microcell.**

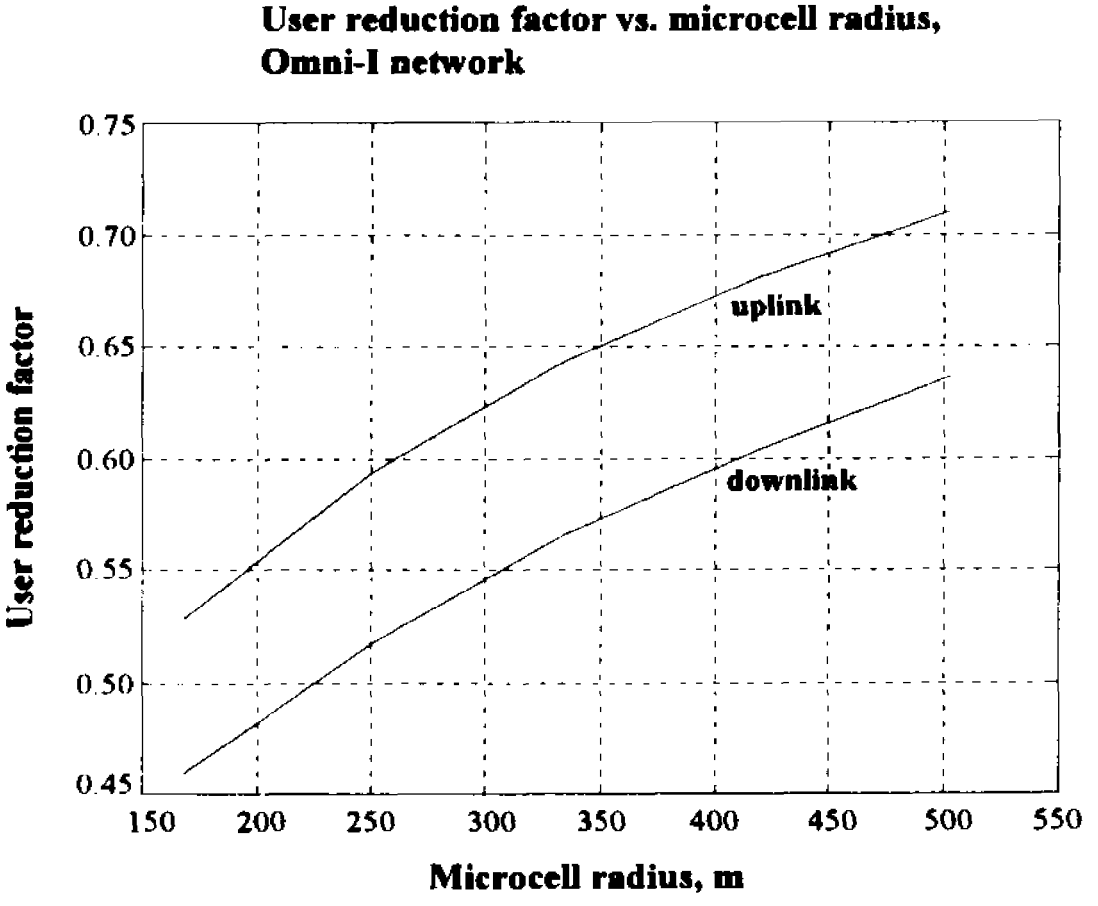


**Figure (5.6.1)**

User reduction factor for uplink and downlink in Omni-I network

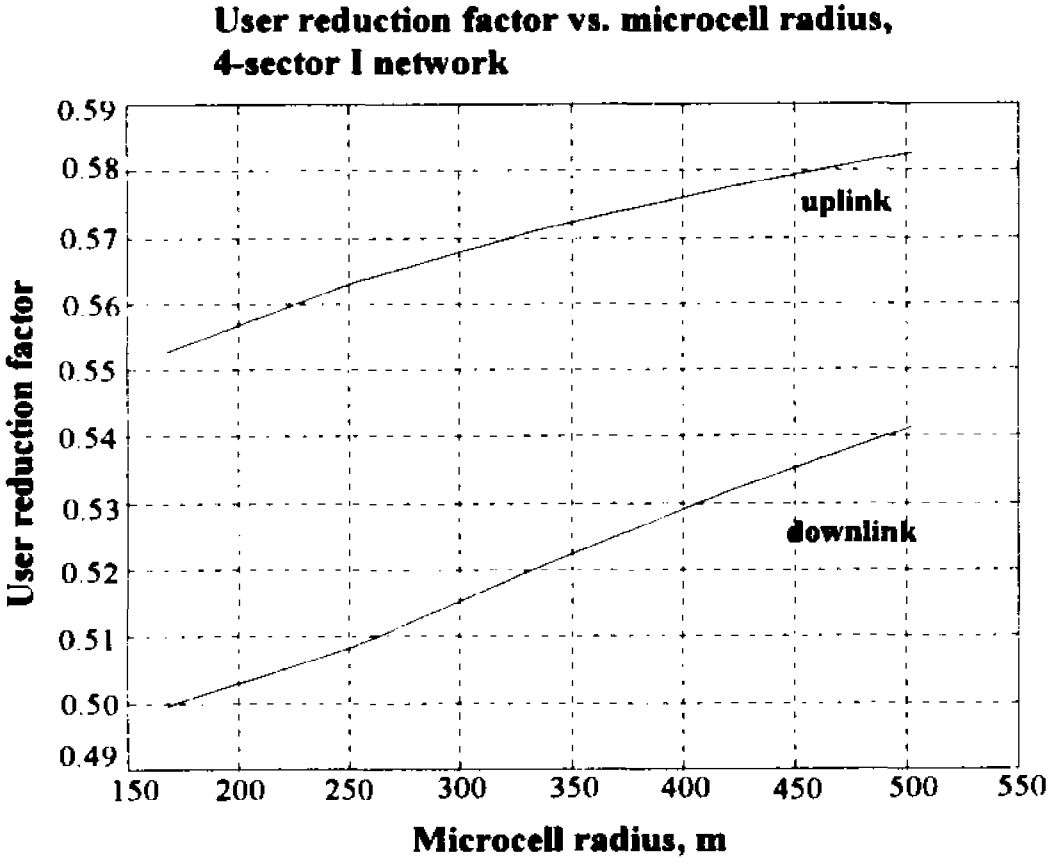


**Figure (5.6.2)**

**User reduction factor for uplink and downlink in 4-I network**

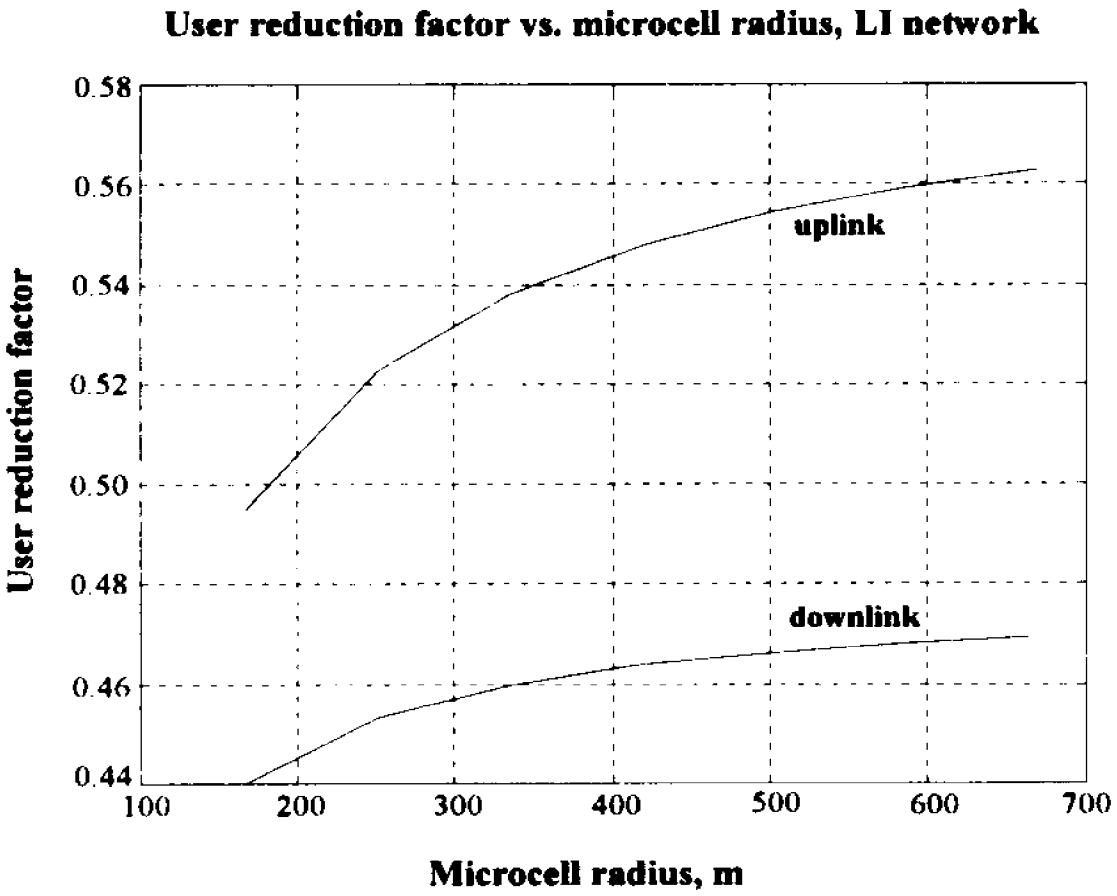


**Figure (5.6.3)**

User reduction factor for uplink and downlink in LI network

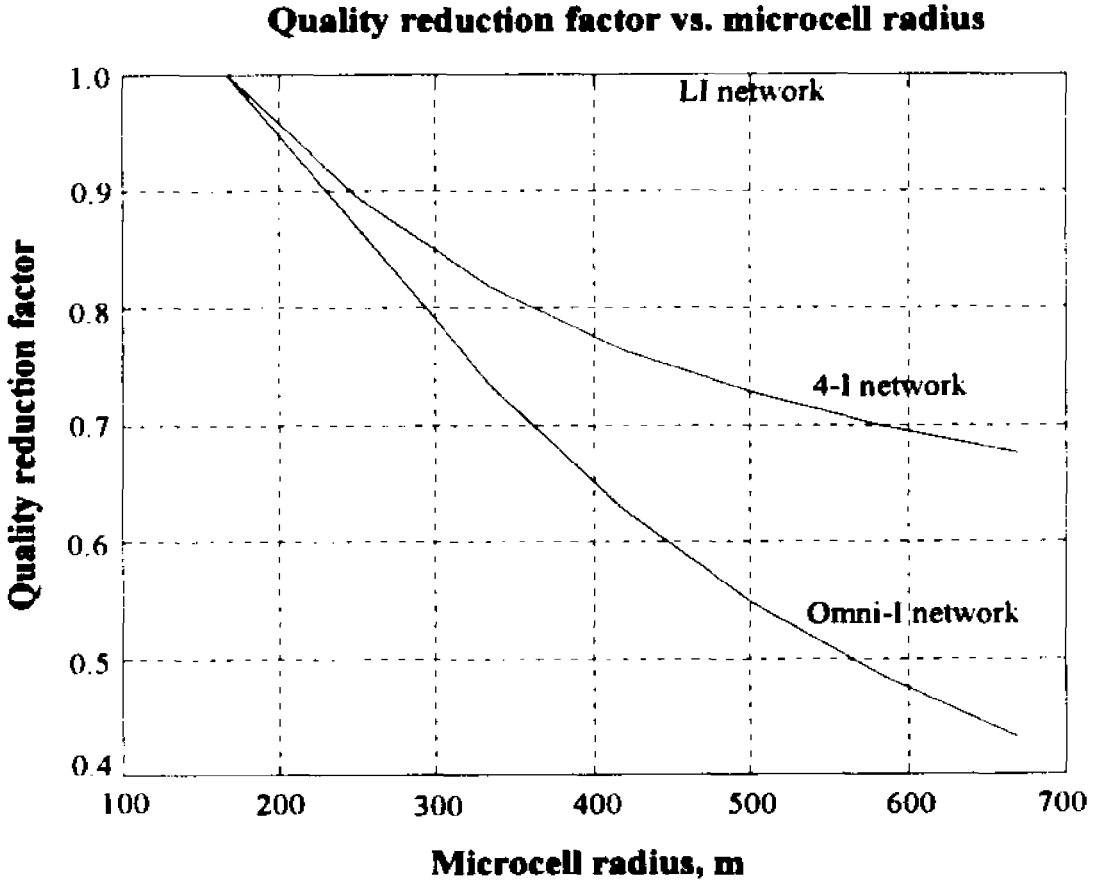


**Figure (5.7.1)**

**Quality reduction factor versus microcell radius**

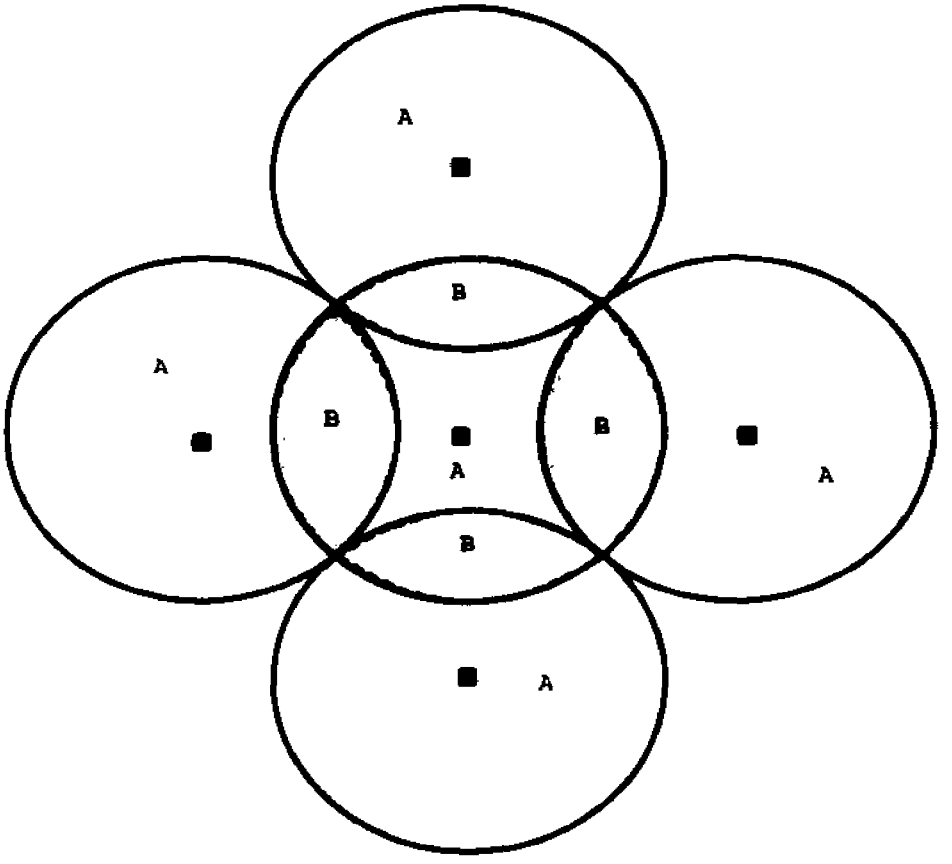


**Figure 6.1**

**Coverage regions on the zeroth floors of adjacent picocells**

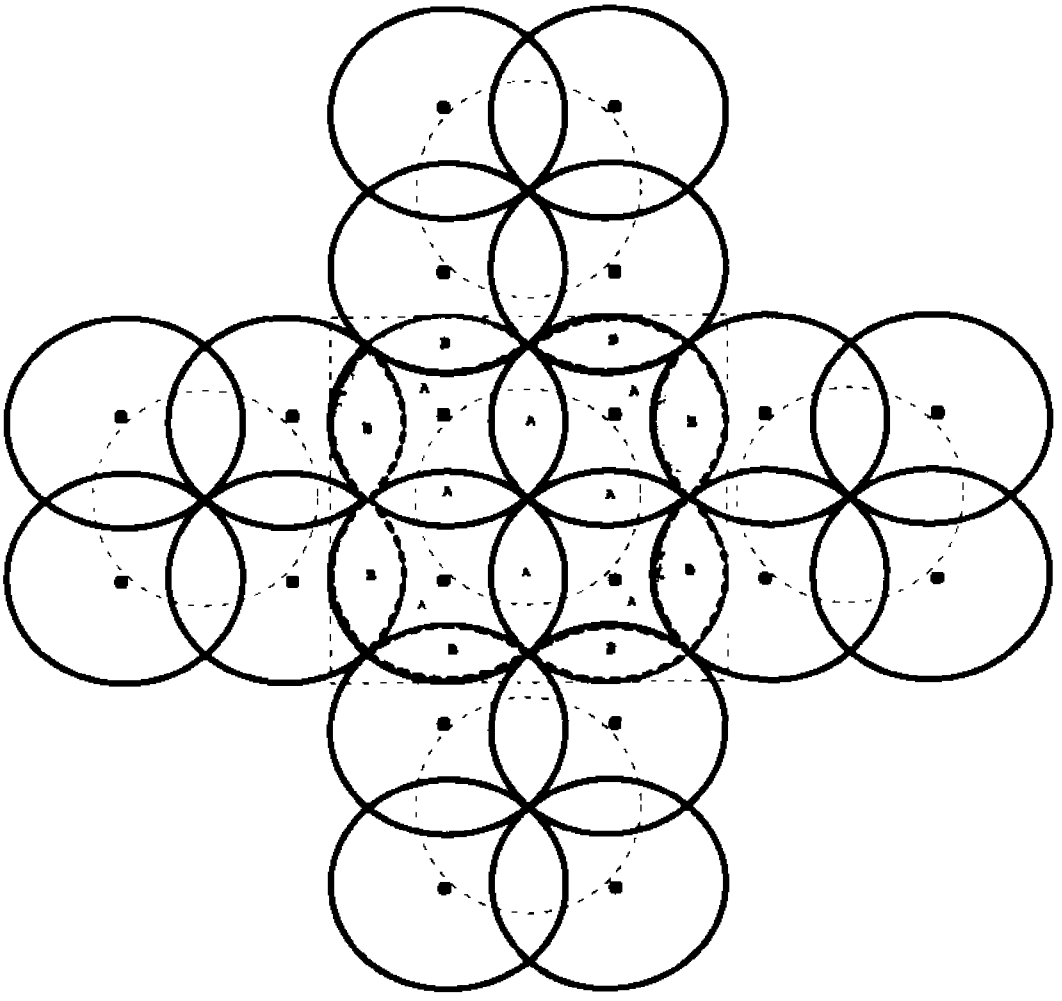

**Figure 6.2**

**Coverage regions on farthest floors from zeroth floors of adjacent picocells.**

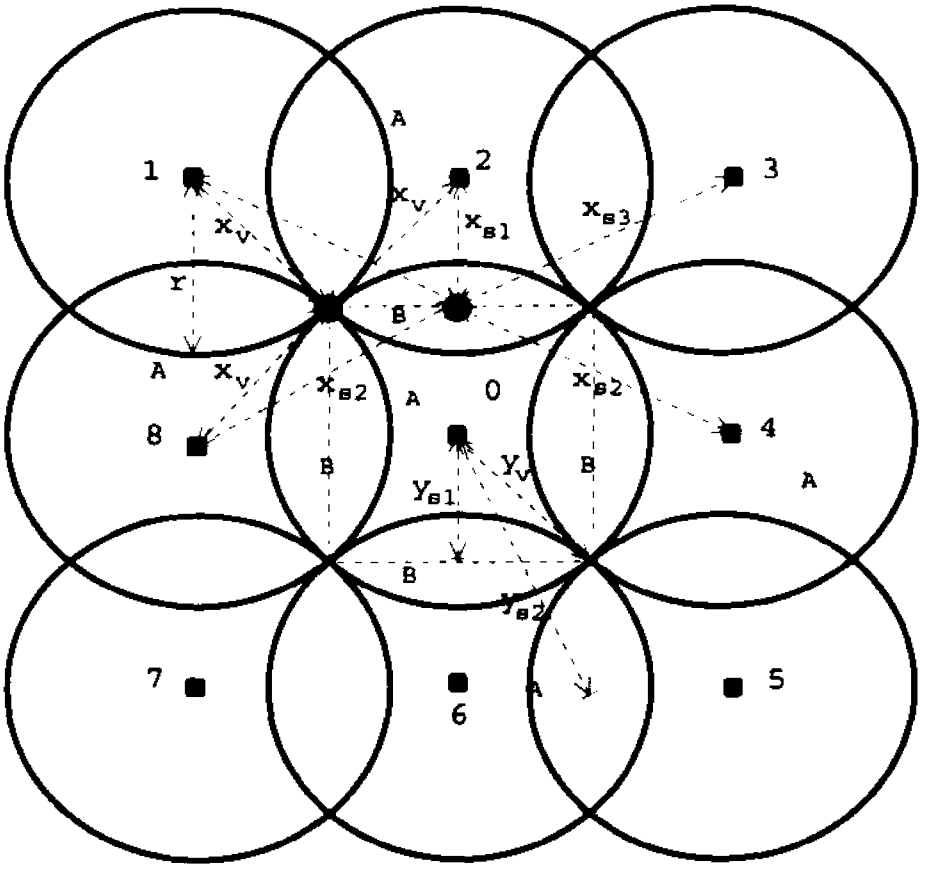


**Figure 6.3**

**Worst case interference scenario on zeroth floor in picocell.**

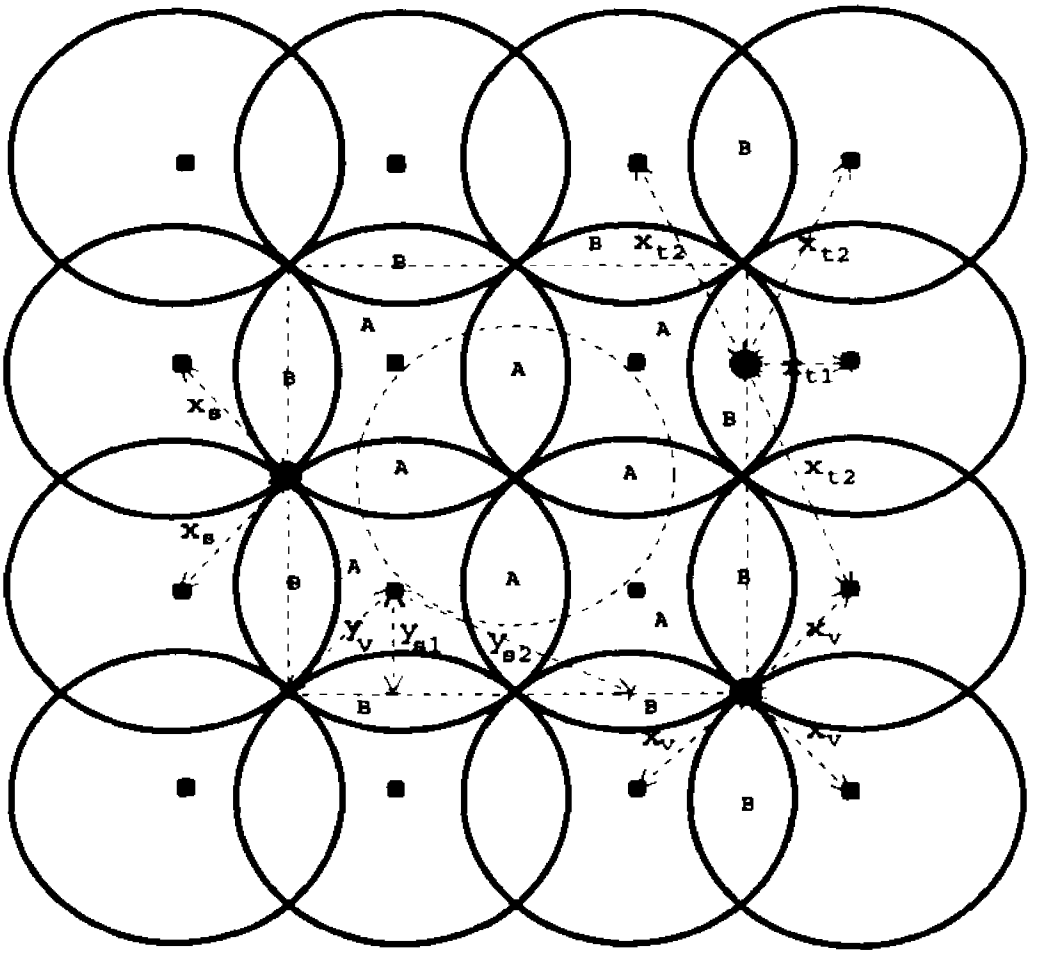


**Figure 6.4**

**Worst case interference scenario on the farthest floor from the zeroth floor in picocell.**

# Appendix A

## Multiple Access Interference (MAI) in PCN CDMA systems

In a Spread Spectrum CDMA system, all the transceivers use the same carrier frequency and bandwidth and operate simultaneously. This results in each user interfering with every other user in a given cell. The interference so generated is called multiple access interference (MAI) and it usually limits the performance of the system. The MAI is determined for the Spread Spectrum system described below.

### Spread Spectrum system

A basic Direct Sequence system (DS) is considered in this analysis. At each user's transmitter, a binary phase shift keyed (BPSK) modulated carrier is further BPSK modulated by a distinct pseudorandom signal, the spreading function. Balanced Gold codes are used as the pseudorandom sequences in the spreading function and no forward error correction coding is used. At the receiver, the signal is demodulated coherently. This is done by de-spreading the received signal with the same spreading function as in the transmitter and correlating over the data bit duration. Switch and stay selection diversity (Appendix B) is used to select the output decision variable.

The following general assumptions are made:

(a) perfect adaptive power control (APC) and automatic gain control (AGC) exist in the system.

(b) the receivers have perfect code acquisition and tracking systems.

(c) The received signals are assumed wide sense stationary and uncorrelated scattered (WSSUS).

From the third assumption above, it can be shown [39,40,41] that the received signal may be resolved into L component signals by the spreading function where

$$L = \mathrm{RND}\left(\frac{T_m}{T_c}\right). \qquad \text{(A.1)}$$

$T_m$ is the delay spread of the channel, $T_c$ is the code chip duration and the function RND( ) rounds the argument to the nearest integer. The kth user's signal, $v_k(t)$, is then

$$v_k(t) = \sum_{i=0}^{L-1} c_{ki}(t)\, d_k(t-\tau_{ki})\, g_k(t-\tau_{ki}) \cos[\omega_0 t - \phi_{ki}(t)], \qquad \text{(A.2)}$$

where $c_{ki}(t)$ and $\phi_{ki}(t)$ are the amplitude and phase of the channel gain of the ith component. $d_k(t)$ and $g_k(t)$ are the user's data and spreading code functions. $\omega_0$ is the carrier frequency and $\tau_{ki}$ is the relative delay of the ith component. The implicit assumption here is that the signals of all users have the same delay spread. If there are K simultaneous users in a cell, then the signal at the zeroth receiver in the uplink

channel[4] is

$$\begin{aligned} r_0(t) &= \sum_{k=0}^{K-1} V_k(t) + n_0(t) \\ &= \sum_{k=0}^{K-1} \sum_{i=0}^{L-1} c_{ki}(t)\, d_k(t-\tau_{ki})\, g_k(t-\tau_{ki}) \cos[\omega_0 t - \phi_{ki}(t)] \\ &\quad + n_0(t), \end{aligned} \tag{A.3}$$

where $n_0(t)$ is Gaussian thermal noise process of the receiver. $\tau_{ki}=\tau_{k0}+iT_c$; $i=0,1,\ldots,L-1$, where $\tau_{k0}$ represents the asynchronism of the system. This is the relative delay in transmission of a data bit by user k compared with the reference (user 0). It is a random variable uniformly distributed in the interval $\{0,T\}$. $T_c$ is the spreading function chip duration.

Assume that the lth component of the zeroth user's signal is acquired in the zeroth receiver, then the de-spread demodulated output is

$$\begin{aligned} X_l &= \int_{\tau_{0l}}^{T+\tau_{0l}} r_0(t)\, g_0(t-\tau_{0l}) \cos[\omega_0 t - \phi_{0l}(t)]\, dt \\ &= \sum_{k=0}^{K-1} \sum_{i=0}^{L-1} \int_0^T c_{ki}(t+\tau_{0l})\, d_k(t-\zeta_{ki})\, g_k(t-\zeta_{ki})\, g_0(t) \\ &\qquad \cdot \cos[\omega_0 t - \phi_{ki}(t+\tau_{0l})] \cos[\omega_0 t - \phi_{0l}(t+\tau_{0l})]\, dt \\ &\quad + \int_0^T n_0(t+\tau_{0l})\, g_0(t) \cos[\omega_0 t - \phi_{0l}(t+\tau_{0l})]\, dt, \end{aligned} \tag{A.4}$$

where

---

[4]The analysis is carried out for the mobile to cell site link (reverse link), but the results are applicable to the opposite link (forward link). This can easily be shown to hold if assumptions are made that the multipath components are statistically independent and the users messages are also statistically independent.

$$\zeta_{kl} = \tau_{kl} - \tau_{0l} = (\tau_{k0} - \tau_{00}) + (l-1)T_c. \qquad \text{(A.5)}$$

Define

$$y_l = \sum_{i=0}^{L-1} \int_0^T c_{0l}(t+\tau_{0l})\, d_0(t-\zeta_l)\, g_0(t-\zeta_l)\, g_0(t) \cdot \cos[\omega_0 t - \phi_{0l}(t+\tau_{0l})] \cos[\omega_0 t - \phi_{0l}(t+\tau_{0l})]\, dt, \qquad \text{(A.6)}$$

$$W_l = \sum_{k=1}^{K-1} \sum_{i=0}^{L-1} \int_0^T c_{kl}(t+\tau_{0l})\, d_k(t-\zeta_l)\, g_k(t-\zeta_l)\, g_0(t) \cdot \cos[\omega_0 t - \phi_{kl}(t+\tau_{0l})] \cos[\omega_0 t - \phi_{0l}(t+\tau_{0l})]\, dt, \qquad \text{(A.7)}$$

and

$$n_l = \int_0^T n_0(t+\tau_{0l})\, g_0(t) \cos[\omega_0 t - \phi_{0l}(t+\tau_{0l})]\, dt, \qquad \text{(A.8)}$$

then $X_l = y_l + W_l + n_l$. $y_l$ is the signal contribution due to the zeroth user; it is the desired part of the output. $W_l$ is the contribution due to the remaining (K-1) users; it is the MAI. $n_l$ is the contribution due to the receiver's thermal noise.

Since the number of users, K, is large, the Gaussian assumption is invoked by the Central Limit Theorem; that is $W_l$ is a Gaussian distributed random variable. Its expected value is zero since the random variables $d_{kl}$ are assumed independent and identically distributed with zero mean. Under the assumption that the coherence time of the channel is very much longer than the correlation interval T, the functions c(t) and $\zeta$(t) are considered fixed in that interval and the variance of $W_l$ is given by

$$\overline{W_I^2} = \frac{1}{2}\sum_{k=1}^{K-1} 2P_k \sum_{i=0}^{L-1} \overline{c_{ki}^2}\ \overline{\cos^2\psi_{ki}}\ \overline{R_{ki}^2(\zeta_{ki})}, \qquad \text{(A.9)}$$

where $(2P_k)$ is the variance of the users data function and $R_{ki}(\zeta_{ki}, j=1,2)$ are the partial cross-correlations of the zeroth and kth user's spreading functions in the ith signal component. The mean square of the partial cross-correlation function can be shown to be given by

$$\overline{R_{ki}^2(\zeta_k)} = T_c^2 \frac{N_d}{6}[3-2\alpha], \qquad \text{(A.10)}$$

where $T_c$ is the chip duration of the spreading function, $N_d$ is the number of code chips per data bit or the processing gain and $\alpha$ is the ratio of the processing gain to the spreading sequence period.

The channel gain amplitude $c_{ki}$ may be written as

$$c_{ki} = a m_{ki} \beta_{ki} \qquad \text{(A.11)}$$

where a is a constant that depends on the receiver AGC system and $m_{ki}$ and $\beta_{ki}$ are the local mean and the variation about the local mean of the ith component gain [38]. Thus $\beta_{ki}$ is a unity mean random variable. If $\beta_{ki}$ is Rayleigh distributed for all i, then the channel is termed Rayleigh fading. When line-of-sight (LOS) condition exists in the physical channel, the first component gain amplitude, $\beta_{k0}$, is Rician distributed and $\beta_{ki}$ is Rayleigh distributed for i=1,...,L-1. The channel is then called a Rician fading channel. In a microcellular

channel in a dense urban environment, there are many strong specular signal paths in addition to the line-of-sight path. The result is that other signal components may be Rician distributed; so $\beta_{ki}$ is Rician distributed for possibly all i.

It may be assumed from the statistics of the received signal (Section 2), that the gain variations are identically distributed for all users; therefore

$$\overline{\beta_{ki}^2} = \overline{\beta_i^2} \quad ;\forall k. \tag{A.12}$$

Substituting for the partial correlation function and the channel gain, The MAI is

$$\overline{W_I^2} = \frac{a^2T^2}{12N}\sum_{k=1}^{K-1} P_k \sum_{i=0}^{L-1} m_{ki}^2 \overline{\beta_i^2} \tag{A.13}$$

where N is the code sequence period (the assumption here is $a=1$). The local mean may be re-written as $m_{ki}=m_k b_i$ so that equation (A.13) becomes

$$\overline{W_I^2} = \frac{a^2T^2}{12N}\sum_{k=1}^{K-1} P_k m_k^2 \sum_{i=0}^{L-1} \overline{\gamma_i^2} \tag{A.14}$$

where $\gamma_i=b_i\beta_i$. The second summation is approximately unity for Rician microcellular channels; therefore

$$\overline{W_I^2} = \frac{a^2T^2}{12N}\sum_{k=1}^{K-1} P_k m_k^2. \tag{A.15}$$

In order for the CDMA system to overcome the near-far problem intrinsic to Spread Spectrum systems, the summand in equation (A.15) must be constant. This is the controlled power, $P_c$, in the cell. Therefore the MAI reduces to

$$W = \rho K P_c \qquad \text{(A.16)}$$

where $\rho$ is a constant and $P_c = P_k m^2_k$. The factor $m_k$ can be approximated by the average propagation path attenuation factor of the kth user channel.

# Appendix B

## Probability of error for Switch and Stay Demodulation in Direct Sequence Spread Spectrum CDMA system

The communication quality of a particular radio link may be determined by the signal to noise ratio (SNR) and bit error rate (BER) out of the receiver demodulator. The subsequent analysis derives these performance parameters for the DS-SS CDMA system described in appendix A. Again the analysis is done for the mobile to cell site link (reverse link). The channel variables that are required are the multipath delay spread and the received envelope statistics. At the data rate to be considered both the microcellular and the picocellular channel can be considered slowly varying channels. Switch and stay diversity is defined later.

### Signal to Noise Ratio

The communication channel model considered is the basic Gaussian model in which additive thermal noise as well as the multiple access interference (MAI) are considered independent, zero mean, Gaussian distributed processes. Standard CDMA analyses [25,40,41] of this model show that the demodulated output SNR, $Q_1$, is given by

$$Q_1 = \frac{y_1^2}{2\sigma_1^2} \qquad \text{(B.1)}$$

where $y_1$ and $\sigma^2_1$ are the mean and variance of the demodulated output decision variable respectively. $y_1$ is given by equation (A.6) in appendix A and $\sigma^2_1$ is the sum of the MAI and the output thermal noise given. Under the Spread Spectrum and channel assumptions given in appendix A, equation (A.6) reduces to

$$y_1 = \frac{1}{2} d_{00} c_{01} T \qquad \text{(B.2)}$$

where $d_{00}=(2P_0)^{1/2}$ is the transmit signal amplitude, $c_{01}$ is the channel gain amplitude and T is the demodulator correlation time. The MAI is given by equation (A.15) and the output noise derived from equation (A.8) is

$$\sigma^2_{01} = \frac{1}{4} \eta_0 T \qquad \text{(B.3)}$$

where $\eta_0/2$ is the thermal noise power spectral density. Substituting equations (B.2), (A.15) and (B.3) into (B.1) gives

$$Q_1 = \frac{\frac{1}{2} a^2 P_c T^2 \gamma_1^2}{\frac{1}{6} a^2 P_c T^2 \frac{K}{N} + \frac{1}{2} \eta_0 T} \qquad \text{(B.4)}$$

where a is a constant, $P_c$ is the controlled power in the cell, K is the number of simultaneous users, N is the processing gain and $\gamma_1$ is the 1th multipath component gain variation. Defining $Q_c=P_cT/\eta_0$, equation (B.4) may be re-written as

$$Q_1 = \frac{a^2 Q_c \gamma_1^2}{\frac{1}{3} a^2 Q_c \frac{K}{N} + 1}. \qquad \text{(B.5)}$$

If the system is interference limited, as is typically the case for CDMA operations, then the first term of the denominator in equations (B.4) and (B.5) is much larger than the second term, hence

$$Q_1 \approx 3\frac{N}{K}\gamma_1^2. \tag{B.6}$$

From equation (B.5), the interference limitation implies that

$$\frac{1}{3}a^2 Q_c \frac{K}{N} > 1, \tag{B.7}$$

hence

$$Q_c > 3\frac{N}{K}\frac{1}{a^2}; \tag{B.8}$$

so for a given channel and receiver thermal SNR, the inequality, as expected, requires a large number of users, K, for a given processing gain, N. Since the Gaussian assumption is used, the probability of error is a function of the SNR and in order to obtain low values, for a given channel, the (N:K) ratio must be very large. This results in fairly large $Q_c$ for low probabilities of error.

**Bit Error Rate in PCN Channel**

Because of the Gaussian assumption, the BER can be expressed in terms of the SNR [39] and is given by

$$P_b = \frac{1}{2}erfc(Q^{\frac{1}{2}}) \quad , Coherent\ BPSK. \tag{B.9}$$

This is a conditional probability as Q is a random variable. The total probability of error for the 1th demodulated component is obtained by averaging over the SNR; that is

$$\begin{aligned} P_{el} &= \int_0^{\infty} p(Q_l)\, P_e(Q_l)\, dQ_l \\ &= \tfrac{1}{2}\int_0^{\infty} p(Q_l)\, erfc(\sqrt{Q_l})\, dQ_l . \end{aligned} \tag{B.10}$$

The random variable $Q_l$, given in equation (B.6), may be written as

$$Q_l = n\gamma_l^2 \tag{B.11}$$

where $n=3N/K$ is a constant and $\gamma_l$ is a random variable. If $\gamma_l$ is Rayleigh distributed, $Q_l$ is chi-square distributed and if Rician distributed, $Q_l$ is non-central chi-square distributed. The density functions of the chi-square variables [42] are given by

$$p(Q_l) = \frac{1}{\bar{Q}_l} e^{-\frac{Q_l}{\bar{Q}_l}} \tag{B.12}$$

for the central case and

$$p(Q_l) = \frac{k_l+1}{\bar{Q}_l} e^{-\left[(k_l+1)\frac{Q_l}{\bar{Q}_l}+k_l\right]} I_0\left(2\sqrt{k_l(k_l+1)\frac{Q_l}{\bar{Q}_l}}\right) \tag{B.13}$$

for the non-central case, where $k_l$ is the Rician power gain and $I_0$ is the zeroth order Bessel function of the second kind.

From equation (B.11), the expected value of $Q_l$ is

$$\overline{Q_l} = n\overline{\gamma_l^2}. \tag{B.14}$$

The mean square gain variations are assumed exponentially weighted so that

$$\overline{\gamma_l^2} = \overline{\gamma_0^2}\, e^{-\frac{\mu l}{L}} \quad ; l=0,1,\ldots,L-1 \tag{B.15}$$

where $\mu$ is a constant for the channel. If a Rician microcellular channel is considered in which all the gain variations are Rician distributed, then the mean square variation may also be given by

$$\overline{\gamma_l^2} = \alpha_l(k_l+1) \tag{B.16}$$

where $\alpha_l$ is the mean square of the implicit Rayleigh distribution and $k_l$ is the Rician power gain. The quantity $\alpha_l$ may also be assumed exponentially weighted; therefore

$$\alpha_l = \alpha_0\, e^{-\frac{\nu l}{L}} \quad ; l=0,1,\ldots,L-1. \tag{B.17}$$

Substituting equation (B.17) into (B.16) and equating to (B.15), the values of $k_l$ are obtained as

$$k_l = \frac{\overline{\gamma_0^2}}{\alpha_0}\, e^{-\frac{(\mu-\nu)l}{L}} - 1 \quad ; l=0,1,\ldots,L-1. \tag{B.18}$$

The higher the component number, the more its distribution tends toward the Rayleigh distribution; therefore $\mu>\nu$. The quantities $E[\gamma_0^2]$ and $\alpha_0$ are found by summing equations (B.15) and (B.17) over all L.

Thus

$$\overline{\gamma_0^2} = \overline{\gamma^2}\,\frac{1-e^{-\frac{\beta}{L}}}{1-e^{-\beta}} \qquad \text{(B.19)}$$

and

$$\alpha_0 = \alpha\,\frac{1-e^{-\frac{\gamma}{L}}}{1-e^{-\gamma}} \qquad \text{(B.20)}$$

where

$$\overline{\gamma^2} = \alpha(k+1)\,. \qquad \text{(B.21)}$$

Equation (B.21) relates the mean square of the received envelope variation to the Rician power gain of the channel. Substituting for $E[\gamma_0^2]$ and $\alpha_0$ in equation (B.18)

$$k_l = (k+1)\,\frac{(1-e^{-\frac{\beta}{L}})\,(1-e^{-\gamma})}{(1-e^{-\frac{\gamma}{L}})\,(1-e^{-\beta})}\; e^{-\frac{|\beta-\gamma|\,l}{L}} - 1 \quad ; l=0,1,\ldots,L-1\,. \qquad \text{(B.22)}$$

The probability of error is now determined for a switch and stay diversity in a Rician microcellular channel. Switch and stay diversity means that the receiver selects the lth resolved signal component, providing its SNR, $Q_l$, is above a set threshold, $Q_T$, and uses that component to provide the output decision variable. When signal fading causes the SNR to fall below the threshold, the receiver searches anew for a component satisfying the selection criterion. The current component, however, is still retained (stay) until the new component is found, at which time the receiver selects the

latter (switch).

The probability of error for this system is the sum of two conditional probabilities, the probability of error given that all components are below the threshold (referred to as a total fade) and the probability of error given this condition does not occur. Let $P_f$ be the probability of total fade; that is the SNR for each component is less than the threshold ($Q_i \leq Q_T$, i=0,...,L-1). Then $P_f$ is given by

$$P_f = \prod_{i=0}^{L-1} F_i(Q_T), \tag{B.23}$$

where $F_i$ is the probability distribution function of $Q_i$. $P_f^c(S)$ defined as $1-P_f$ is the probability of the complement event; it is the probability that some component is above the threshold. The average probability of error, $P_e$, for the diversity system is then

$$\begin{aligned} P_e &= P_f^c \sum_{i=0}^{L-1} q_i P_{ei} + P_f \sum_{i=0}^{L-1} q_i P_{ei}^* \\ &= \sum_{i=0}^{L-1} q_i P_{ei} + P_f \sum_{i=0}^{L-1} q_i [P_{ei}^* - P_{ei}]. \end{aligned} \tag{B.24}$$

$q_i$ is the selection probability for the ith component, $P_{ei}$ and $P^*_{ei}$ are the probabilities of error for the ith component above and below threshold respectively. The error probabilities $P_{ei}$ are found by substituting equation (B.13) into equation (B.10) with the lower integration limit set to $Q_T$.

The selection probabilities $q_i$ are given by

$$q_i = \frac{1-F_i(Q_T)}{\sum_{i=0}^{L-1}[1-F_i(Q_T)]}. \qquad \text{(B.25)}$$

It was shown in section 2 that, for the general PCN channel in the urban areas, the signal distribution is Rician with k=5-10 dB indoors and 10-15 dB outdoors and the delay spread is typically 250 ns. If a 30 MHz signal bandwidth is assumed (a possible choice for the emerging PCNs), then about four multipath components will be resolved. Substituting equations (B.10), (B.23) and (B.25) in equation (B.24) gives the average probability of error for the diversity system. Figure (B.1) shows these probabilities as functions of the mean signal to noise ratio of the received signal for different Rician power gain k.

For the error calculations, the threshold SNR was taken as $E[Q][1+10/\sqrt{k})$, where E[Q] is the mean SNR of the signal. This value was chosen so that only significant values of Q would be used, thereby biasing stronger components. The channel constants $\mu$ and $\upsilon$ were chosen to satisfy the following constraints: (1), $k_i>0$ for all i, and (2), $E[\gamma^2_L]$ 25 dB or more below $E[\gamma^2_0]$. The first condition is true for all Rician channels and the second is typical for the microcellular channels under consideration.

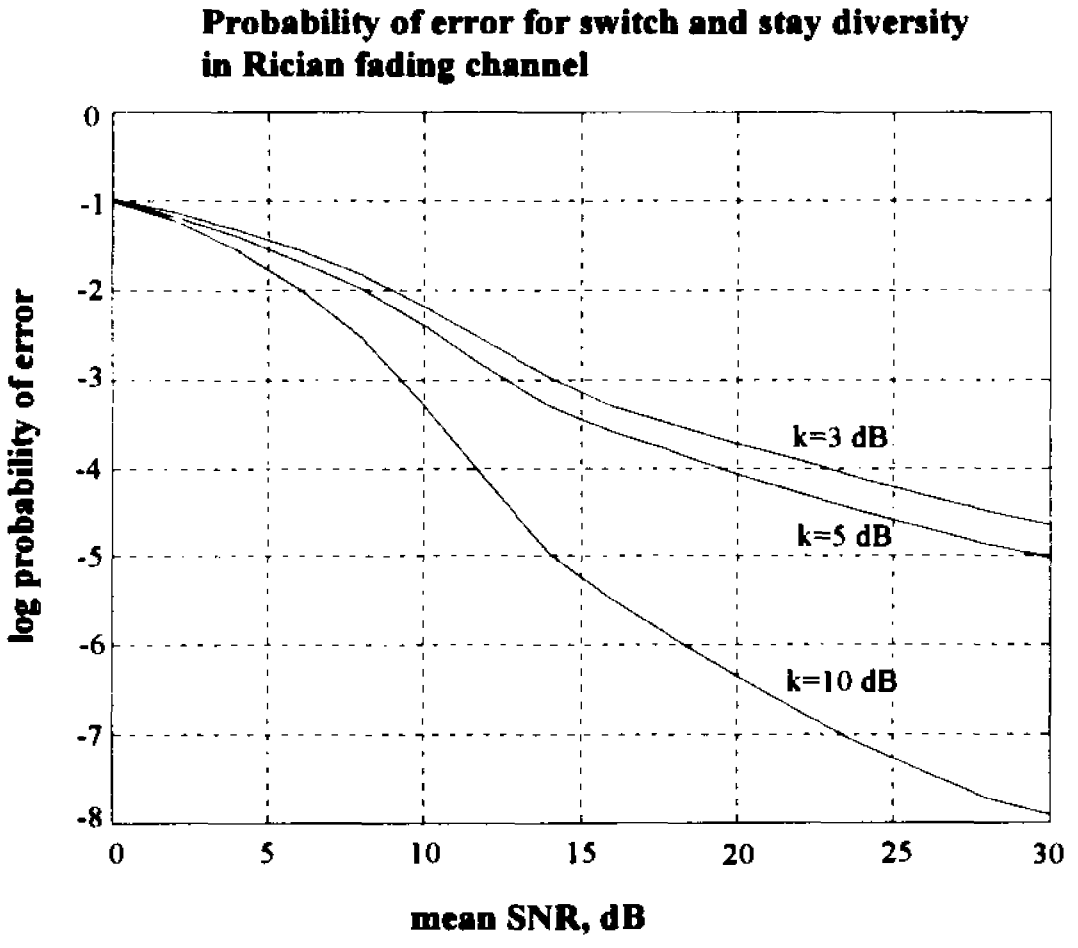


Figure (B.1)

Probability of error for
switch and stay diversity
in Rician fading channel

# Appendix C

## Maximum number of simultaneous users in isolated microcell

When the bit error rate (BER) of the system is set, the mean signal to noise ratio (SNR) required to realize this BER can be found from the graphs in figure (B.1) in Appendix B. Assuming a BER of $10^{-3}$ (a typical value for digital mobile radio systems), a mean SNR of approximately 9.0 dB is obtained for a Rician power gain of 10 dB. The mean SNR of the lth resolved signal component was also given in Appendix B by equation (B.6). Therefore summing over all l in that equation, the mean SNR, Q, of the received signal is given by

$$\overline{Q} = 3\frac{N}{K}\sum_{l=0}^{L-1}\overline{\gamma_l}. \qquad \text{(C.1)}$$

The sum in the above equation is approximately unity for the Rician microcellular channel, so

$$\overline{Q} = 3\frac{N}{K}. \qquad \text{(C.2)}$$

Substituting for the mean SNR in equation (C.2) gives an N:K ratio of 2.64. So for a code length of 1023, **K=387**. Likewise substituting for Q in equation (B.8), Appendix B, gives a required receiver thermal SNR of approximately 19 dB. The value found for K represents the maximum number of simultaneous users that can operate in the cell for the given BER.

Because of bandwidth limitations and the use long codes, the code sequence length, N, and the processing gain, PG, often are not the same; PG is usually less than N. If the system uses Gold codes or any other pseudorandom codes with non-zero cross-correlation functions, then when N is not equal to PG there is an additional factor in the denominator of equation (B.6) (Appendix B). This results in a larger N:K ratio than calculated above, which implies a smaller K for a given N. Thus the value of K found when **N=PG** may be considered an upper bound.

The Thermal SNR can now be used to find the maximum permissible path loss in the network. The power budget is given by the equations

$$P_T = L_c - G_T - G_R + P_R \qquad \text{(C.3)}$$

$$P_R = Q_0 + N \qquad \text{(C.4)}$$

where $P_T$ is the transmit power

$P_R$ is the received power

$Q_0$ is the thermal SNR

N is the demodulator noise output

$L_c$ is the path loss at the cell boundary

$G_T, G_R$ are the transmitter and receiver antenna gains respectively.

The following are assumed for a typical PCN:

(1) The maximum transmit power in the cell is taken to be 100 mW (20 dBm) for microcellular networks and 10 mW (10 dBm) for picocellular networks.

(2) The overall antenna gain is 3 dB.

(3) The data rate is 16 kbps.

(4) The transmit bandwidth is 30 MHz.

The thermal noise power N is given by

$$N = 2kTB \qquad \text{(C.5)}$$

where k is Boltzmann's constant, T is the Kelvin temperature and B is the output data bandwidth. Substituting the assumed values in equation (C.5) gives a noise power of -126 dBm. This results in a received power, $P_R$, of -107 dBm, and for 20 dBm transmit power the maximum path loss is -127 dB for microcells. For picocells the maximum path loss is -117 dB.

# Appendix D

## Number of blocks and intersections in Omni-I network

Consider a microcell network on a general grid with standard block length L, avenue spacing mL and street spacing L. m is assumed a non-zero positive integer. Let $n_c$ be the radius of the microcell in standard blocks and the avenue and street spacings be $n_c$ and $mn_c$ respectively, then if $N_I$ and $N_B$ are the total number of blocks and intersections in the microcell are given as follows:

### Number of nodes

(a) $m \mid n_c$, that is $n_c = km$, then

$$N_I = (2n_c+1) + 2\sum_{i=1}^{k}[2(n_c - mi) + 1] = \frac{2n_c(n_c+1) + m}{m} \qquad (D.1)$$

(b) $m \nmid n_c$ that is $n_c = km + l$ ,$k,l \in I$, $k\neq 0$, $l\neq 0$, $l < m$, then

$$N_I = (2n_c+1) + 2\sum_{i=1}^{k}[2(n_c - mi) + 1] = \frac{2n_c(n_c+1) - 2l(l-m+1) + m}{m}. \qquad (D.2)$$

Comparing both equations, it is seen that the second gives a general relationship; therefore

$$N_I = \frac{2n_c(n_c+1) - 2l(l-m+1) + m}{m} \quad , l = n_c \,(\mathrm{mod})\, m. \qquad (D.3)$$

**Number of boundary nodes**

(c) $m \mid n_c$

$$N_v = 2 + 2(2k-1) = 4k = 4\frac{n_c}{m} \tag{D.4}$$

(d) $m \nmid n_c$

$$N_v = 2(2k+1) = 4k+2 = \frac{4(n_c-l)+2m}{m}. \tag{D.5}$$

**Number of blocks**

(a) $m \mid n_c$

$$\begin{aligned} N_b &= 4n_c + 2\sum_{i=1}^{k} 2(n_c - mi) + 2\sum_{i=1}^{n_c} 2(n_c - i) \\ &= 2n_c^2 + \frac{2n_c^2}{m} = 2n_c^2\left(\frac{m+1}{m}\right) \end{aligned} \tag{D.6}$$

(b) $m \nmid n_c$

$$\begin{aligned} N_b &= 4n_c + 2\sum_{i=1}^{k} 2(n_c - mi) + 2\sum_{i=1}^{n_c} 2(n_c - i) \\ &= 2n_c^2 + 2n_c + (n_c - l)\frac{2(n_c+1)-2m}{m} \\ &= 2n_c^2\left(\frac{m+1}{m}\right) + 2l\left(\frac{m-l}{m}\right). \end{aligned} \tag{D.7}$$

The second equation here is also a general expression; therefore

$$N_b = 2n_c^2\left(\frac{m+1}{m}\right) + 2l\left(\frac{m-1}{m}\right) \quad , l = n_c \,(\mathrm{mod})\, m. \tag{D.8}$$

## References


[1] Sam Ginn; "Personal Communication Services: Expanding the Freedom to Communicate"; IEEE Communications Magazine, Feb.91, pp.30-32, 39

[2] Ian M. Ross; "Wireless Network Directions"; IEEE Comm. Mag., Feb.91, pp.40-42

[3] Douglas G. Smith; "Spread Spectrum for Wireless Phone Systems: The Subtle Interplay between Technology and Regulation"; IEEE Comm. Mag., Feb.91, pp.44-46.

[4] Jack T. Taylor; "Spread Spectrum Technology: A Solution to the Personal Communications Services Frequency Allocation Dilemma"; IEEE Comm. Mag., Feb.91, pp.48-51

[5] Carson E. Agnew; "Efficient spectrum allocation for Personal Communications Services"; IEEE Comm. Mag., Feb.91, pp.48-51

[6] Richard J. Lynch; "PCN: Son of Cellular? The Challenges of Providing PCN Service"; IEEE Comm. Mag., Feb.91, pp.56-57

[7] Richard M .Singer; "Personal Communications Services: The Next Technological Revolution"; IEEE Comm. Mag., Feb.91, pp.62-66

[8] W.C.Y. Lee; "Smaller Cells for Greater Performance"; IEEE Comm. Mag., Vol.29, No.11, Nov.91, pp.19-23

[9] Theodore S. Rappaport; "The Wireless Revolution"; IEEE Comm. Mag., Vol.29, No.11, Nov.91, pp.52-71

[10] Donald L. Schilling, Lawrence B. Milstein, Raymond L. Pickholtz; "Spread Spectrum for Commercial Communications", IEEE Comm. Mag., Apr.91, pp.66-79

[11] D.L. Schilling, L. Milstein, R.L. Pickholtz, et.al; "Broadband CDMA for Personal Communications Systems", IEEE Comm. Mag., Nov.91, pp.86-93

[12] R.L.Pickholtz, L.B. Milstein, D.L. Schilling; "Spread Spectrum for Mobile Communications"; IEEE Transaction on Vehicular Technology, May 91, pp.313-322

[13] L.B.Milstein, D.L. Schilling, R.L. Pickholtz, et.al "On the Feasibility of a CDMA Overlay for Personal Communications Network", IEEE Journal on Selected Areas of Communications, Vol.10, No.4, May 92, pp.655-668

[14] Andrew Viterbi, Roberto Padovani; "Implications of Mobile Cellular CDMA", IEEE Comm. Mag., Vol.30, No.12, Dec.92, pp.38-41

[15] Larry J. Greenstein, Noach Amitay; "Microcells in Personal Communications Systems"; IEEE Comm. Mag.,Vol.32, No.12, Dec.92, pp.76-88

[16] R.Steele, V.H. Prabhu; "High-User-Density Digital Cellular Mobile Radio Systems"; IEE Proceedings, Vol.132,Pt.F, No.5, Aug.85, pp.396-404

[17] R. Steele; "Towards a High-Capacity Digital Cellular Mobile Radio System"; IEE Proc., Vol.132, Pt.F, No.5, pp.405-415

[18] Donald C. Cox; "Universal Digital Portable Radio Communications"; IEEE Proc., Vol.75, No.4, Apr.87, pp.436-477

[19] E. S. K. Chien, D. J. Goodman, J. E. Russell; "Cellular Access Digital Network (CADN): Wireless Access to Networks of the Future"; IEEE Comm. Mag. Vol.25, No.6, Jun.87, pp.22-31

[20] Raymond Steele; "The Cellular Environment of Lightweight Handheld Portables"; IEEE Comm. Mag., Jul.89, pp.20-29

[21] David J. Goodman; "Second Generation Wireless Information Networks; IEEE Trans. on Vehic. Tech., Vol.40 No.2 May 91, pp.366-374

[22] Vinko Erceg; "Propagation Characteristics of 2.0 GHz Microcellular channel"; Ph.D thesis, City University of New York, 1992

[23] V. Erceg, S. Ghassemzadeh, M. Taylor, et.al; "Urban and Suburban Out-of-Sight Propagation Modeling"; IEEE Com. Mag., Jun.92, pp.56-60

[24] S. Ghassemzadeh, V. Erceg, M. Taylor, et.al.; "Indoor Propagation and Fading Characteristics of Spread Spectrum Signals at 2 GHz"; Conference Tutorial, Globecom 92.

[25] Raymond L. Pickholtz, Donald S. Schilling, Lawrence B. Milstein; "Theory of Spread-Spectrum Communications-A Tutorial"; IEEE Transactions on Communications, Vol.30, No.5, May 82, pp 855-884

[26] Saeed S. Ghassemzadeh; "Effects of Channel Fading on a Direct Sequence Spread Spectrum Signal at 2 GHz"; Ph.D thesis, City University of New York, 1994

[27] Shigeru Kozono, Akira Taguchi; "Mobile Propagation Loss and Delay Spread characteristics with a Low Base Station Antenna on an Urban Road; IEEE Trans. Vehic. Tech. Vol.42, No.1, Feb.93, pp.103-109

[28] Robert J.C. Bultitude; "Measurement, Characterization and Modeling of Indoor 800/900 MHz Radio Channels for Digital Communications"; IEEE Com. Mag., Jun.87, pp.5-12

[29] Robert J.C. Bultitude, Samy Mahmoud and William A. Sullivan; "A comparison of Indoor Radio Propagation Characteristics at 910 MHz and 1.75 GHz"; IEEE J.S.A.C., vol.7, No.1, Jan.89, pp.20-30

[30] Hamilton W. Arnold, R.R. Murray and Donald C. Cox; "815 MHz Radio Attenuation Measured within Two Commercial Buildings"; IEEE Transaction on Antennas and Propagation, Vol.37, No.10, Oct.89, pp.1335-1339

[31] J-F. Lafortune, M. Lecours; "Measurement and Modeling of Propagation Losses in a Building at 900 MHz"; IEEE Vehic. Tech. Vol.39, No.2, May 90, pp.101-108

[32] Scott Y. Seidel and Theodore S. Rappaport; "914 MHz Path Loss Prediction Models for Indoor Wireless Communications in Multifloored Buildings"; IEEE Trans. Ant. and Prop., Vol.40, No.2, Feb.92, pp.207-217

[33] Daniel M.J. Devasirvatham; "Time Delay Spread and Signal Level Measurements of 850 MHz Radio Waves in Building Environments"; IEEE Trans. Ant and Prop. Vol.34, No.11, Nov.86, pp.1300-1305

[34] ------; "A comparison of Time Delay Spread and Signal Level Measurements within Two Dissimilar Office Buildings"; IEEE Trans. Ant. and Prop., Vol.35, No.3, Mar.87, pp.319-324

[35] ------; "Multipath Time Delay Spread in the Digital Radio Environment"; IEEE Comm. Mag., Vol.25, No.6, Jun.87, pp.13-21

[36] Adel A.M. Saleh and Reinaldo A. Valenzuela; "A Statistical Model for Indoor Multipath Propagation"; IEEE J.S.A.C., Vol.5, No.2, Feb.87, pp.128-137

[37] Michel Daoud Yacoub; "Foundations of Mobile Radio Engineering"; CRC Press, 1993, Boca Raton

[38] William Y.C. Lee; "Mobile Communication Engineering", 1st Ed.; McGraw-Hill, 1982, New York

[39] Seymour Stein; "Fading Channel Issues in System Engineering"; IEEE J.S.A.C., Vol.5, No.2, Feb.87, pp.68-89

[40] George L. Turin; "The Effects of Multipath and Fading on the Performance of Direct-Sequence CDMA Systems"; IEEE J.S.A.C., Vol.2, No.4, Jul.84, pp 597-603

[41] Heinz Ochsner; "Direct-Sequence Spread-Spectrum Receiver for Communication on Frequency-Selective Fading Channels"; IEEE J.S.A.C., Vol.5, No.2, Feb.87, pp.188-193

[42] John G. Proakis; "Digital Communications", 2nd Ed. (Ch.7); McGraw-Hill, 1989, New York;